R.P.I. Technical Report MP-28

A Progress Report for
July 1, 1971 to June 30, 1972

ANALYSIS AND DESIGN OF A CAPSULE LANDING SYSTEM AND SURFACE VEHICLE CONTROL SYSTEM FOR MARS EXPLORATION

National Aeronautics and Space Administration

Grant NGL 33-018-091

Submitted by the Special Projects Committee

D.K. Frederick
P.K. Lashmet
G.N. Sandor
C.N. Shen
E.J. Smith
S.W. Yerazunis

School of Engineering
Rensselaer Polytechnic Institute

ABSTRACT

Investigation of problems related to the design and control of a mobile planetary vehicle to implement a systematic plan for the exploration of Mars has been undertaken. Problem areas receiving attention include: vehicle configuration, control, dynamics, systems and propulsion; systems analysis; navigation, terrain modeling and path selection; and chemical analysis of specimens. The following specific tasks have been under study: vehicle model design, mathematical modeling of dynamic vehicle, experimental vehicle dynamics, obstacle negotiation, electromechanical controls, collapsibility and deployment, construction of a wheel tester, wheel analysis, payload design, system design optimization, effect of design assumptions, accessory optimal design, on-board computer subsystem, laser range measurement, discrete obstacle detection, obstacle detection systems, terrain modeling, path selection system simulation and evaluation, gas chromatograph/mass spectrometer system concepts, chromatograph model evaluation and improvement and transport parameter evaluation.

These tasks are defined in detail and the progress which has been achieved during the period July 1, 1971 to June 30, 1972 is summarized. Projections of work to be undertaken in certain areas during the period July 1, 1972 to June 30, 1973 are included.

TABLE OF CONTENTS

Analysis and Design of a Capsule Landing System and Surface Vehicle Control System for Mars Exploration

I. Introduction

Current national goals in space exploration include a detailed study and examination of the planet Mars. The effectiveness of Mars exploration missions would be enhanced according to the extent to which the investigative devices which are landed are mobile, to the range of their mobility, and to the ability to control their motion. In order to achieve basic mission objectives, and beyond that, to maximize the return on the commitment of resources to the mission, formidable technical problems must be resolved. The major factor contributing to these problems is the round trip communications time delay between martian and earth control stations which varies from a minimum of about 9 minutes to a maximum of 25 minutes. This time delay imposes stringent requirements on the vehicle, on its control and communication systems and on those systems included on board to make the scientific measurements, in terms of their ability to function autonomously. These systems must be able to operate with a high degree of reliability and must be capable of calling for earth control under appropriate circumstances.

A number of important problems originating with these factors and relating directly the basic mission objectives of an unmanned exploration of Mars have been and are currently being investigated by a faculty-student project team at Rensselaer Polytechnic Institute with the support of NASA NGL-33-018-091.

This progress report describes the tasks which have been undertaken and documents the progress which has been achieved in the interval July 1, 1971 to June 30, 1972.

II. Definition of Tasks

The delay time in round trip communication between Mars and Earth gives rise to unique problems relvant to martian and/or other planetary explorations. All phases of the mission from landing the capsule in the neighborhood of a desired position to the systematic traversing of the surface and the attendant detection, measurement, and analytical operations must be consummated with a minimum of control and instruction by earth based units. The delay time requires that on board systems capable of making rational decisions be developed and that suitable precautions be taken against potential catastrophic failures. Four major tasks areas, which are in turn divided into appropriate sub-tasks, have been defined and are listed below.

A. Vehicle Configuration, Control, Dynamics, Systems and Propulsion. The objectives of this task are to investigate problems related to the design of a roving vehicle for Mars exploration with respect to configuration; motion and attitude control; obstacle avoidance; control, information and power systems; and propulsion systems. In addition, the design concepts must accommodate the equipment and instruments required to automate the vehicle and to perform the scientific objectives of the mission.

B. General Systems Analysis. The objective of this task is to develop a framework within which decisions in design involving conflicting requirements can be made rationally and in the context of the whole system and mission. Relationships between alternative mission profiles and specifications and weight, energy and space allocation and management will be sought.

C. Surface Navigation and Path Control. Once the capsule is landed and the roving vehicle is in an operational state, it is necessary that the vehicle can be directed to proceed under remote control from the landing site to specified positions on the martian surface. This task is concerned with the problems of terrain modeling, path selection and navigation between the initial and terminal sites when major terrain features precluding direct paths are to be anticipated. On board decision making capability must be designed to minimize earth control responsibility except in the most adverse circumstances.

D. Chemical Analysis of Specimens. A major objective of martian surface exploration will be to obtain chemical, biochemical or biological information. Many experiments proposed for the mission require a general duty, gas chromotograph-mass spectrometer for chemical analysis. The objective of this task is to generate fundamental data and concepts required to optimize this chemical analysis system.

III. Summary of Results

Task A. Vehicle Configuration, Control, Dynamics, Systems and Propulsion

This broad task has been divided into the following subtasks: vehicle model design, mathematic modeling of vehicle dynamics, experimental dynamics analysis, obstacle negotiation, electromechanical control systems, collapsibility and deployment, wheel testing apparatus, wheel analysis and payload design. A brief summary of the progress achieved in the prior interval in each of these areas follows below.

A.1.a. Vehicle Model Design

A new phase in the design of a vehicle model was undertaken during this period to overcome deficiencies in the first generation model. The major change has been in the design of the rear wheel suspension system which now involves a torsion bar concept. This change should improve the dynamic characteristics as well as to permit an effective collapsibility and deployment system. Although the new design eliminates the original three-wheeled operating mode for the vehicle which permitted considerable flexibility for maneuver and obstacle avoidance, the new arrangement can also be used to overcome unusual terrain features through a shift-back maneuver. On the basis of dynamic studies of the 0.184 model of the new vehicle, it was concluded that a 0.4 model should be constructed for testing and evaluation.

A.1.b. Mathematical Model of Dynamic System

The mathematical modeling of the dynamics of the vehicle has been completed. On the basis of prediction of response of the vehicle to periodic disturbances, conclusions with regard to dampening components have been drawn and are being considered in the design of the 0.4 model.

A.1.c. Dynamic Analysis

Experimental dynamic analysis of the 0.184 model has verified the mathematical model except for a coupling which is believed to be due to imperfect symmetry of the rear wheel spring rates and weight distribution. Improvements in the torsion bar dampener as well as adjustments in the vehicle spring rates are indicated if an exceptional dynamic behavior is to be achieved.

A.1.d. Obstacle Negotiation

A number of tools for determining limiting values of obstacle negotiating capabilities of roving vehicles have been developed. Computer programs relating the wheel torque and coefficient of friction required to negotiate step, crevasse and slope obstacles have been developed. Vehicle hangup can now be predicted from configurational parameters and obstacle descriptions. These tools can now be used to define the crucial MRV dimensions and to provide quantitative comparisons between alternative vehicle concepts.

A.1.e. Electromechanical Controls

Control systems for the 0.184 RPI MRV model for payload leveling, steering and rear wheel motion have been developed. Some modification of these systems for the 0.4 scale vehicle will be required in the future.

A.2. Collapsibility and Deployment

The collapsibility and deployment of the RPI MRV design has been studied. On the basis of these studies, more reliable design constraints can be defined and are reflected in the present MRV configuration. Consideration has been given to the collapse of the vehicle within the Viking capsule and to a Mars landing sequence.

A.3.a. Wheel Tester

A wheel testing system has been designed and constructed. This apparatus will permit the testing of 0.4 scale wheels under various conditions of wheel slip, load, cant angle and soil condition to provide data necessary for optimization of wheel design.

A.3.b. Wheel Analysis

Improved mathematical methods for the analysis of the toroidal wheel have been developed and evaluated. The new method, based on

finite elements, computes radial stiffness for any combination of hoop and rim stiffnesses within an accuracy of 5%. The computer program has been used to develop a wheel design "handbook".

A.4. Payload Design

The objective of the payload design task is to coordinate the MRV subsystems into an effective and reliable MRV design capable of executing the stated mission functions. Constraints and assumptions serving as design guidelines have been defined and have led to design concepts which have identified areas requiring further study. The relation of the form of the vehicle and its payload to the aerodynamic forces is being investigated. Once payload form is defined, placement of subsystem components will be undertaken. Analysis of the composite vehicle design including vehicle dynamics, systems operation and reliability, collapsibility, stability, etc. will be pursued and comparisons with alternative vehicle concepts will be made.

Task B. General Systems Analysis

This major task is subdivded into four subtasks: systems design assumptions on the system model, accessory optional solutions for design parameter perturbation and the on-board computer system.

B.1. Systems Design Optimization

The systems design optimization task has been concerned with the problem of optimizing the design of the vehicle system including science, communication, propulsion, etc. The approach which has been taken involves the mathematical modeling of all of the physical components of the system and the reduction of the resulting equations to a group of relationships involving a set of state variables. All design parameters are related in some direct fashion to these state variables. The problem is to determine what particular set of state variables, and therefore what set of design parameters, optimize the desired objective function values related to the mission.

The original set of equations was nonlinear and considerable difficult was encountered in obtaining reasonable solutions. On review of the basic model equations, simplifications and modifications have been made to improve the description of the physical system or to eliminate unnecessary features which complicate the analysis. Although the problem remains nonlinear, the updated model appears to be more realistic and some preliminary results which probably represent "local" optimums have been obtained. Future work is aimed at initiating the optimization at other starting points to determine the sensitivity of the "optimum point" to the initial point. Refinement of the mathematical model will be continued to improve the description of the physical system. Ultimately, the method will be applied to other major mission alternatives as identified below.

B.2. Effect of Design-Dependent Assumptions

The effect of changing design-dependent assumptions on the system model has been determined for two cases. First, the addition of an active stationary orbiter linking the vehicle with earth has been studied. The net effect of this assumption is to eliminate restrictions on data rate and to reduce on-board power and weight requirements. Second, model equations describing a conventional six-wheeled, three compartment vehicle have been developed. Future work includes optimization of each of these major mission models and comparison with the original model representing the RPI MRV vehicle concept.

B.3. Accessory Optimal Solutions

The task dealing with accessory optimal solutions for design parameter perturbations originates with several factors. First, the optimal solution may suggest parameters awkward from an implementation point of view; second, new constraints may be added and perturb the solution; and third, off-the-shelfware hardware may not coincide with optimal values. In these cases, it is desired to know how the design parameters should be adjusted to retain optimality when small perturbations are made. The objective of the task is to determine the optimal manner in which to make this adjustment. A sensitivity approach has been used because it has the advantage of linearity even though the original optimization problem is non-linear. A method for determining the required adjustment of design parameters has been developed and it has been applied to simple problems where the true optimum is known. Work in this area has been deferred pending completion of Task B.1 on optimization of the original model and will be reactivated in the near future.

B.4. On-Board Computer Subsystem

The on-board computer subsystem task is intended to allow the investigation of alternative internal computer structures and to provide a device for testing alternative structures and the operation of model and/or hardware subsystems. Vehicle objectives and operating requirements were determined to establish demands on the on-board computer. A simulator has been developed using a GEPAC-30 computer which achieves the desired objectives. When the vehicle systems have been modeled to the point where they can be interfaced with the computer, the computer architecture which has been developed will be tested. Long range plans include interfacing the 0.4 scale RPI MRV with this computer and testing the combined system performance.

Task C. Navigation, Terrain Modeling and Path Selection

This task deals with problems of terrain sensing, terrain modeling, obstacle detection and path selection for an autonomous roving vehicle. Specific tasks receiving active effort include laser beam range measurement, discrete obstacle detection, obstacle detection systems, terrain modeling and path selection system evaluation.

C.1.a. Range Measurement

The use of a laser beam range measurement system has been analyzed. It has been determined that present day technology can be employed to measure distances in the 3 to 30 meter range with an accuracy of 5 cm. The required components are small and do not require high voltages or large amounts of power. The feasibility of using a gallium-arsenide laser, a silicon p-i-n photodiode and electronic scanning has been established. However, terrain reflectivity requires further investigation. Should the dynamic range prove to be large, it may be necessary to control the output of the laser. Future work should include experimental studies on terrain reflectivity, the circuitry of the range finding system and the optics of the scanning system.

C.1.b. Discrete Obstacle Detection

Discrete obstacle detection, i.e. steps, boulders, mounds, craters, etc, by use of a split beam laser system has been investigated. The concept is based on a comparison of the return times of a split laser pulse emitted from unit at a fixed height and angle relative to the vehicle. The difference of the return time can be interpreted as a positive or a negative obstacle reliably as long as the beams intersect the terrain at the nominal range. A major drawback to this system is that pitching of the vehicle which causes the split beam to intersect the terrain at a shorter or longer distance than the nominal range leads to a misinterpretation of the terrain. It is concluded that additional data will be required for this type of a system to provide reliable obstacle detection data.

C.1.c. Obstacle Detection System

The obstacle detection system task represents an alternative approach towards an effective path selection system. In this case, a single beam laser range finder is attached at a fixed elevation angle to the mast of the vehicle. On scanning the terrain before the vehicle, range data are obtained and when combined with measurements of the deviation of the mast from local vertical can be used to calculate both the height of the terrain relative to horizontal and the apparent slope between the vehicle and the terrain point. One proposed decision rule is based on the exclusion of all paths involving excessive heights which are not preceded by an acceptable slope. A second rule involves selection of a minimum energy path from all acceptable paths. A range error analysis for a system using angular measurements as opposed to a stereo system relying on two sensors shows no advantage for the stereo system unless angle errors exceed 3^{o}.

C.1.d. Terrain Modeling

The terrain modeling task has been concerned with the reliability of the interpretation of terrain data in the range of approximately 30 meters. Using as a reference a known mathematical plane, some 1.5 by 1.0 meters in area, the error in estimating the in-path and cross-path slope due to range, azimuthal and elevation angle errors was

calculated for three, four and six point fits. In making these calculations, it was assumed that the range and angle errors are gaussian. On the basis of standard deviations for range of between 1 and 10 cm and for angles of between 0.001 and 0.005 radians, errors in the estimation of the in-path and cross-path slopes of between -1.2 and 16.6° were determined. These slope errors were found to increase linearly with angle error in the range from one to four milliradians and to reach a steady state value at the ten milliradian level. Six point fits were superior to four point fits which were superior to three point fits. Cross-path slope errors of three to five degrees were noted even with angle errors of one milliradian. A terrain modeling algorithm independent of angle measurements may prove superior.

C.2. Path Selection System Evaluation

The path selection system evaluation task is intended to provide a tool by which alternative terrain sensing, modeling, obstacle detection and path selection concepts can be simulated and evaluated. A computer simulation package has been developed for this purpose. The package was designed to provide a user with a high degree of flexibility. The real terrain desired can be specified by defining polynomial parameters for low frequency terrain characteristics, (gaussian features are to be added shortly), and special features such as boulders, crevasses, craters, etc. The user can specify his choices of specific terrain sensor, terrain modeler and path selection rule. Sensor errors and the effects of finite vehicle response can also be specified. The effect of high frequency disturbances on the vehicle, i.e. small rocks, etc., and the consequent measurement errors can be simulated.

Methods by which to evaluate alternative path selection systems both quantitatively and heuristically have been developed.

The computer package has been tested on two simple path selection systems and is operational.

Future work will include software implementation of the model display block, the addition of gaussian terrain features and the extension of the vehicle dynamics and attitude block. Efforts to improve and refine the evaluation criteria will be continued along with evaluation of alternative path selection systems which have been or will be proposed.

Task D. Chemical Analysis of Specimens

This task which is concerned with developing the fundamental concepts which will be required to optimize a gas chromatograph-mass spectrometer analysis system is divided into the following subtasks: mass spectrometer characteristics, carrier gas generation and removal, chromatograph model evaluation, chromatograph model improvement and estimation of chromatograph model parameters.

D.1. Mass Spectrometer Characteristics and Carrier Gas Generation and Removal

Prior work in small mass spectrometers has been reviewed and analyzed to obtain the quantitative relationships between mass-range

and resolution as functions of the magnetic and electrical fields, scan rate and scan method, effect of operating pressure on performance, and power, weight and volume requirements as controlled by system parameters. Mathematical modeling of these gross characteristics has been initiated and major model equations suitable for component (mass spectrometer) and system (GC/MS) simulation are expected by September 1972.

The carrier gas generation and removal studies are intended to identify the basic characteristics and limitations of the more promising concepts to provide support for the final system design. Principal emphasis has been directed to the gas generation problem and specifically to a high pressure gas storage concept which would be suitable for short duration or low frequency analysis missions. Storage vessel volume and weight requirements as a function of charge pressure and anticipated operating time have been determined. Although a review of methods of carrier gas removal has been completed, alternative systems have not yet received a quantitative evaluation.

D.2. Chromatographic Model Evaluation Using Multicomponent Systems

This task is intended to verify experimentally the mathematical chromatograph model using superposition of single component data. The test facility was modified to provide more accurate carrier gas flow and pressure data. The mathematical model was updated to reflect more reliable Peclet number data. Initial studies involving n-pentane/n-heptane indicate that the superposition principle applies only approximately in a first order sense with the actual data lagging the predicted results. It is intended to extend these studies to other packing materials and other multicomponent systems.

D.3. Chromatograph Model Improvement

The objective of this task is to improve the model being evaluated under D.2. Extension of the present model from the equilibrium assumption to the non-equilibrium case (finite column length) does not improve significantly the fit between theory and experiment. Of the single component studies, acetone was best fitted while ethylene was most poorly fitted. It is believed that intraparticle diffusion in which constituents may transport into the bulk of the packing material as opposed to adsorbing on the particle surface may be responsible for the lack of agreement between theory and experiment. Work is underway to develop a theoretical model incorporating intraparticle diffusion.

D.4. Transport Parameter Estimation

The chromatograph model requires knowledge of the transport parameters: Peclet number and the number of transfer units. Analysis of literature data and correlations have resulted in correlations which appear to be adequate for the requirements of this project. Apart from developing estimates of the reliability of these results and preparing a technical report, this task is essentially completed.

IV. Detailed Summaries of Progress

Task A. Vehicle Configuration, Control, Dynamics, Systems and Propulsion

This broad task is concerned with all aspects of the design of a roving vehicle for Mars exploration. Included within this major effort are the following subtasks: vehicle model design, mathematical model of the vehicle dynamics, experimental dynamic analysis, obstacle negotiation, electromechanical control systems, collapsibility and deployment, wheel testing apparatus, wheel analysis, and payload design.

Progress made in these areas during the past interval is summarized in the sections which follow.

A.1.a. Vehicle Model Design - Mark C. Rodamaker
Faculty Advisor: Prof. G. N. Sandor

The first operational model of the RPI MRV, Figure 1, was built to 0.184 scale for reasons of dynamic analysis and ease of construction. Dynamic testing of this first generation model pointed out areas where redesign was required. Changes and alterations to this first model led to a second generation model, Figure 2, incorporating the torsion bar rear suspension. Dynamic testing of this second-generation model has pointed out problem areas requiring additional design considerations. The additional design and testing work will require a larger, more refined model. Problems of excessive motor size and weight as well as the modeling of torsion bar spring rate for the 0.184 model also demand a larger model for more refined testing.

The next operational model of the RPI MRV should include the vehicle refinements to date, incorporate the collapsibility scheme and payload, and scaled so the motors are not grossly out of proportion as they are on the 0.184 model. The design of the RPI MRV is stabilized, so ease of making large changes is not a critical consideration. These factors indicate the need for an operational model which is larger than the 0.184 model presently being used.

Physical Model

Consideration of new performance requirements including collapsibility and payload isolation resulted in significant design changes. The original transverse-mounted rear suspension proved very difficult to collapse in a simple manner and the rigid angular coupling between the payload and the suspension did not provide good payload isolation. To overcome these problems, a transverse mounted torsion bar with longitudinal suspension arms was installed. As shown in Figure 2, a motor is attached to the center of the torsion bar which is used to adjust the nominal position of the suspension. The vehicle's payload may thus be raised or lowered depending on the terrain and the vehicle's needs at any time, proximity to the ground for soil sampling or stability and elevated position for a laser "look around".

A modified tilt-back maneuver, renamed the shift-back, is possible in which the payload is lowered to the ground, but the suspension motor continues to drive the suspension arms in the same direction until the rear wheels contact the ground ahead of the torsion bar. At this point,

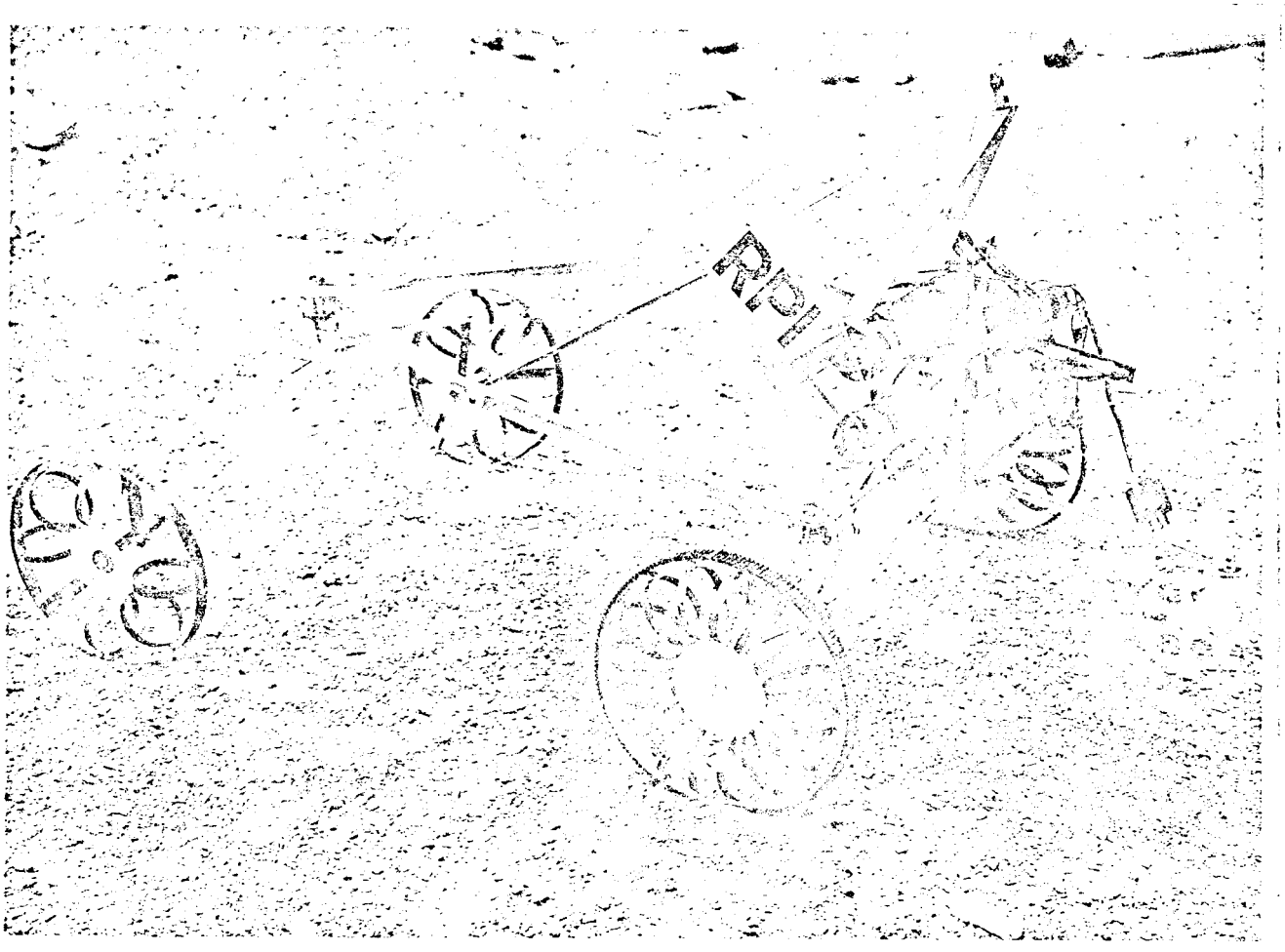

Figure 1 Original 0.184 Scale Model

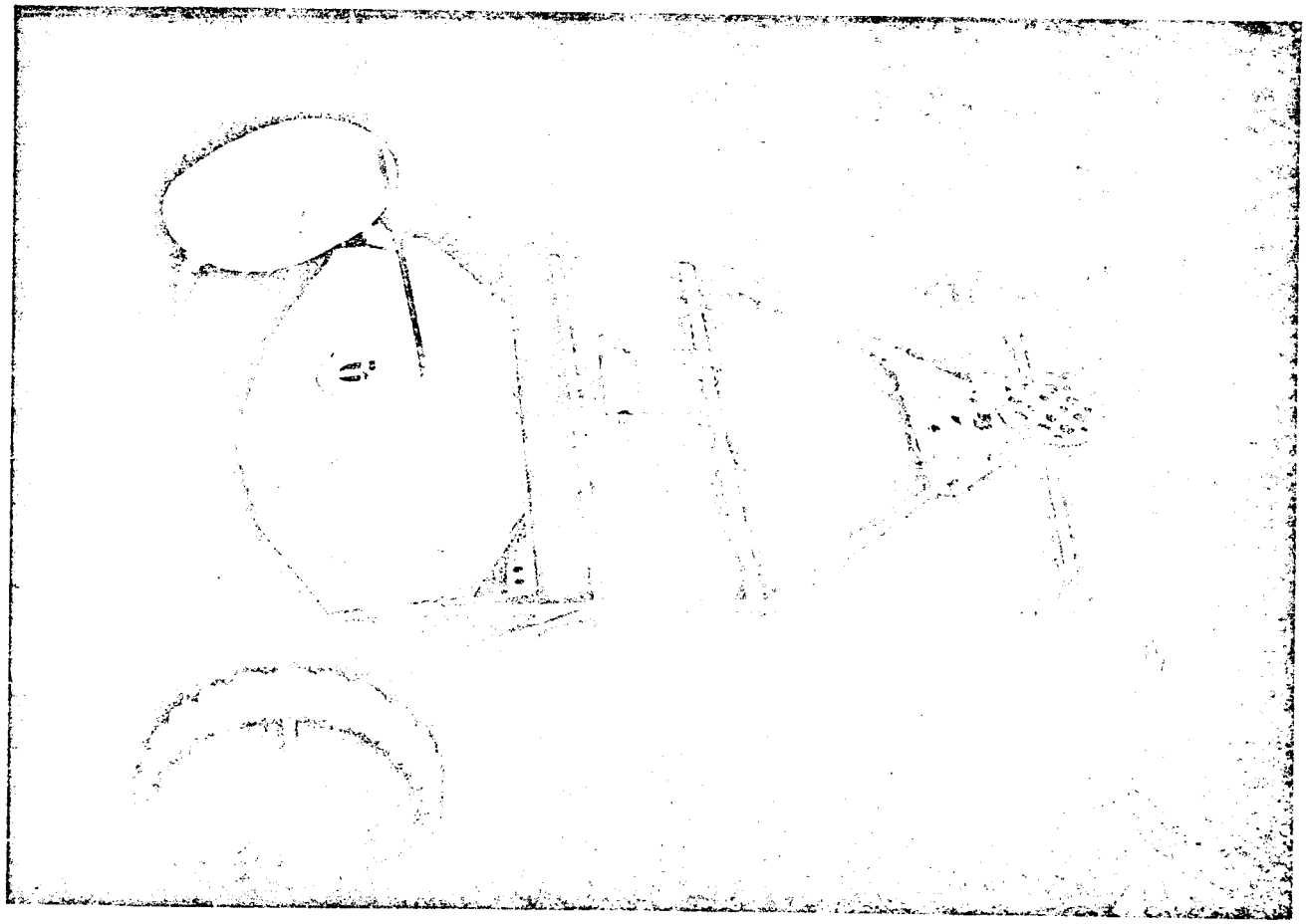

Figure 2 Revised 0.184 Scale Model

the torsion bar motor may lift the front wheels off the ground. In this mode, the payload may be pushed backwards by the drive motors. Return to the 4-wheel mode is accomplished by reversing the previous sequence. This maneuver could also be used to unstick the rear wheels should they become bogged down in sand or otherwise immobilized. The roving capabilities of the modified MRV in the shifted-back mode are not as good as the previous vehicle's capability in its tilted-back mode, but the ability to extricate rear as well as front wheels from "bog-downs" and the greatly increased stability should make the shift-back more useful than the previous tilt-back maneuver.

In order to provide better similarity between a full-sized vehicle and the .184 scale model and also to improve payload isolation, the steering has been moved to the steering axis and the drive motors have been placed in the wheel hubs thus reducing the inertia of the payload section and also sparing the levelizing system from having to counteract the torques from the control motors.

By June, 1972 dynamic tests of the RPI MRV were concluded. It was decided that a larger model would be desirable for further tests and for better scaling of the structural members. Three possible alternatives were considered:

1. Build a .4 model for compatibility with the the .4 scale wheel tester;
2. Build a full scale model;
3. Build a full size model at a later date with the benefit of experience with the .4 model.

A feasibility analysis of the three alternatives was made. This analysis compared the three models by listing several categories which might influence the building of one model or another and each category was given a degree of importance as to how much it would affect the building of a model. Then a relative merit factor was given to each of the three models in each of the categories to compare within the category the effect that category would have on the building of a certain model. The importance factor was then multiplied by each of the relative merit factors to give each model in each category a cumulative comparison number. For example: the man-hours to build a .4 model now would be a good deal less than the full scale models due to the difference in size of the material used, and the building of a full scale model would be better in the future due to the increase in manpower available during the school year. These factors might give relative merit factors at 8 for the .4 scale model, of 2 for the full scale model now, and of 3 for the full scale model in the future. Also, an importance factor at 3 might be given for the manpower category. This would give cumulative comparison numbers of $8 \times 3 = 24$ for the .4 scale model, $2 \times 3 = 6$ for full model now, and $3 \times 3 = 9$ of full model in the future in the category of man-hours to build. Other aspects of consideration entering into the decision making process were: cost, stability of rover design, functional capabilities, material availability, production difficulties, storage,

transportability, demonstrability, test practicality and accuracy of test results, and power requirements.

The cumulative comparison number for all of the categories were added for each of the three models and this gave a feasibility factor for each of the models. The largest feasibility factor corresponds to the most feasible model.

Three of the lists were filled out by project personnel (J. Almstead, W. Embleton, M. Rodamaker) to encompass all significant design parameters. From these reports an average was made of the feasibility factors and it was found that the .4 model would be the most feasible.

With this decided, planning began on a .4 scale model of the MRV. The weight for the .4 scale model was calculated using linear scaling based on a 1170 lb full-size vehicle, Ref. 1.

A structural analysis was performed to find the allowable size of the structural members for assuming maximum deflection in each member. The weight used in this analysis was twice the .4 model weight to allow for dynamic loadings. This produced an allowable area moment of inertia and from this, beam dimensions could be calculated for the structural members. A half-scale drawing of the .4 model was made, Figure 3, and the material was ordered for its production.

The new design of the MRV to be built at a .4 scale has a 6' x 5' x 1½' payload size. The platform stabilizing motor is located outside of the payload. The torsion bar now runs through a pipe and the pipe, which is driven by the platform stabilizing motor off the payload, drives the torsion bar at its middle through a pin connection. Collapsibility features will be included in the design.

Work is now being done on designing the hinges of the collapsibility scheme. Also work has begun on wheel construction. An empirical formula relating force deflection characteristics to wheel dimensions is being sought to allow proper wheel dimensions to be found easily. The .4 scale model should be completed by the middle of August, 1972.

A.1.b. Mathematical Model of Dynamic System - M.C. Rodamaker
Faculty Advisor: Prof. G. N. Sandor

Two methods of analysis involving energy techniques were applied to the mathematical model, Figure 4, this past year. One utilized an input force as an excitation while in the other a displacement was specified. The latter was considered more realistic since a vehicle normally experiences terrain inputs which can best be modeled as displacements. The differential equations of motion for the second analysis are shown in Table 1. Damping of the torsion bar has been added for stability and to more closely simulate the physical model. These equations have been programmed on an analog computer with the following parameters inserted which were measured from the .184 scale model, Table 2.

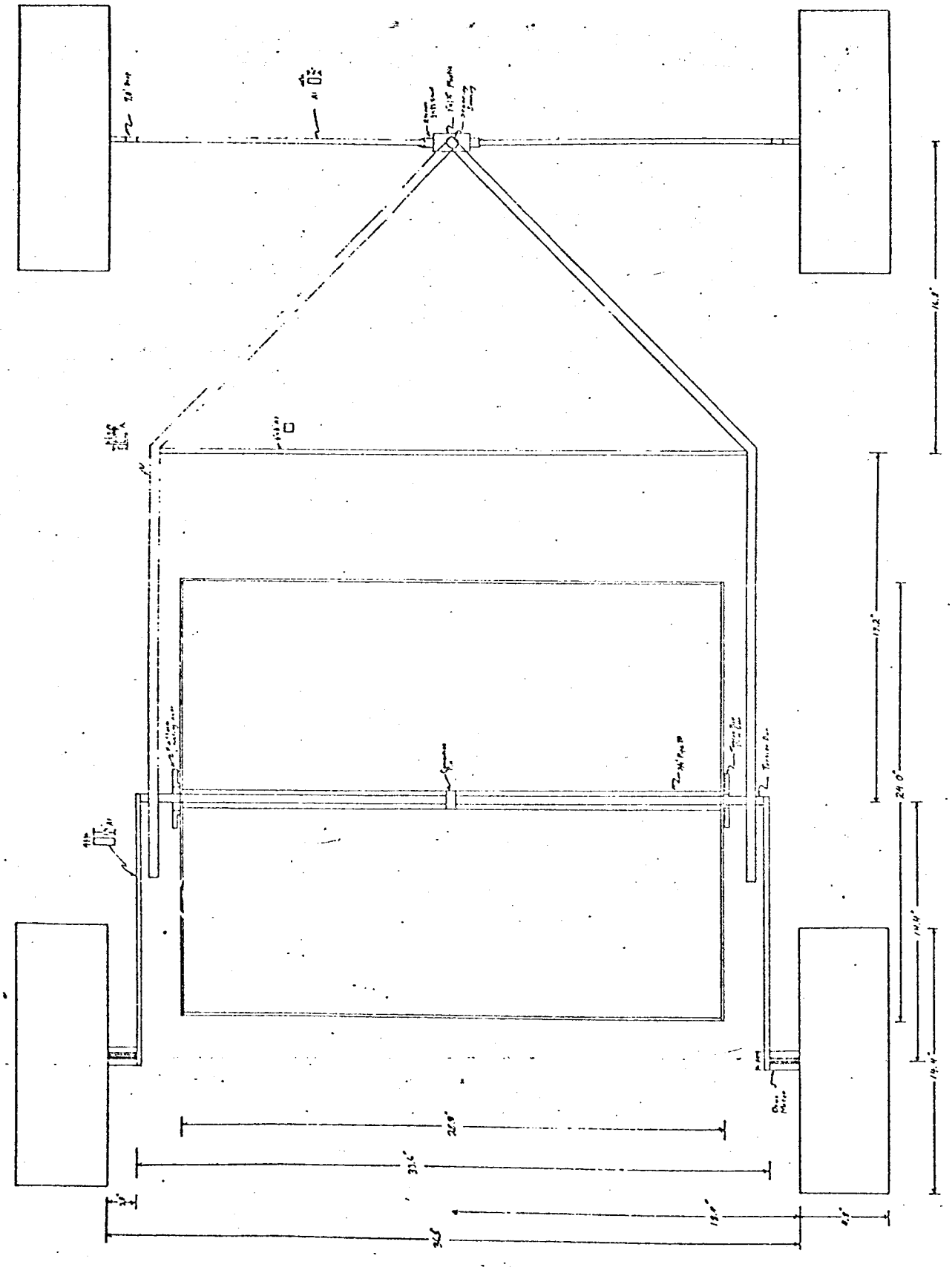

Figure 3. 0.4 Model Scale Drawing

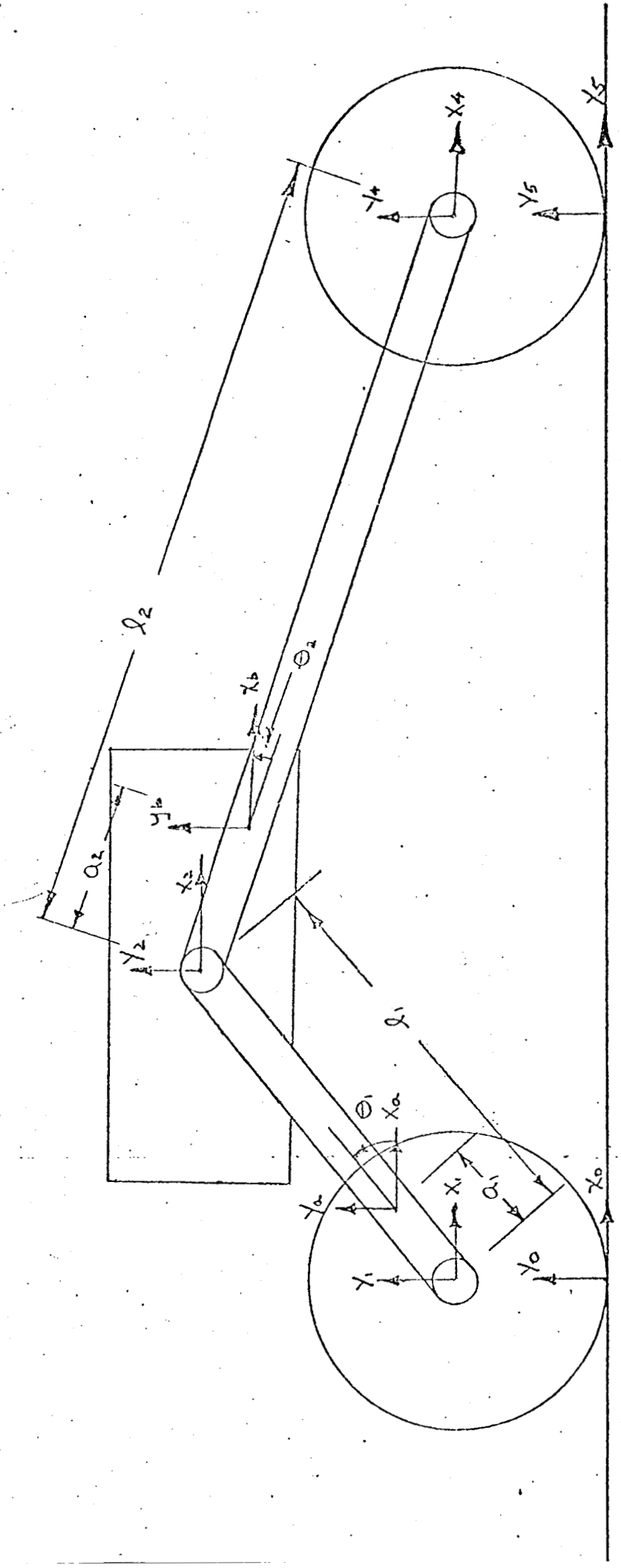

Figure 4. Mathematical Model of MRV

Table 1

$$m_r \ddot{y}_0 + K_{\omega r}(y_0 - y_1) = 0$$

$$m_a \ddot{y}_1 + m_a a_1 \cos\theta_1 \ddot{\theta}_1 + K_{\omega r}(y_1 - y_0) = 0$$

$$(2m_r + m_a)\ddot{X}_1 - m_a a_1 \sin\theta_1 \ddot{\theta}_1 + \frac{K_{\omega t}}{R^2}(X_1 - R\Delta\theta_1) = 0$$

$$m_2(\ddot{y}_2 - a_2 \cos\theta_2 \ddot{\theta}_2) + K_{\omega f}(y_2 + \ell_2 \cos\theta_2 \Delta\theta_2 - y_5)$$

$$m_r \ddot{y}_5 - K_{\omega f}(y_2 + \ell_2 \cos\theta_2 \Delta\theta_2 - y_5) = 0$$

$$I_2 \ddot{\theta}_2 + K_{\omega f}(y_2 + \ell_2 \cos\theta_2 \Delta\theta_2 - y_5)(a_2 + \ell_2)\cos\theta_2 + K_t(\Delta\theta_2 - \Delta\theta_1) = 0$$

$$\left(I + \frac{2m_r m_a a_1^2 \sin^2 Q_1}{2m_r + m_a}\right)\ddot{\theta}_1 + K_{\omega r} a_1 \sin\theta_1 y_1 - K_{\omega r} a_1 \sin\theta_1 y_0 + \left(\frac{2m_r}{2m_r + m_a} a_1 \sin\theta_1 \frac{K_{\omega t}}{R} - \frac{K_{\omega t}}{R} a_1 \sin\theta_1 + K_{\omega t} + K_t\right)\Delta\theta_1 + \left(\frac{K_{\omega t}}{R^2} a_1 \sin\theta_1 - \frac{2m_r}{2m_r + m_a} a_1 \sin\theta_1 \frac{K_{\omega t}}{R^2} - \frac{K_{\omega t}}{R}\right) X_1 - K_t \Delta\theta_2 = 0$$

where y_0 and y_5 are the input displacements.

Table 2

m_r = .0007 slug

$I_r = m_r R^2$ = .00856 in-lb-sec^2

m_a = .0375 slug

I_a = .0310 in-lb-sec^2

m_2 = .116 slug

I_b = 1.458 in-lb-sec^2

I_1 = .0318 in-lb-sec^2

I_2 = 4.058 in-lb-sec^2

$K_{\omega t}$ = 63.5 in-lb/rad

$K_{\omega r}$ = 2.94 lb/in

$K_{\omega f}$ = 1.572 lb/in

K_t = 425 in-lb/rad

R = 3.5 in

ℓ_1 = 9 in

ℓ_2 = 14.5 in

a_1 = .46 in

a_2 = -1.50 in

Response curves, Figures 5 and 6, indicate that a high frequency transient appears, which damps out quickly, but a lower frequency oscillation remains for an unacceptably long time. The lower frequency resonance has been identified as a rear wheel resonance. The high frequency transient is due to the torsion bar system. It is hoped that only one damping unit will be necessary and it would be easier to damp the torsion bar than the wheels. In order for the entire system to be damped, the damped unit must have a lower natural frequency than the other spring-mass systems.

To verify the ineffectiveness of the damped torsion bar system, cross-plots of θ_1 vs θ_2 were made for initial condition and step inputs, Figures 7 and 8. It is clear that the system is effective for only 2 or 3 cycles after which θ_1 and θ_2 rotate in-phase with their difference being very small. To increase this effectiveness, the natural frequency of the torsion bar system should be reduced and the wheel resonance raised so that the torsion bar resonance occurs at a lower frequency than the wheel resonance. This corresponds to employing a softer torsion bar and stiffer wheels. These alterations will be made on the analog model as well as the new .4 scale model.

A.1.c. Dynamic Analysis - W. Cobb
Faculty Advisor: Prof. G.N.Sandor

The previous .184 scale model had undergone dynamic tests during the summer of 1971. An electromagnetic shaker system was used to excite the rear wheels and displacements of various vehicle components were measured using a blurred-image photographic technique. It soon became clear that angulation of the payload section was a serious problem. The rear suspension system which was causing the difficulties was also proving difficult from a collapsibility viewpoint so a new torsion bar suspension system was installed. The resulting vehicle was sufficiently different from the original vehicle that new and more thorough dynamic tests were deemed necessary.

For these tests which are described in detail in Ref. 2, a shaker system similar to that used previously was employed with either an optical tracker or a capacitance displacement device for displacement measurements. Data was recorded onto an F.M. tape deck and replayed at a slower than recorded speed to minimize X-Y recorder errors. A typical Bode Plot is shown in Figure 9. Plots taken for other variables always resulted in similar plots with peaks around 3.7 Hz and 7½ to 9 Hz. The 3.7 Hz resonance has been identified as a rear wheel resonance which is very lightly damped. The higher frequency peak is due to the torsion bar suspension system. A torsion bar damper is planned for next year's vehicle to improve overall vehicle damping. The torsion bar will clearly have to be softened if it is to absorb the wheel resonance.

Transient response measurements were also made. Figure 10 shows a typical trace for a step input to the body section. The output is almost purely 3.7 Hz or wheel resonance frequency. The damping is small ($\xi \sim .03$). Around 6 seconds, coupling or beating is observed, but this is most probably side to side coupling due to slightly

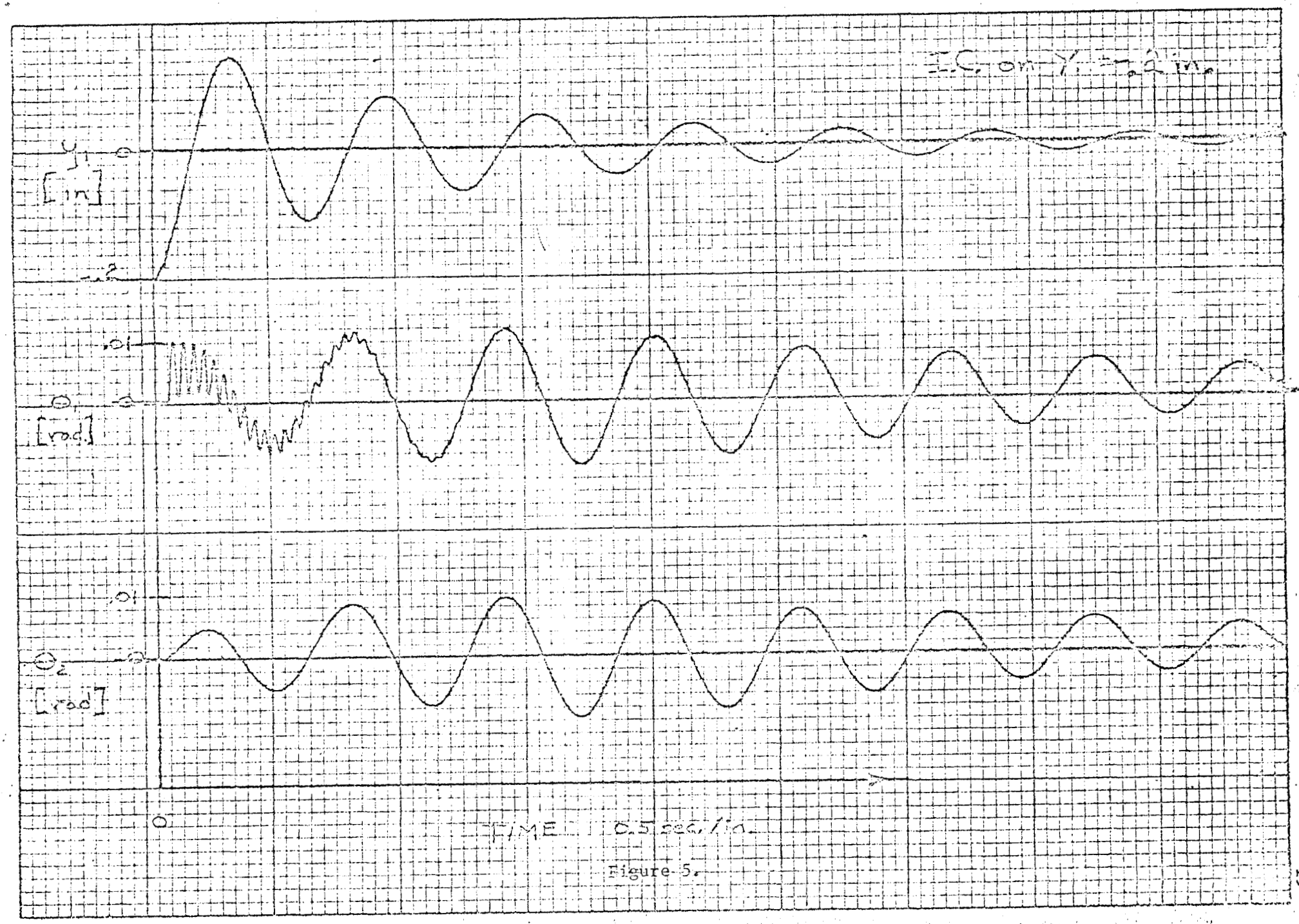

Figure 5.

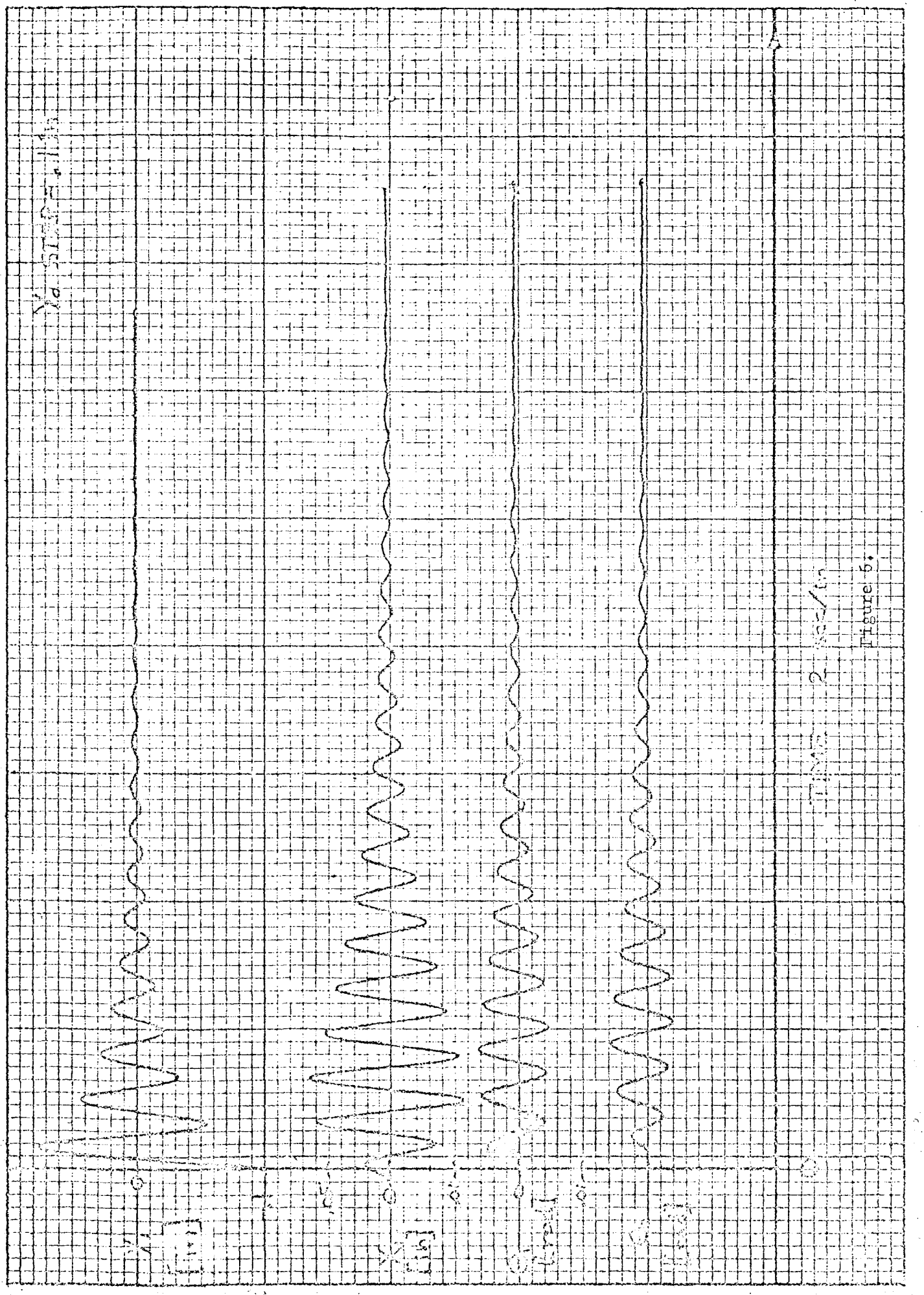

Figure 6.

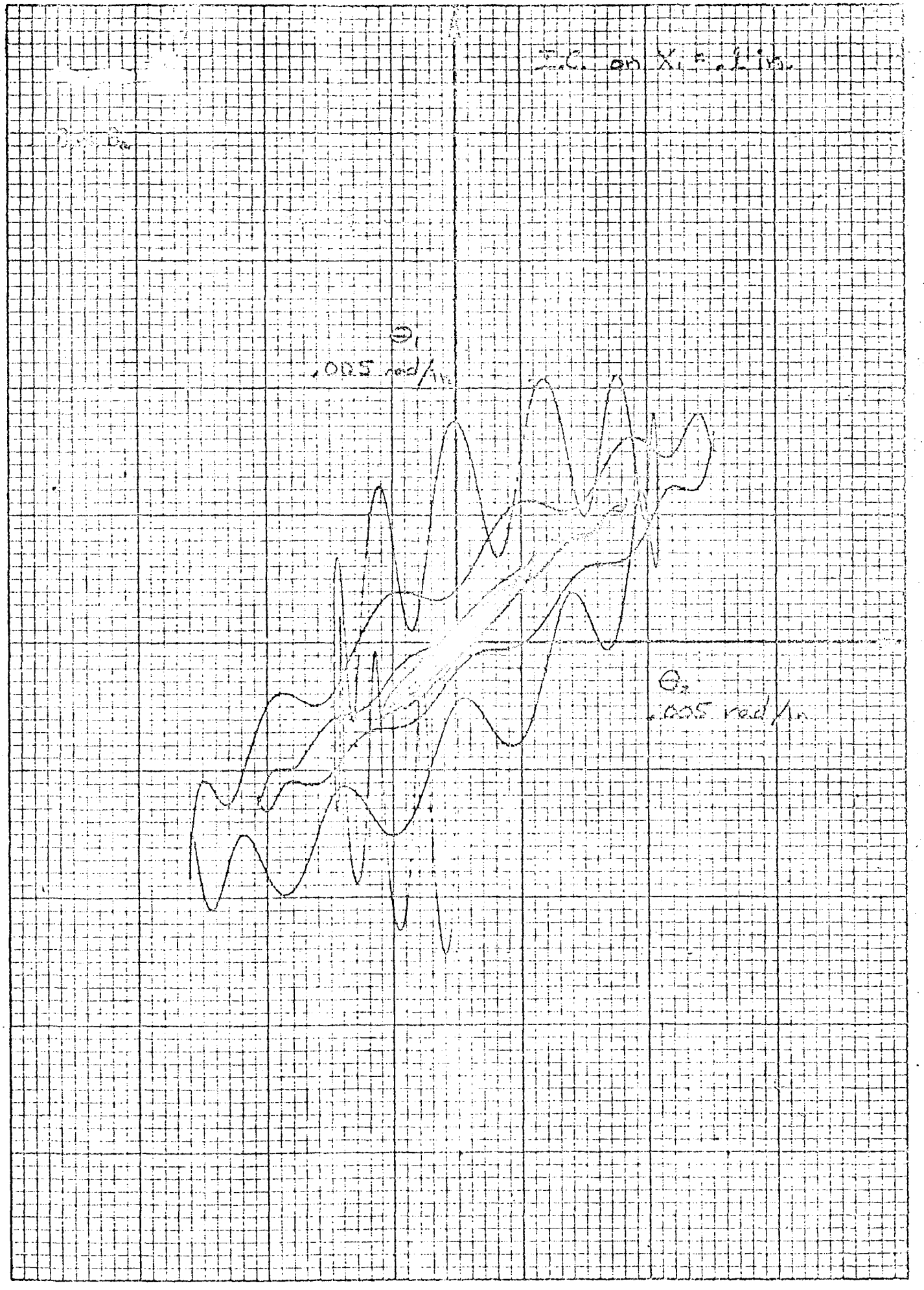

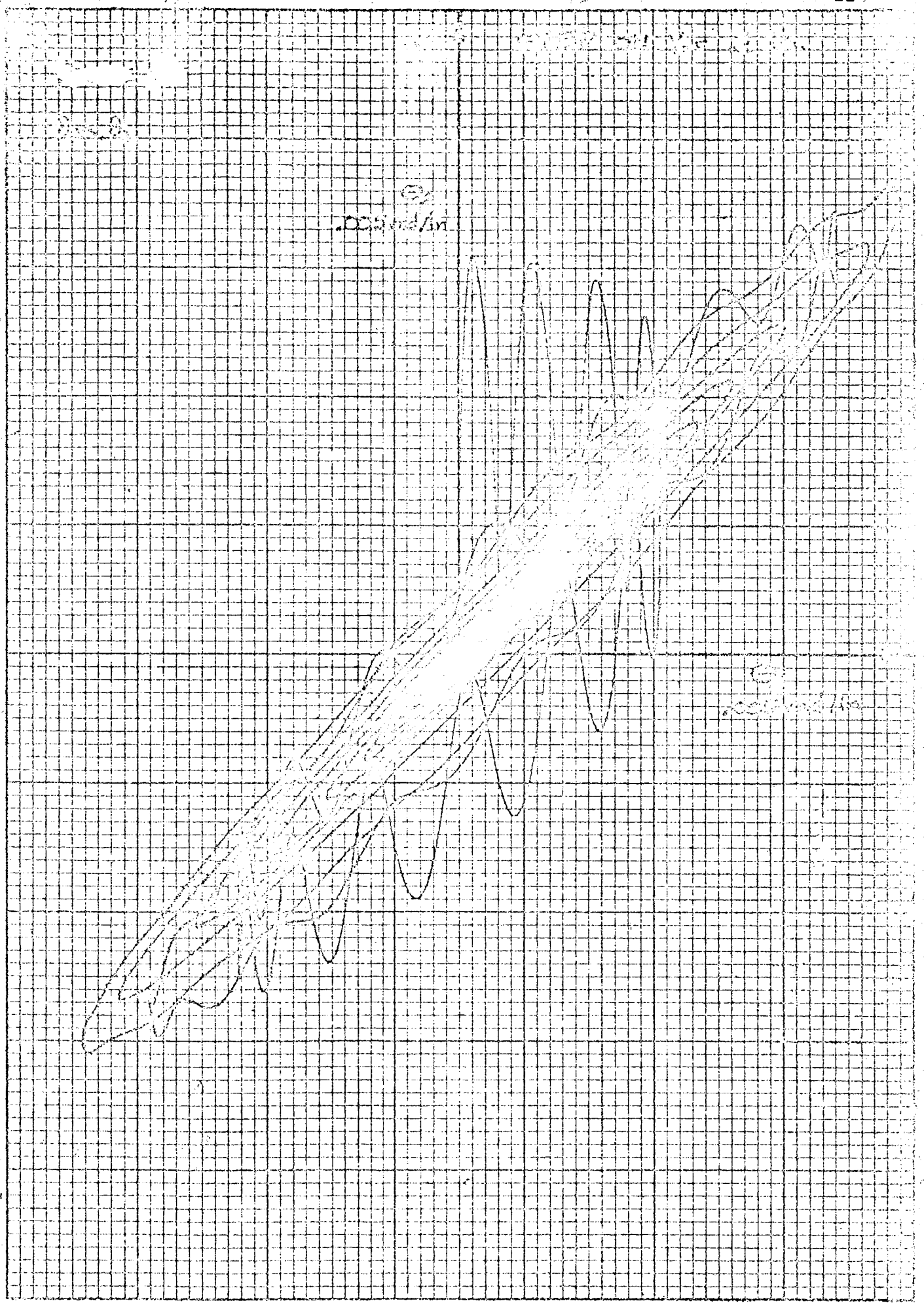

Figure 8.

FIGURE 9. VERTICAL RESPONSE OF FRONT SECTION TO REAR WHEEL INPUT . SHAKER AMPLITUDE = .01 INCH PEAK TO PEAK .

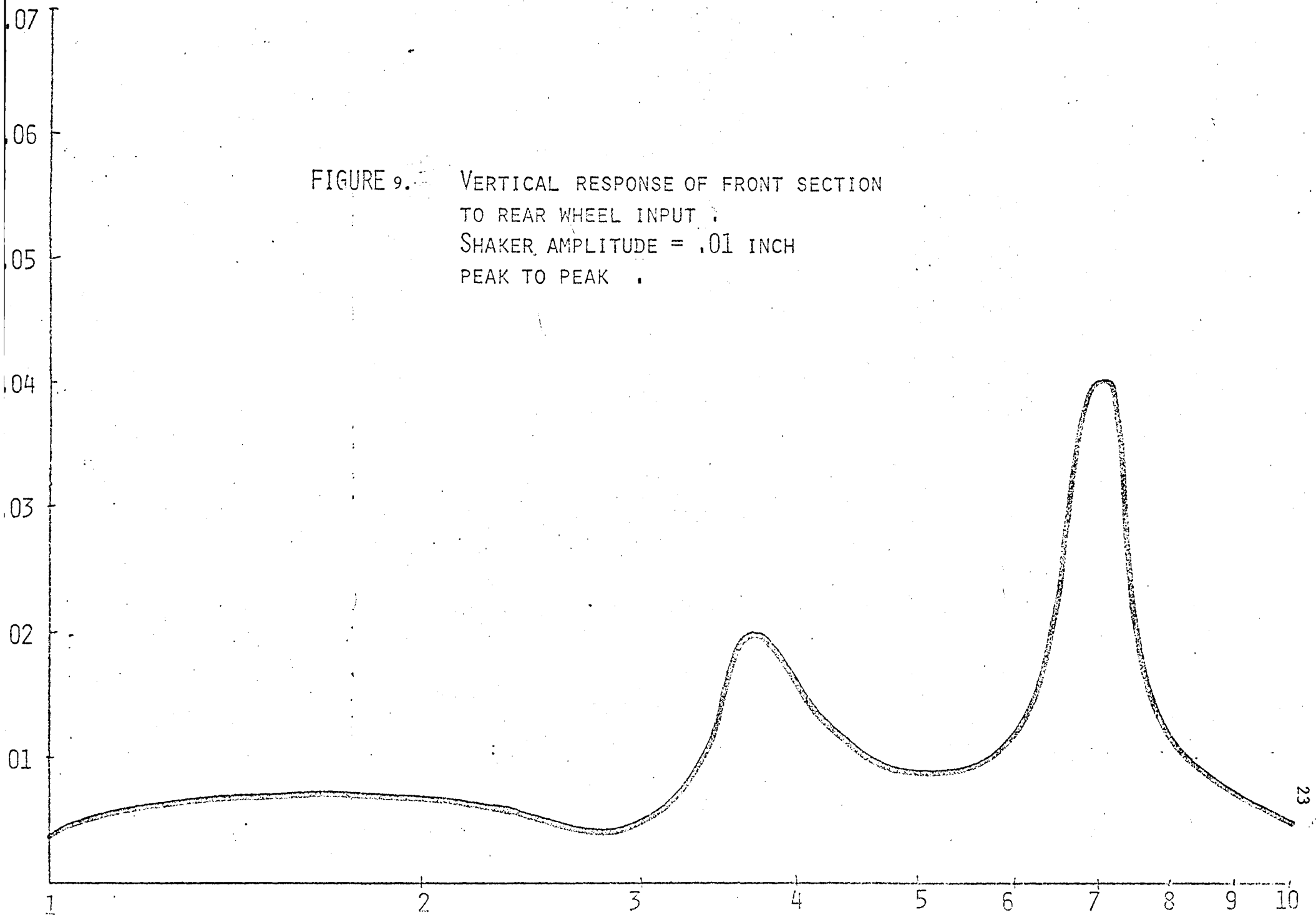

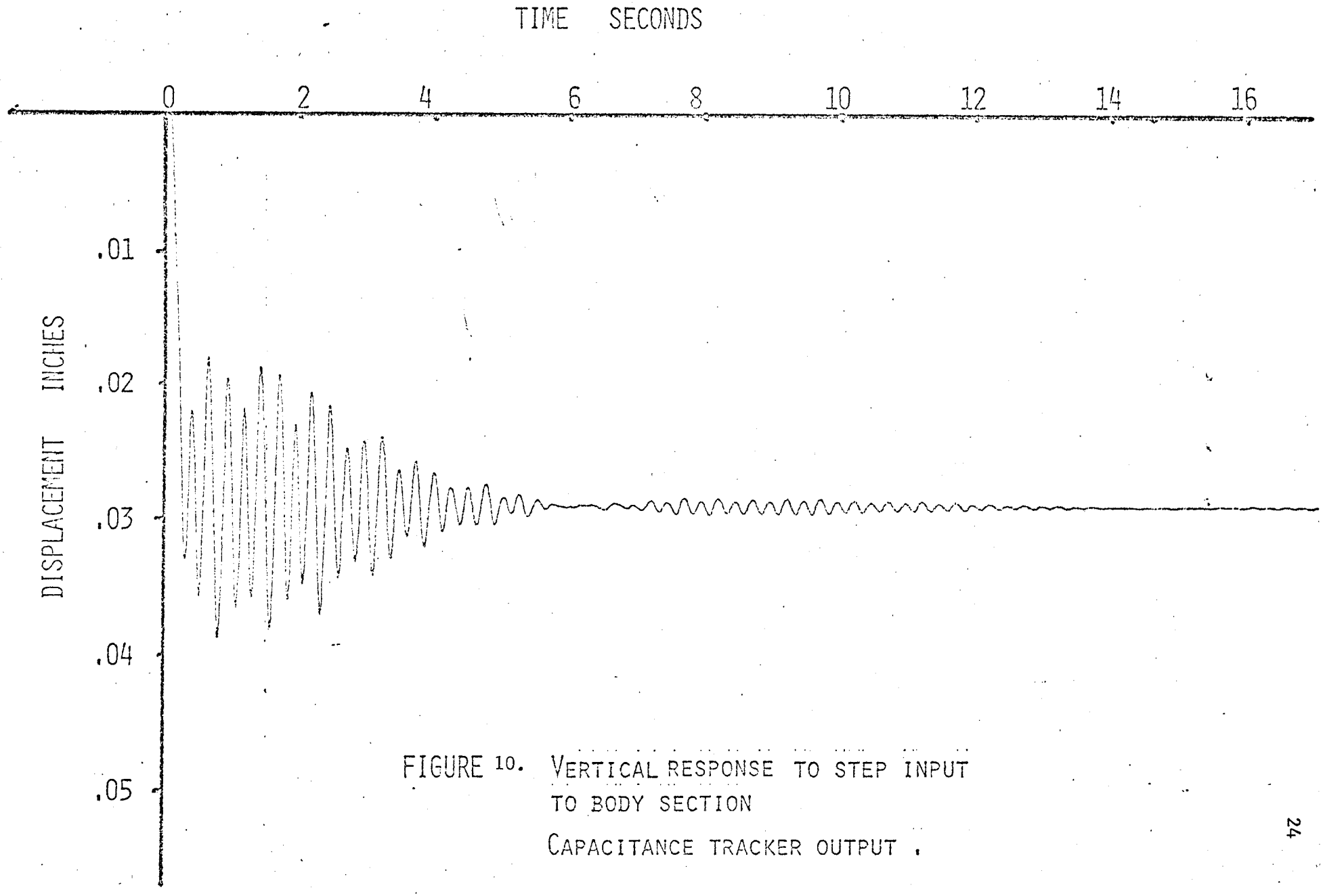

FIGURE 10. VERTICAL RESPONSE TO STEP INPUT TO BODY SECTION

CAPACITANCE TRACKER OUTPUT .

imperfect symmetry of the rear wheel spring rates and vehicle weight distribution. If this coupling is dismissed, very good verification of the mathematical simulation results. Regardless, a torsion bar damper as well as altered vehicle spring rates are necessary in order to provide the exceptional dynamic behavior possible with the present vehicle.

A.1.d. Obstacle Negotiation - A.F. Steinbock
Faculty Advisor: Prof. G.N. Sandor

Many tools for determining limiting values of obstacle negotiation capabilities have been developed and refined during this past year, Ref. 3. All tools have been developed in general form so that they are useful in vehicle optimization and also in comparison between competing designs.

Computer programs have been developed which calculate rear wheel torque and coefficient of friction required to traverse step, crevasse and slope obstacles. Using these programs, it is easy to determine whether traction (wheel and cleat design), drive motor torque or vehicle geometrical factors are the limiting parameters in obstacle negotiation. Results from these programs are shown on Figures 11, 12, and 13 for a full-size RPI MRV.

One cause of vehicle failure in obstacle negotiation seldom considered is vehicle hang-up. This occurs when the terrain contacts the vehicle body. In some cases, vehicles are unable to free themselves and the mission is ended. Clearly, when traveling on level ground, any obstacle as high as the undercarriage may cause hang-up, but a better method of rating this behavior exists. Specifically, any vehicle traversing a ridge or two-plane obstacle as shown in Figures 14a and 14b will contact the ridge if the angle of the ridge is large (sharp) enough. From the definition of β (the hang-up angle) a large β capability is clearly desirable. The method of analysis employs geometrical relationships derived by rotating the obstacle through a stationary vehicle as in Figures 14a and 14b. Data derived from this method is given in graphical form in Figures 15 and 16.

At present, only obvious conclusions have been drawn from these results. In all cases, larger wheels are advantageous. Higher ground clearance is desirable, but a higher c.g. accompanies this parameter which lessens stability so a trade-off area as longer vehicles perform better on obstacles in general except that their hang-up behavior is not so good. In all cases, the RPI MRV is expected to excel due to the variable ground clearance and configuration associated with the torsion bar system. Very few trade-offs will be necessary allowing optimal performance in many areas.

In the coming year, these tools will be used to finalize the dimensions of the RPI MRV as well as size the motors and determine cleat requirements. These parameters will be set so as to outperform competing designs in as many areas as possible.

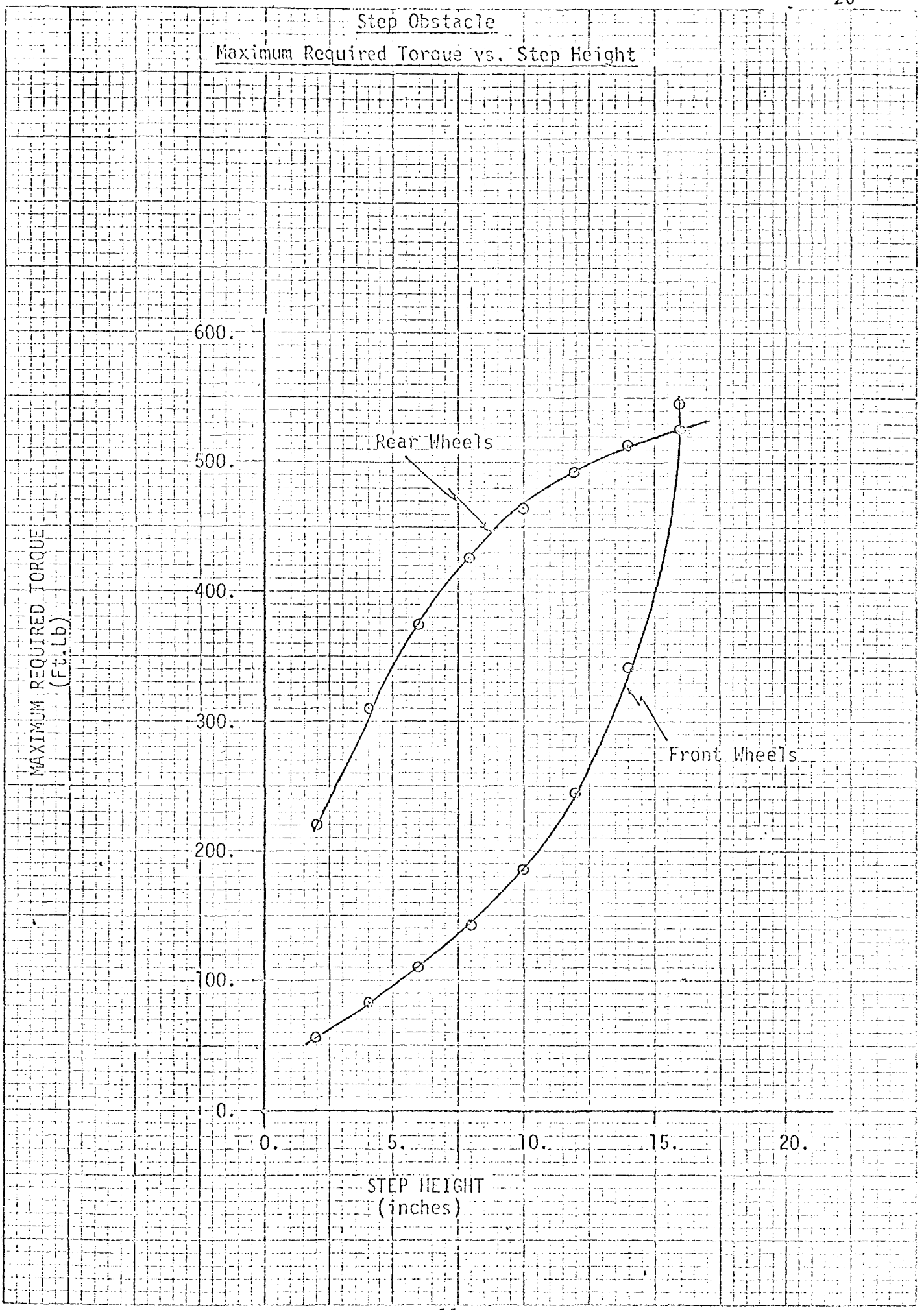
Step Obstacle
Maximum Required Torque vs. Step Height
MAXIMUM REQUIRED TORQUE (Ft.Lb)
600.
500.
400.
300.
200.
100.
0.
Rear Wheels
Front Wheels
0.
5.
10.
15.
20.
STEP HEIGHT (inches)

FIGURE 11.

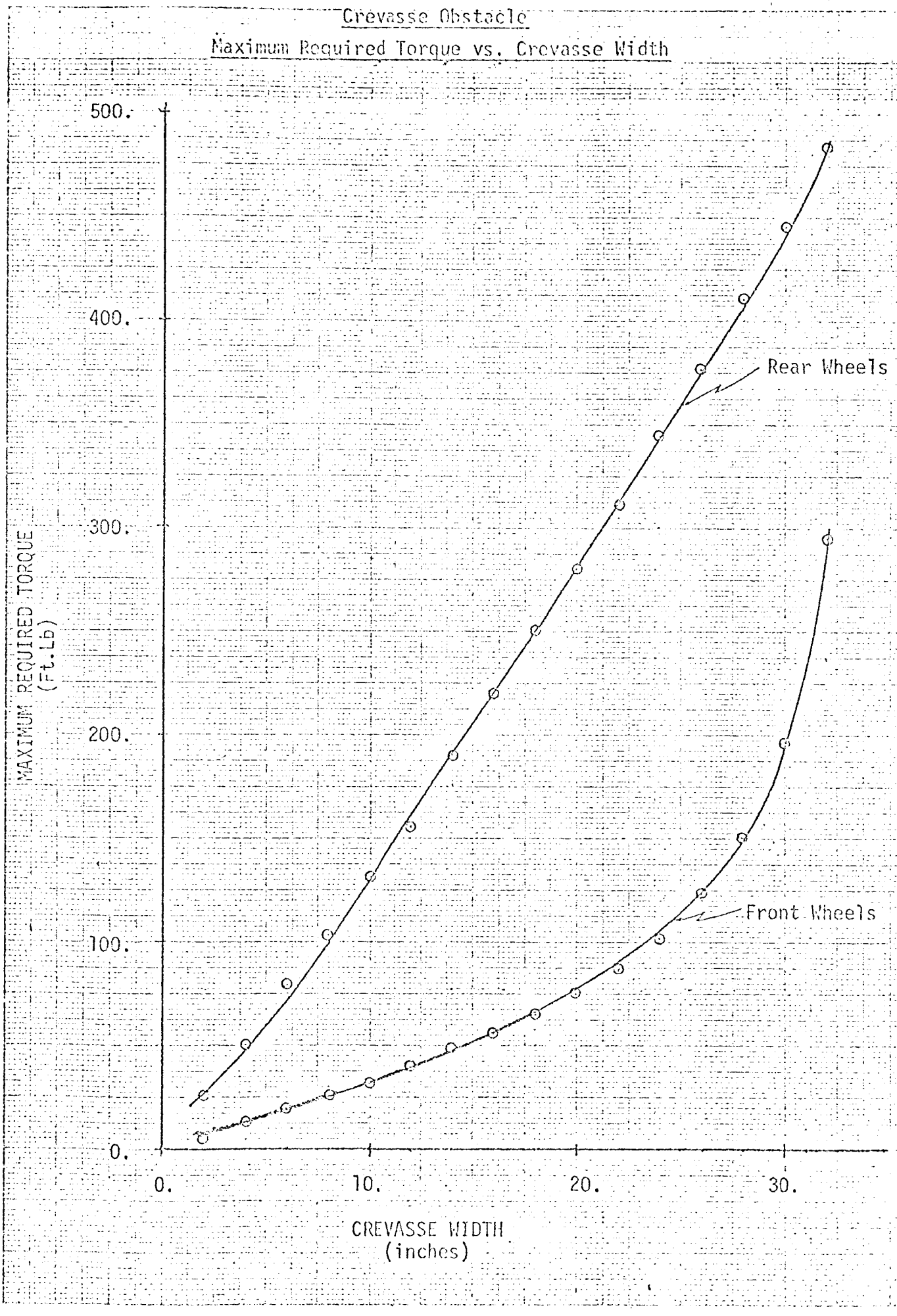
Crevasse Obstacle
Maximum Required Torque vs. Crevasse Width
500.
400.
300.
200.
100.
0.
MAXIMUM REQUIRED TORQUE
(Ft.Lb)
Rear Wheels
Front Wheels
0.
10.
20.
30.
CREVASSE WIDTH
(inches)

Figure 12.

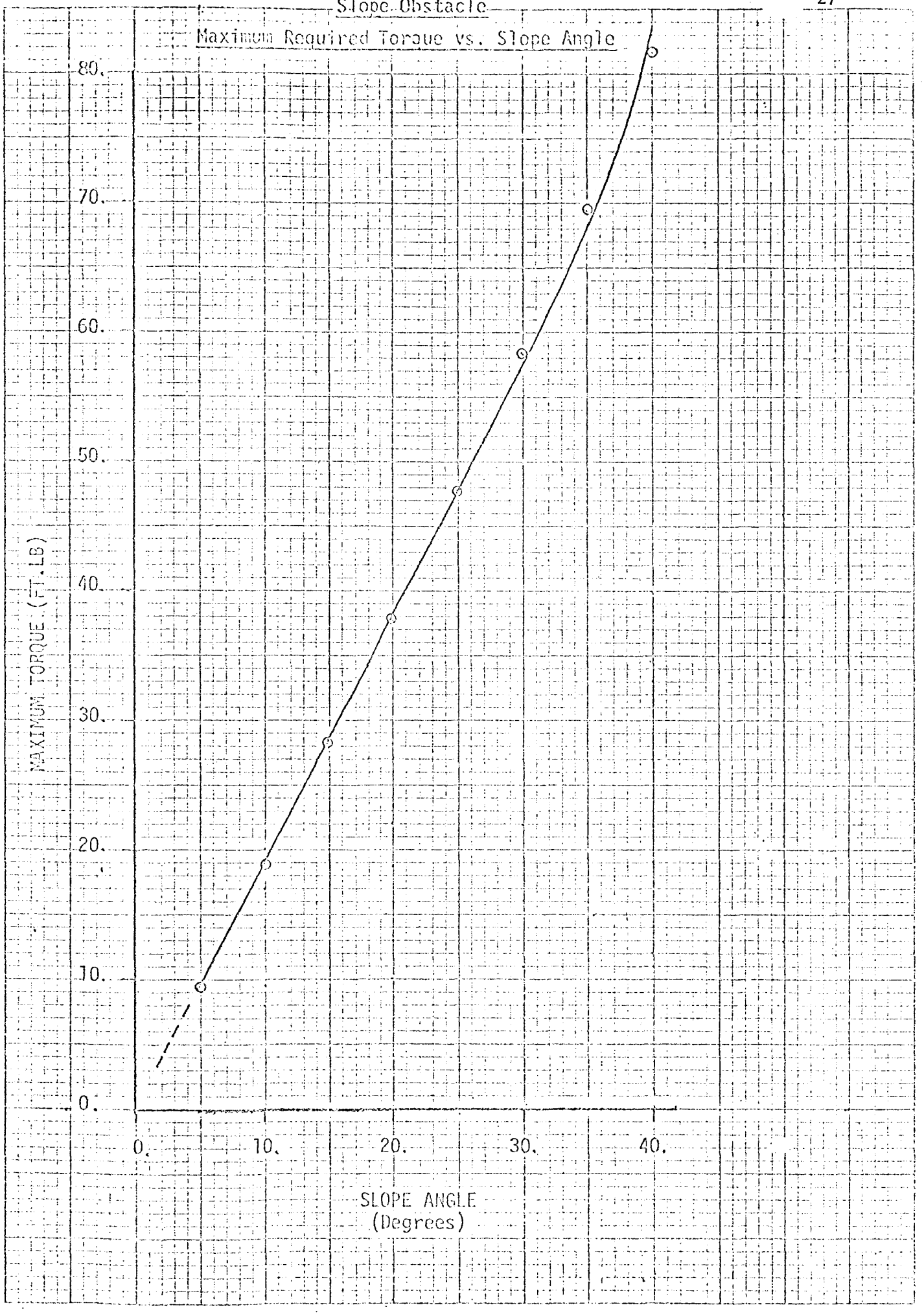

10 Squares to the Inch

Figure 13.

LONGITUDINAL TWO-PLANE OBSTACLE NEGOTIATION

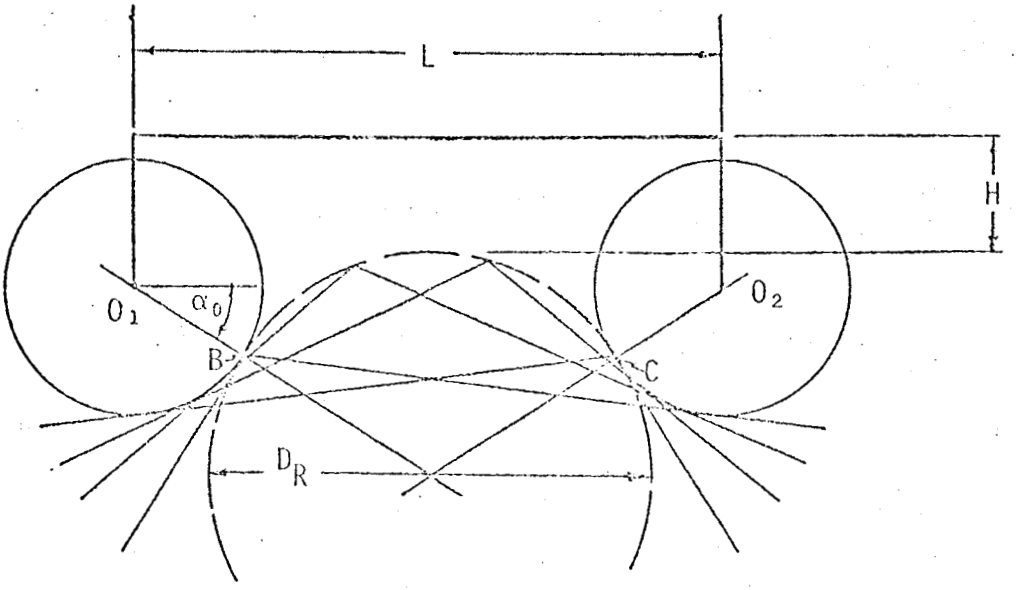

Figure 14a.

TRANSVERSE TWO-PLANE OBSTACLE NEGOTIATION

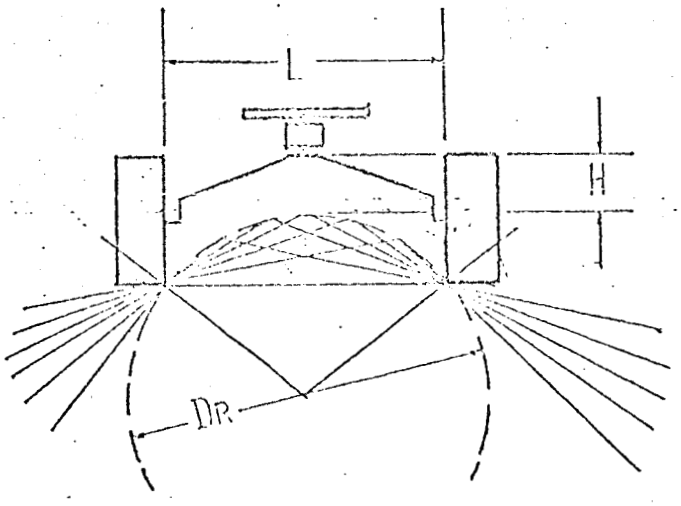

Figure 14b.

Part A. The Longitudinal Case

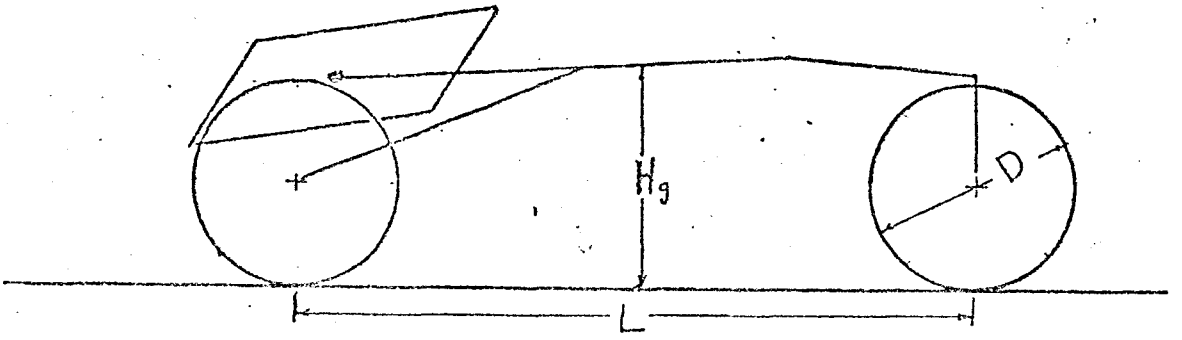

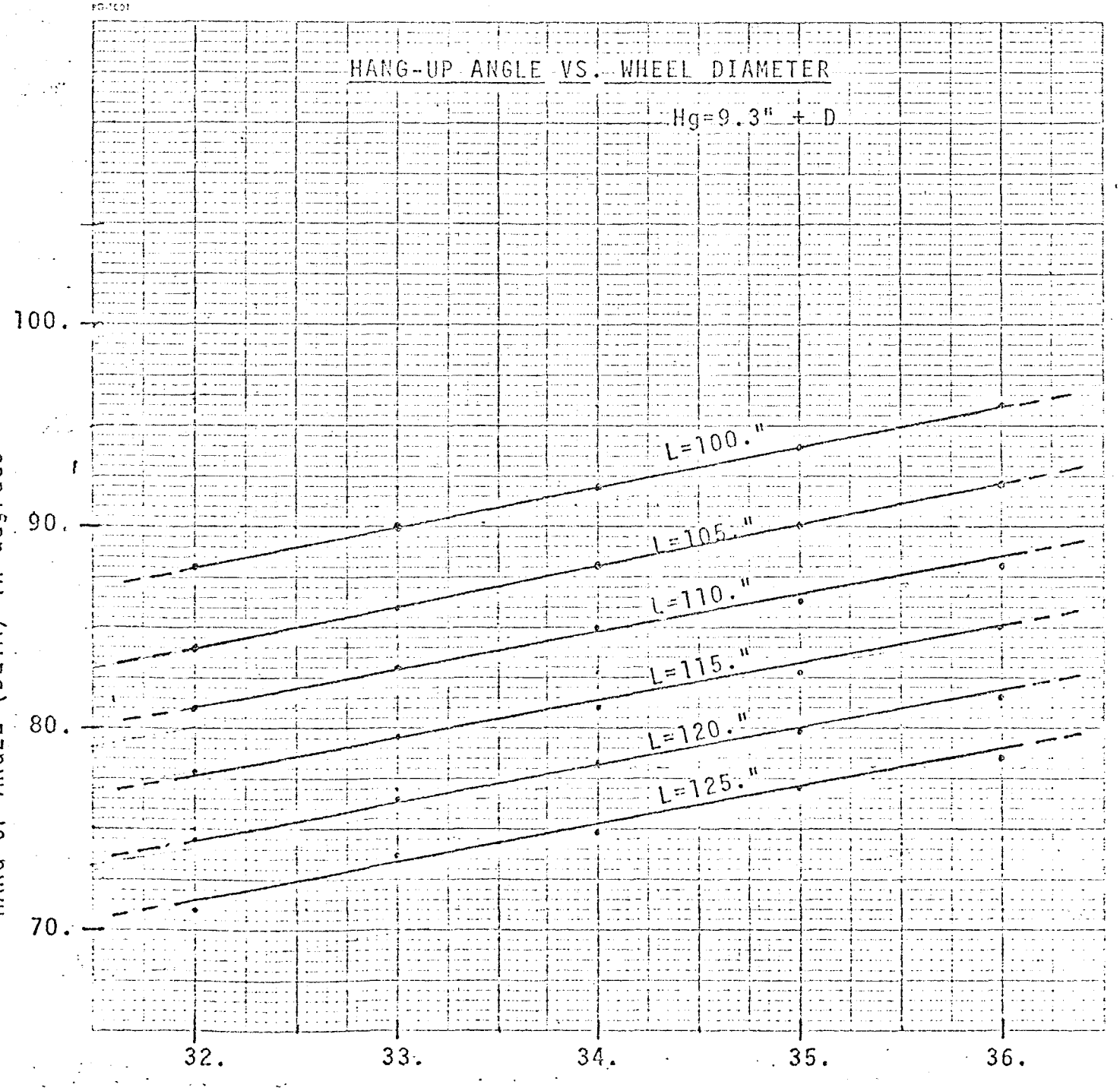

Figure 15. Obstacle Negotiation

Part B. The Transverse Case

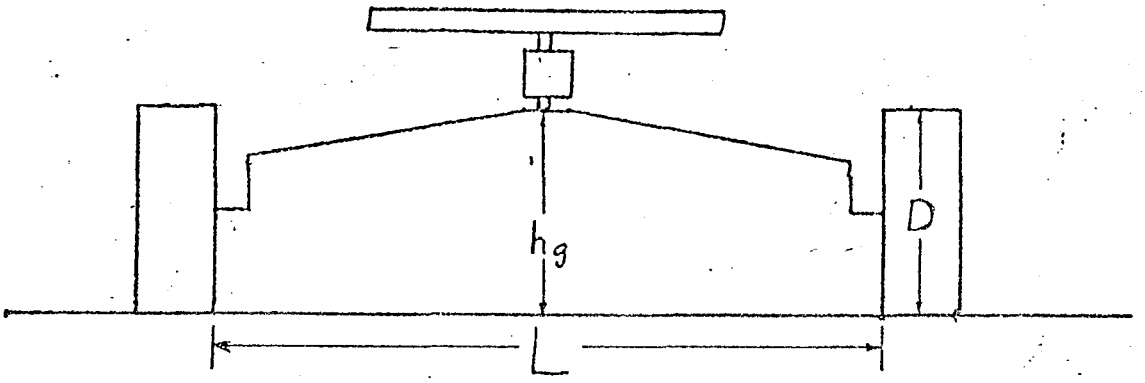

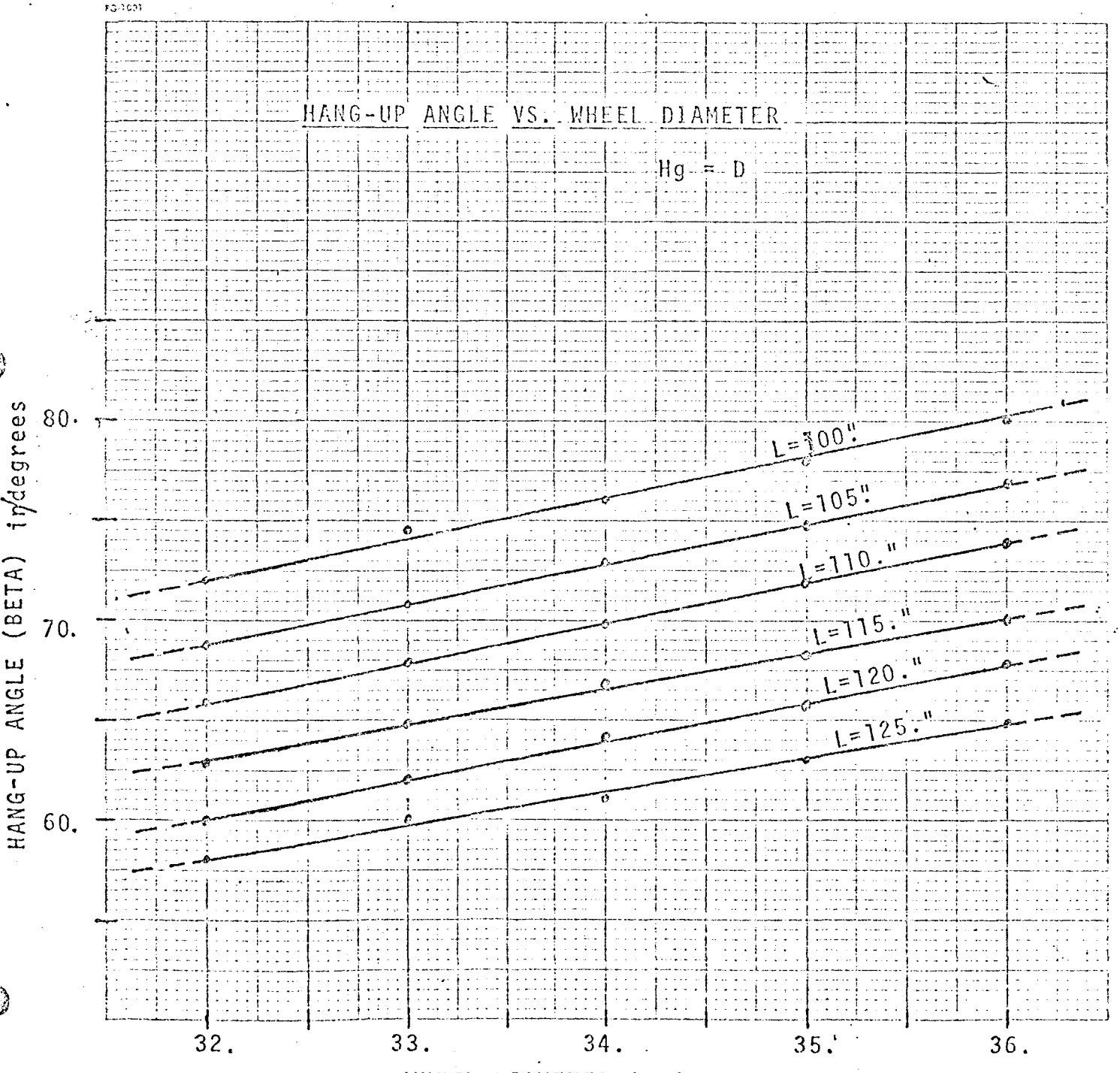

Figure 16. Obstacle Negotiation

A.1.e. Electromechanical Controls - Dennis Rosenthal
Faculty Advisor: Prof. G. N. Sandor

The control system for the 0.184 RPI MRV encompassed three areas: payload leveling, steering, and rear wheel motion. Due to the size/weight ratio of the model involved, leveling of the payload was temporarily discontinued. Constraints involved were size of sensors, weight of payload, size and weight of motor needed to control payload, sensitivity of available sensor types, and the complete weight of the model.

The steering system uses the same basic components as the movement motors and further description will be postponed until later in the report.

Power control for the rear wheel drive motors comes from two solid state complementary D.C. amplifiers each rated at 60 watts steady-state power out. The new Motorola complementary-darlington power output transistors were incorporated along with a modified (for D.C.) circuit given in their manual. The closed loop gain becomes feedback resistor R6 divided by zero-point resistor R5. Resistor R6 provides for full D.C. feedback to maintain the output at the selected level regardless of load (within operating range of the amplifier). The motors used are 24 volt 1 amp. D.C. permanent magnet instrumentation type with approximately 100:1 reduction gears. Feedback from back emf of the motor is essentially nonexistent due to the gear reductions (for small variations of output change) but given a constant voltage the motor maintains a constant speed over wide variations of load.

The low output impedance of the amplifier (approximately .03 ohms) gives a high dampening factor ($\sim$400) which provides excellent regulation over most operational regions. Input impedance is 10 K ohms. Use of the D.C. amplifier provides both forward and reverse operation by reversing the voltage at only one terminal of the motor, the other being at 'ground' potential. The drawback of using this type of control is that both a positive and negative supply voltage must be provided with both having the capability to handle the peak power required for the motor, or about 60 watts.

When the front wheels are turned, each rear wheel has a different speed to maintain or maximize the nonskid traction; hence a differential is required. This must be electronic since each motor is driven independently and gear reductions on the motors do not allow skid 'sensing'. The function involved is complex and involves the wheelbase, distance from front to rear, and width between wheels in tagent function. A piecewise linear approach was used to model the curves, Figure 17, as both are similar (as can be seen if reversed side for side). To register the steering angle two potentiometers are connected to the steering axle to give a voltage proportional to the angle. This voltage is then sent through an emitter follower for isolation and on to a resistor-zener diode matrix for the piecewise-linear approximated output, Figure 18. This output current, which represents the y coordinate of the graph, is passed through a resistor and this voltage is sent to the power amplifiers. There must be complete power supply isolation between power amp

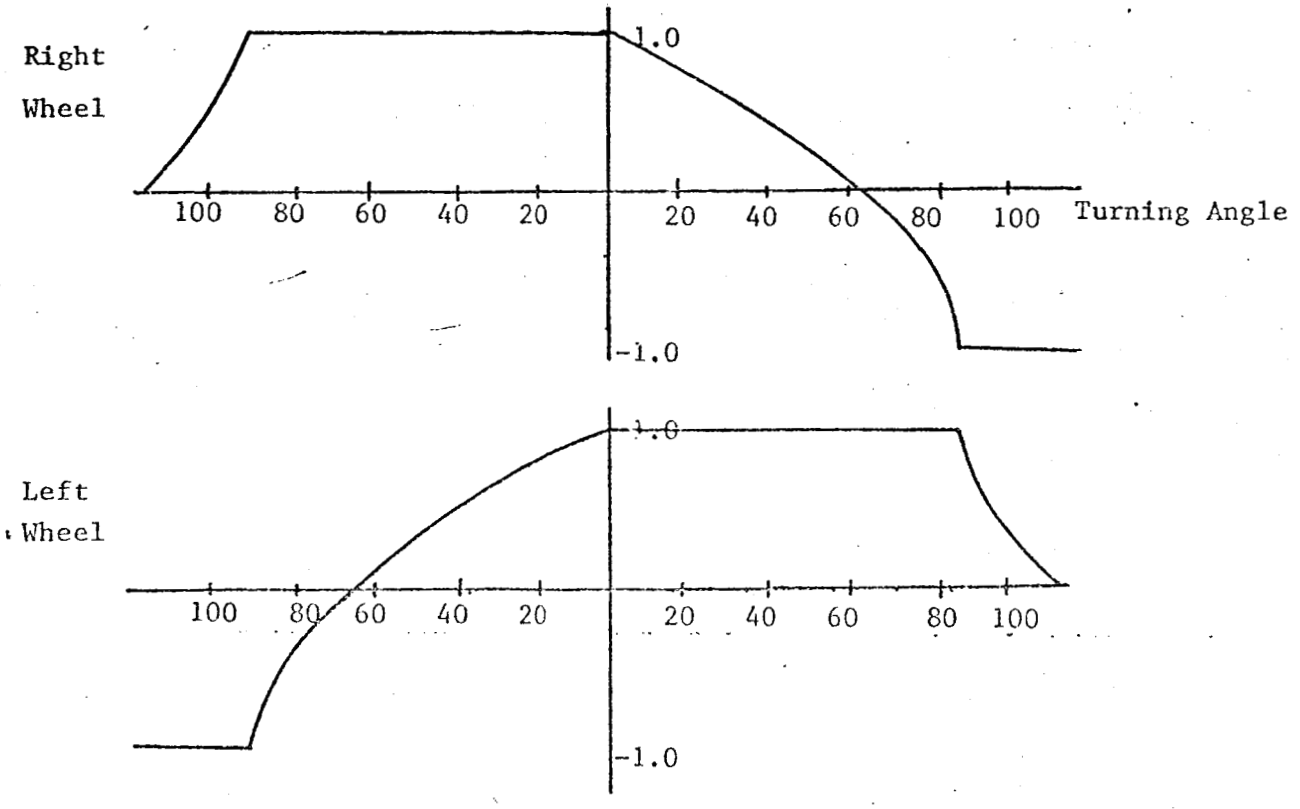

Figure 17
WHEEL MOTION VS. TURNING ANGLE

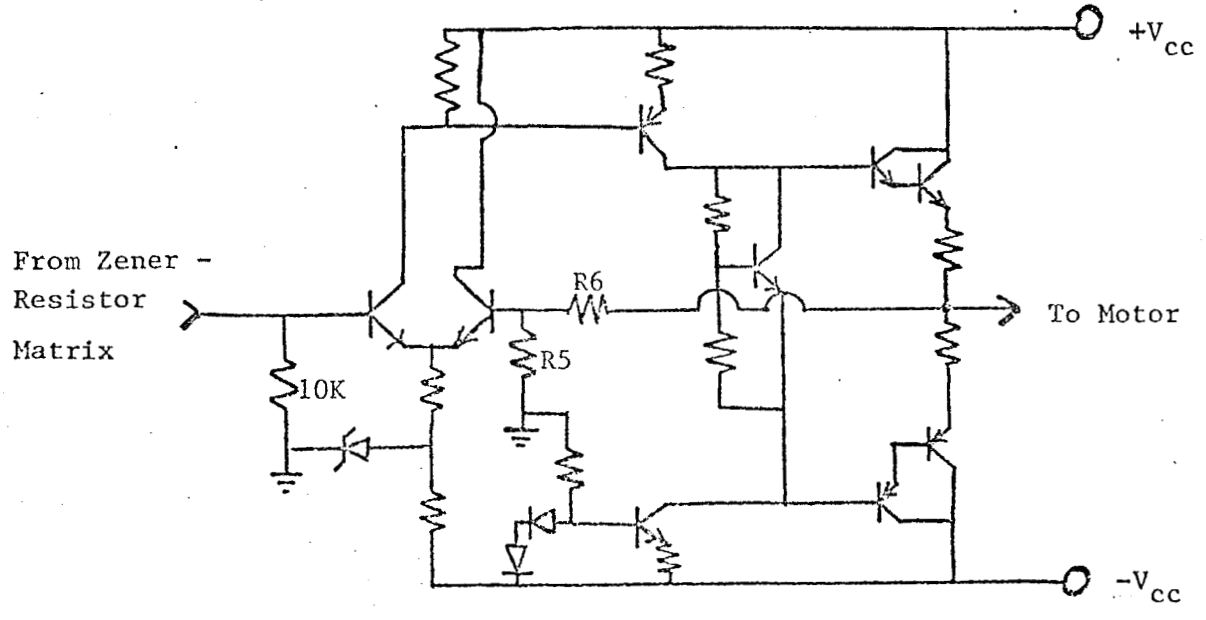

Figure 18
POWER AMP CIRCUIT

and sensor due to the fact that the ground or center potential must be adjustable.

The deadband voltage of the motors is around 4 volts and for certain headings, errors are incurred due to this. To eliminate this feedback from a wheel motion sensor will have to be incorporated into the power amps, but due to size limitations this is not possible for the present model.

Referring back to the steering system the same type of power output is used but a nulling bridge is used to derive the output signal.

In the future many changes will have to be made and with a larger vehicle, more area for finer instrumentation will be available and finer control can be maintained.

A.2. Collapsibility and Deployment - T. Janes
Faculty Advisor: Prof. G. N. Sandor

The objectives of this subtask are to investigate the design of the RPI MRV with respect to collapsibility, stowage within the Viking capsule, and deployment on the Martian surface.

Several design concepts combining various features of collapsibility and deployment have been explored in an effort to optimize the overall design, Ref. 4. The following three assumptions and constraints were developed in determining the present collapsibility scheme:

1. the payload body width must be decreased to 72" to fit the vehicle within the capsule;
2. the elastic behavior of the wheels is preserved after prolonged deformation; and
3. the location of the rover center of gravity within the Viking capsule may be adjusted to be within the established limits of the center of the capsule.

To achieve collapsibility under the above conditions, it is necessary to alter the present vehicle design in three places.

1. A spring-loaded, self-locking, ratchet type joint must be mounted on the rear wheel struts, 23" from the center of the rear wheel. This will permit the rear wheels to be folded against the rear face of the payload body.
2. A temporary rigid connection between the side of the payload body and the rear wheel strut will be required in the deployment phase and will be discussed later.
3. A spring-loaded, self-locking, ratchet-type joint must be placed on the forward part of the vehicle frame, at the base of the triangular section, to permit folding the front axle under the vehicle body, and the front wheels along side the payload body.

Once the collapsing operations, made possible by the above design-changes, are performed the RPI MRV will fit within the Viking capsule. Figures 19 and 20 show the collapsed state of the vehicle within the Viking capsule.

The rover and its scientific payload are protected from extreme shock and vibration while in the capsule by the resilience of the four wheels in direct contact with the upper and lower sections of the aeroshell. Future work should determine whether further protection is required; if so, light-weight dampers should be placed at the upper and lower corners of the payload body.

The landing sequence calls for soft-landing the rover on its wheels, aided by small rocketry.

There are three areas for future research associated with the collapsibility, stowage and deployment of the RPI MRV. Studies should be conducted into the aerodynamics of soft-landing the rover on its wheels with small rocketry, and alternatives to that system. Vibration analysis of vehicle-capsule assembly is needed to insure sufficient isolation of the instrumentation from shock during launch and landing. A computer program to analyze the composite center of gravity to determine subsystem locations is necessary to satisfy the capsule center of gravity requirements. Upon landing, the rear wheels will be driven so as to swing the wheel-support segment back into operational configuration. The force on the strut, due to this action, will be countered by the rigid attachment outlined above in alteration #2, and will cause the rover to move forward somewhat as the segment swings. Once the rear segment is locked, the payload body should be raised, the front wheels locked, and the rover driven in reverse. The skidding action of the front wheels, and the action of the spring-loaded assembly will bring the front section to its operational configuration.

A.3.a. Wheel Tester - C. Klette
Faculty Advisor: Prof. G. N. Sandor

In the development of the wheel, analysis and further development in the area of wheel traction and mechanics of the wheel-soil interface are required. The best method for obtaining information concerning soil and wheel interaction is to physically simulate anticipated conditions and test various prototypes under these conditions. Variations on the hub, hoops, hinges, rim and grousers can be tested under similar soil conditions while attempting to maximize tractive effort and minimize the energy expenditure. The objectives of this subtask are the design and construction of wheel test facilities, and testing of the RPI MRV toroidal wheel, Ref. 5.

Specifications showed the need for large and cumbersome test apparatus and the associated cost and labor involved in building a full scale test facility. The decision was made to scale the wheels and tester to 0.4. The main difficulty arising in the use of scaled test apparatus is the scaling of the various parameters associated with the full scale wheel such as velocity, mass, gravitational forces, etc. These parameters must be weighted as to their relative importance.

(Top View)

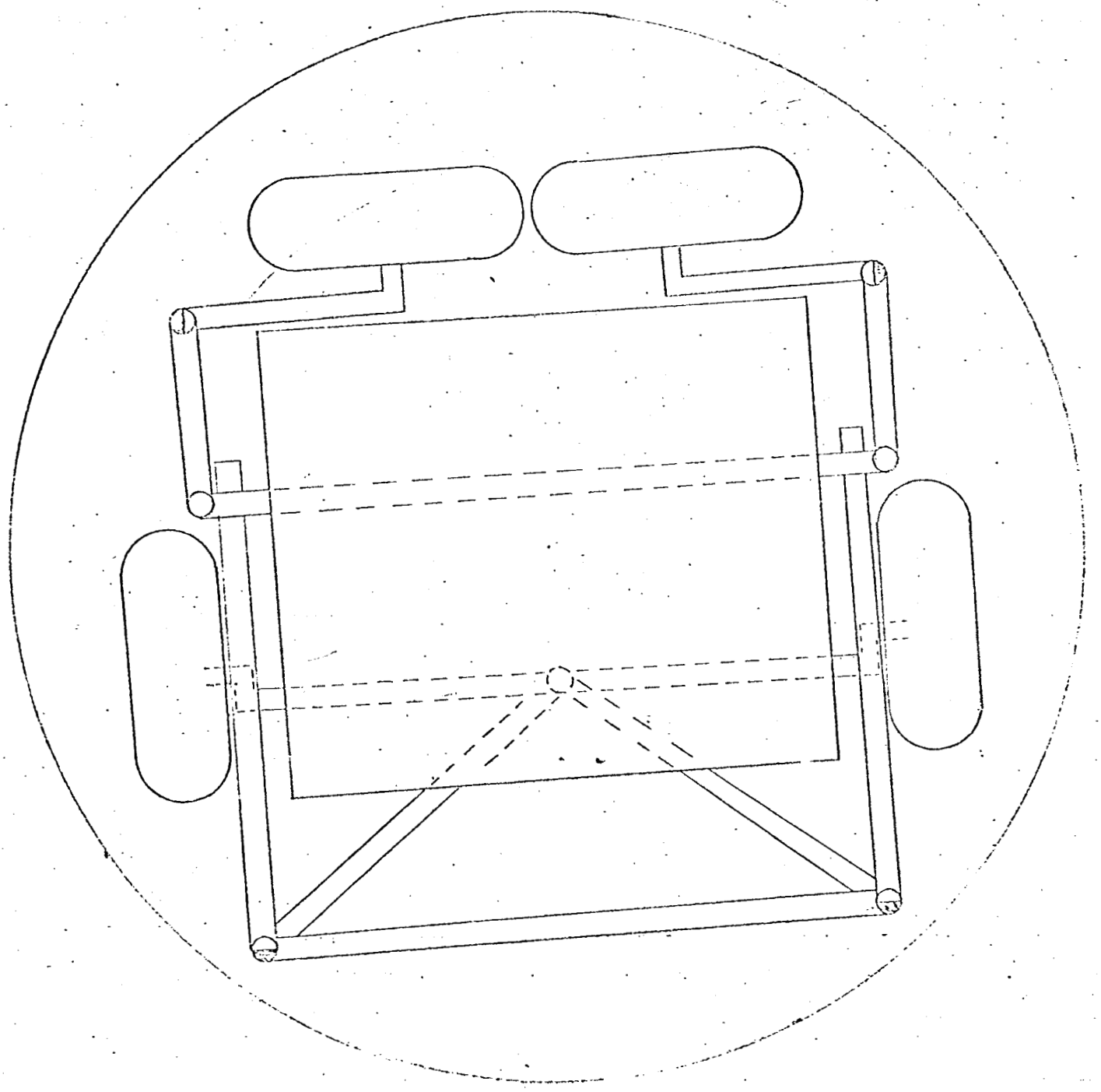

Figure 19. Collapsed MRV & Superimposed Viking

Collapsed MRV & superimposed Viking (Rear View)

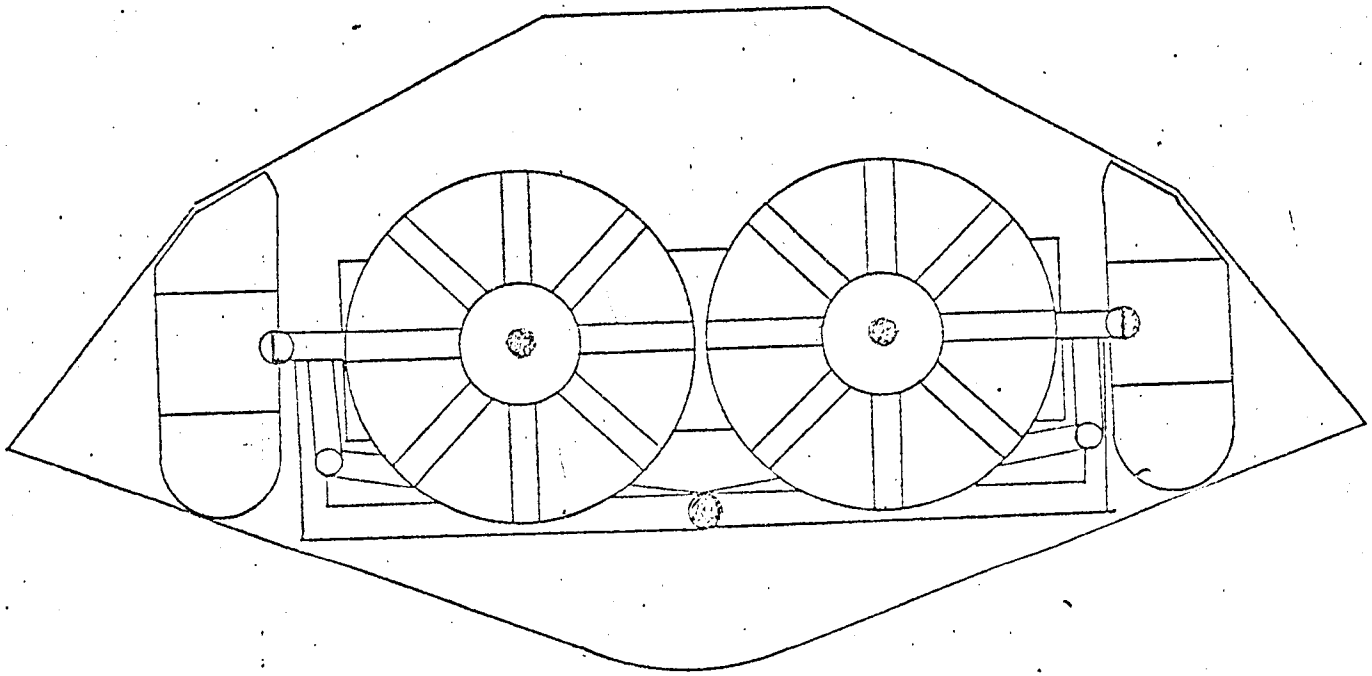

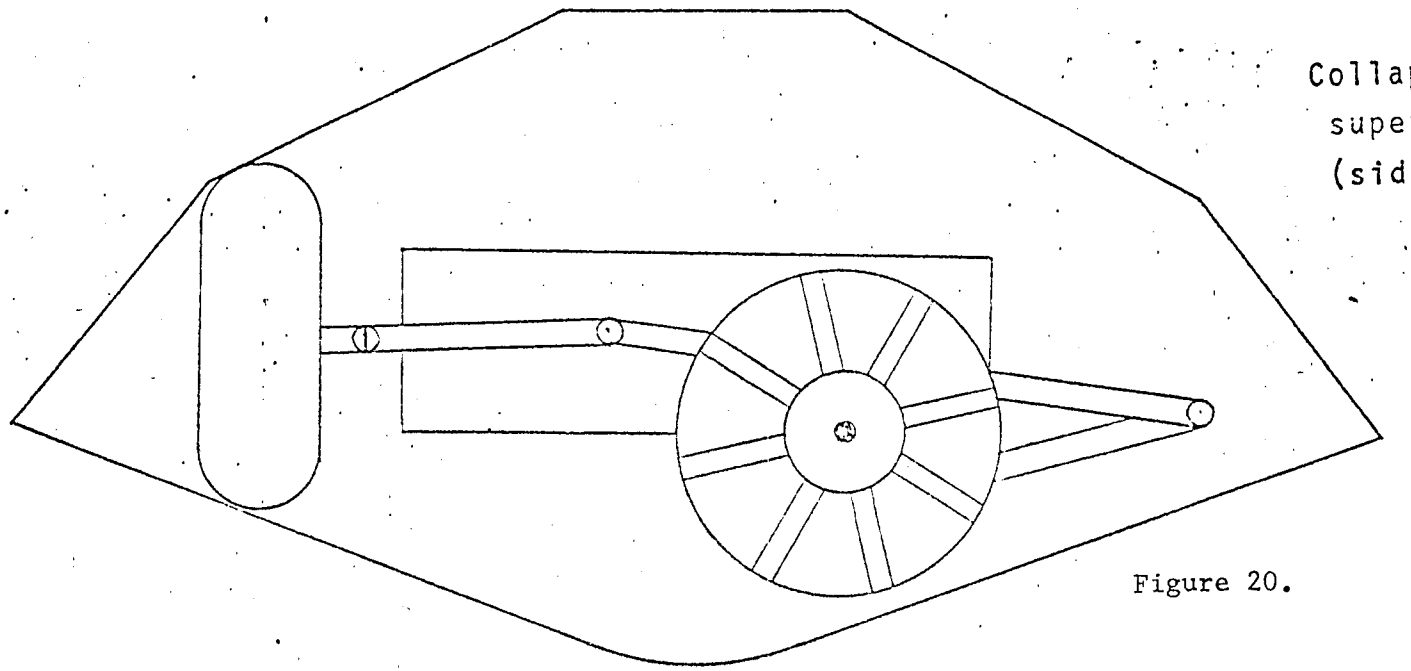

Collapsed MRV & superimposed Viking (side view)

Figure 20.

Design Criteria

To design the test appratus and its functions a set of design criteria were drawn up. In the final design, the wheel is free to move vertically to compensate for irregularities in the soil. Constant velocity of the carriage is provided by a constant speed motor mounted on one end of the soil bin. Stability and durability were needed for accurate measurements and long range testing. Provisions for load and inertia characteristics are included in the carriage design. Both the test wheel and the carriage are powered. Canting of the wheel while loaded is also possible. The test wheel is to be scaled in size and the scaling of dynamic characteristics must be considered. The hoops and rim of the wheel are to be interchangeable for variability of design. The test soil will approximate anticipated terrain conditions on Mars. Provisions for monitoring instrumentation are necessary.

The wheel tester as built is shown in Figures 21 and 22.

Test Bin Soil

The moisture content of Martian soil is small as indicated by infrared spectral analysis although the exact amount is unknown. Since presence of water in the soil will create a slightly cohesive soil condition, a conservative estimate of the wheel effectiveness will be illustrated by a test conducted under cohesionless soil condition.

Although the Mars surface appears to be smoother than that of the moon, the lunar Mars analogy appears to provide a safer upper limit on the particle size distribution.

If a linear .4 scale of the grain size diameter is adopted the type of soil necessary would be on the order of a fine silt. Silt would be extremely difficult to work with in a soil bin because of its higher natural cohesion, the ease of scattering, the retention of water and effect of humidity. The scaling of parameters such as the internal friction, cohesion and density would complicate testing beyond feasibility. The assumption necessary at this point is that the same soil model can be used for the scale version as for the full-sized version. This assumption is justified by the fact that the grain size to grouser and rim size ratio is very small and the scale version is equivalent to the full size version because of weight, inertia and speed scaling characteristics.

Test Procedures

Test procedures will permit changing wheel slip, load, cant angle and soil conditions for each wheel tested.

Controlled Slip

In a programmed slip test, the wheel speed is linearly varied from a higher to a lower speed relative to the cart speed. Tachometers mounted on the test wheel and on the motor driving the wheel test

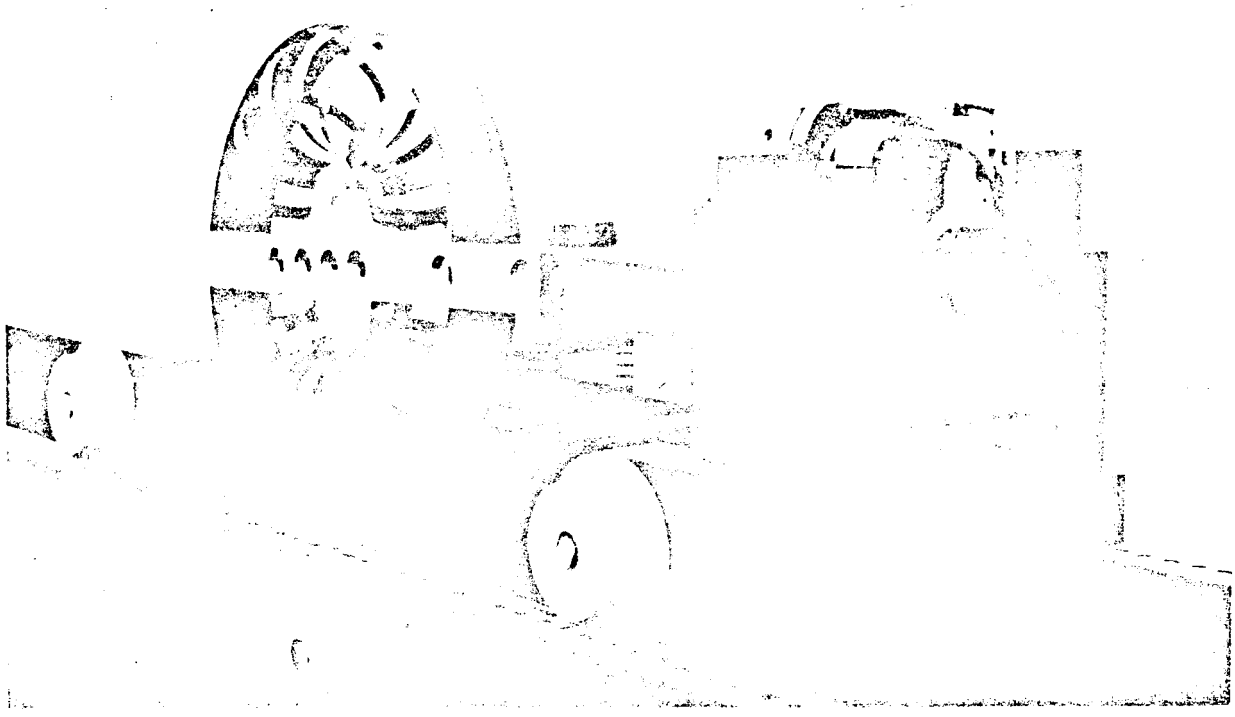

Figure 21. Test Carriage on Wheel Test Bin

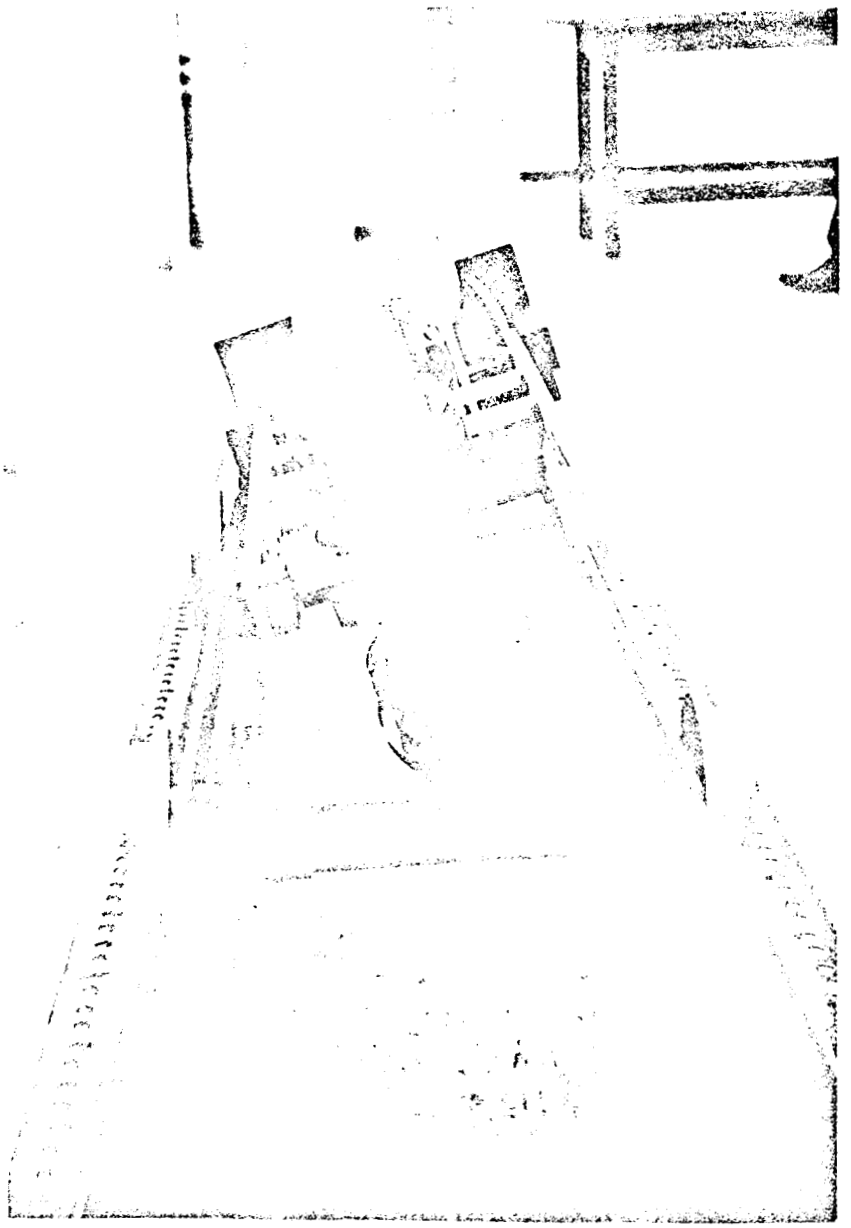

Figure 22. Canted Position of Wheel and Test Carriage

apparatus give the rotational and translational speeds respectively of the wheel and provide the information for the amount of slip.

The controlled slip test also is valuable in conservatively estimating the slope climbing capability of the wheel. The degree of difference from actual slope appears to be small and validates this interpretation of data. The information necessary for prediction of the slope climbing abilities from level soil bin tests is the determination of the pull coefficient, P/N, which is drawbar pull divided by the wheel load. This number is equivalent to the tangent of the critical slope angle for slip rates of 20 percent or larger.

Load Variations

The load can be varied to simulate the inertia and load characteristics that the wheel will be subjected to. The load variations are effected in two different ways. The hub of the wheel is loaded by weights attached to the arms with the center of mass of the weight on line with the hub center. These weights constitute a mass approximation. The springs on the arm can be compressed to attain the desired force at the wheel to simulate gravitational effects. If the gravitational force is higher than the inertia load approximation, tension rather than compression springs can be used. The reaction force due to the springs can be measured by adjusting the centerpost that is attached to the arms and pulling the arms down to the horizontal position with a spring scale. The springs can represent the suspension of the vehicle when the actual suspension is decided upon.

Cant Angle

The main purpose of the cant angle experiment is to test the flexibility of the wheel rim and optimize the footprint characteristics. Cant angle experiments can be made by the rotation of the back plate and adjustment of the spring assembly. The bearing connected to the centerpost of the spring assembly can be rotated to maintain a vertical orientation of the spring assembly. The possible cant angles of the test apparatus are equivalent to a 31 degree rotation. Beyond this point the wheel would hit the test cart or become influenced by the side of the test bin. The 31 degree limit was decided upon because of the nature of the vehicle and hinges on the wheel. Beyond this point the hinges of the reduced size could break under maximum load conditions. The vehicle will probably not be required to operate under greater cant angle conditions for safety reasons.

Soil Variations and Tests

The soil preparation should be accomplished in the following manner. Water is added to the soil in the desired amount (.5 to 1.8 percent of the dry density in keeping with the Waterways Experiment Station procedure). The soil is thoroughly mixed to provide an even distribution of water. The soil is compacted at the surface and leveled. The combination of moisture and compaction will vary all the soil parameters. As the amount of soil compaction increases the friction angle increases as well as the apparent cohesion and the density characteristics of the soil. As the moisture content is increased the cohesion increases.

The compaction affects the friction angle and the density while the moisture content regulates the soil cohesion.

Additional work is required in the instrumentation and calibration of the test tequipment. The wheel testing will be closely associated with the development work performed on the .4 scale model. Of particular interest will be the areas of radial and lateral stiffness.

A.3.b. Wheel Analysis - J. Kobus
Faculty Advisor: Prof. G. N. Sandor

The previous wheel analysis involved a great deal of computer time and possible round-off errors. Therefore, a new method, based on finite elements, has been applied, Ref. 6. This method is a matrix displacement technique which gives a closed form solution for the system displacements as the bottom of the wheel is loaded. Only five lower right side hoops are analyzed in order to keep the matrix sizes low. This program quickly calculates radial stiffness for any combination of hoop and rim stiffnesses with accuracy within 5%. Thus, sizing of wheel parameters to give a predetermined spring rate is now easily accomplished.

The computer program has been run for several input parameter values, the resulting output taking the form of a wheel design "handbook". An example of the output is given in Figure 23.

Future work in this area should include extension to torsional and lateral stiffness calculations as stability problems related to these parameters have been encountered.

A.4. Payload Design - J. Almstead
Faculty Advisor: Prof. G. N. Sandor

The objective of the payload subtask is the coordination of all of the MRV subsystems into an effective and reliable MRV system design capable of executing the stated mission functions. The subtask has the responsibility of giving form to the RPI MRV system. While none of the subsystems have been specifically designed as to their make-up, it is necessary to begin the payload design to insure that the RPI MRV system is integrated with respect to all its subsystems and their requirements. The work has been most closely related to the mobility subsystem and its associated collapsibility and deployment requirements, and the systems analysis task, Task B, which involves developing a means of making design decisions when conflicting subsystem requirements occur, Ref. 7.

The first task in payload design was the definition of constraints and assumptions which will serve as design guidelines. A description of the subsystems to be included as well as the system and subsystem constraints was required. The following is a partial list of the areas where assumptions and constraints apply.

```
HOOP MATERIAL= ALUMINUM ALLOY.
                                                        WHEEL CONFIGURATION NUMBER=      7.      1
    WHEEL RADIUS=      16.00    NUMBER OF HOOPS=        12.    HOOP RADIUS=       3.50
RIM WIDTH=       5.00    RIM THICKNESS=     0.0150    HOOP WIDTH=       1.00    HOOP THICKNESS=     0.1330
    MASS OF RIM=     0.7389    MASS OF HOOPS=     3.4386    INITIAL WHEEL LOAD=     100.00    HOOP SPRING  CONSTANT=      30.0000
DEFLECTION HOOP 1=  0.3300807E 01    REACTION FORCE 1=  0.9902423E 02    BENDING LOAD ON RIM=  0.9757651E 00    JENNY=   4
DEFLECTION HOOP 3=  0.2769306E-01    REACTION FORCE HOOP 3=  0.8367918E 00    BENDING LOAD RIM 3=  0.8245580E-02KATHY=   4
    MOMENT AT 3  0.4087274E 01    MOMENT AT 5=  0.4073666E 01
FOOTPRINT HALF-LENGTH=  0.4459340E 01


                                                        WHEEL CONFIGURATION NUMBER=      7.      2
    WHEEL RADIUS=      16.00    NUMBER OF HOOPS=        12.    HOOP RADIUS=       3.50
RIM WIDTH=       5.00    RIM THICKNESS=     0.0150    HOOP WIDTH=       1.00    HOOP THICKNESS=     0.1576
    MASS OF RIM=     0.7389    MASS OF HOOPS=     4.0769    INITIAL WHEEL LOAD=     100.00    HOOP SPRING  CONSTANT=      50.0000
DEFLECTION HOOP 1=  0.1988244E 01    REACTION FORCE 1=  0.9941225E 02    BENDING LOAD ON RIM=  0.5877530E 00    JENNY=   3
DEFLECTION HOOP 3=  0.1012034E-01    REACTION FORCE HOOP 3=  0.3060173E 00    BENDING LOAD RIM 3=  0.2991716E-02KATHY=   4
    MOMENT AT 3  0.2461972E 01    MOMENT AT 5=  0.2458998E 01
FOOTPRINT HALF-LENGTH=  0.4477139E 01


                                                        WHEEL CONFIGURATION NUMBER=      7.      3
    WHEEL RADIUS=      16.00    NUMBER OF HOOPS=        12.    HOOP RADIUS=       3.50
RIM WIDTH=       5.00    RIM THICKNESS=     0.0150    HOOP WIDTH=       1.00    HOOP THICKNESS=     0.1764
    MASS OF RIM=     0.7389    MASS OF HOOPS=     4.5608    INITIAL WHEEL LOAD=     100.00    HOOP SPRING  CONSTANT=      70.0000
DEFLECTION HOOP 1=  0.1422564E 01    REACTION FORCE 1=  0.9957947E 02    BENDING LOAD ON RIM=  0.4205298E 00    JENNY=   3
DEFLECTION HOOP 3=  0.5180825E-02    REACTION FORCE HOOP 3=  0.3626580E 00    BENDING LOAD RIM 3=  0.1531525E-02KATHY=   3
    MOMENT AT 3  0.1761510E 01    MOMENT AT 5=  0.1760421E 01
FOOTPRINT HALF-LENGTH=  0.4484810E 01


                                                        WHEEL CONFIGURATION NUMBER=      7.      4
    WHEEL RADIUS=      16.00    NUMBER OF HOOPS=        12.    HOOP RADIUS=       3.50
RIM WIDTH=       5.00    RIM THICKNESS=     0.0150    HOOP WIDTH=       1.00    HOOP THICKNESS=     0.1918
    MASS OF RIM=     0.7389    MASS OF HOOPS=     4.9593    INITIAL WHEEL LOAD=     100.00    HOOP SPRING  CONSTANT=      90.0000
DEFLECTION HOOP 1=  0.1107473E 01    REACTION FORCE 1=  0.9967261E 02    BENDING LOAD ON RIM=  0.3273848E 00    JENNY=   3
DEFLECTION HOOP 3=  0.3139947E-02    REACTION FORCE HOOP 3=  0.2825953E 00    BENDING LOAD RIM 3=  0.9282127E-03KATHY=   3
    MOMENT AT 3  0.1371346E 01    MOMENT AT 5=  0.1370831E 01
FOOTPRINT HALF-LENGTH=  0.4489082E 01


                                                        WHEEL CONFIGURATION NUMBER=      7.      5
    WHEEL RADIUS=      16.00    NUMBER OF HOOPS=        12.    HOOP RADIUS=       3.50
RIM WIDTH=       5.00    RIM THICKNESS=     0.0200    HOOP WIDTH=       1.00    HOOP THICKNESS=     0.1330
    MASS OF RIM=     0.9852    MASS OF HOOPS=     3.4386    INITIAL WHEEL LOAD=     100.00    HOOP SPRING  CONSTANT=      30.0000
DEFLECTION HOOP 1=  0.3257253E 01    REACTION FORCE 1=  0.9771759E 02    BENDING LOAD ON RIM=  0.2282405E 01    JENNY=   5
DEFLECTION HOOP 3=  0.6438351E-01    REACTION FORCE HOOP 3=  0.1931505E 01    BENDING LOAD RIM 3=  0.4511447E-01KATHY=   5
    MOMENT AT 3  0.9560513E 01    MOMENT AT 5=  0.9487032E 01
FOOTPRINT HALF-LENGTH=  0.4285589E 01
```

Figure 23. Example Output from Wheel Stiffness Program

1. Capsule
    a. size
    b. shape
    c. weight
    d. center of gravity location
2. Vehicle
    a. front/rear weight ratio
    b. collapsibility
3. Science
    a. access to soil samples
    b. storage and test bays
    c. chemical storage
    d. imaging
    e. test equipment
4. Communications
    a. high gain antenna and antenna pointing
    b. low gain antenna
5. Thermal Control
    a. radiators
    b. compressor
    c. insulation
6. Landing
    a. terminal descent rocketry and fuel
    b. landing radar
    c. ability to deploy
7. Power
    a. RTG
    b. battery
8. Martian Atmosphere
    a. winds 200 mph to 500 mph
    b. dust storms

The constraints and assumptions were then translated into design concepts. For example, the high velocity Martian winds require a payload package which minimizes the aerodynamic forces; the thermal control requires radiator panels on the sides of the payload; the power system requires space and thermal shielding for large RTG packages; and the landing sequence requires placement of rocketry and fuel on the vehicle for descent.

The definition of design concepts pointed out areas where additional information and testing is required. The most critical testing at this point concerns the winds which the vehicle will experience on the Martian surface. Results from this analysis and dust accumulation testing will be significant in determining the form and shape of the vehicle system.

The wind testing has been designed to clarify the effect of the

winds on appendage location, RTG location and orientation, payload body angle relative to the surface, overturning moments, stability, and an estimation of the vehicle drag coefficient for several orientations of the vehicle relative to the wind direction. This will be a result of the analysis of the experimental aerodynamic loading data.

For the wind testing it is necessary to define the Martian atmosphere. It is thought to be composed of mostly CO_2, with a density in the range of 10^{-5} gms/cm^3, pressure of 10 millibars and temperatures which vary in the range of 150°K to 250°K, Ref. 8. For modeling purposes the basic flow regime of the Martian atmosphere must be determined requiring an estimate of the Reynolds number for the atmosphere.

$$Re = \frac{U L \rho}{\mu}$$

where U = velocity
L = length
ρ = density
μ = dynamic viscosity

A velocity of 9.0×10^3 m/sec was chosen as a starting point for calculations. The viscosity figure of 1.35×10^{-4} gm/cm sec is that of CO_2 at 1.3°C. Support for this value comes from the viscosity of the earth atmosphere at 100,000 ft. where the physical characteristics are similar to the Martian atmosphere with a viscosity of 9.9306×10^{-6} lbs/ft sec or about 1.5×10^{-4} gm/sec cm). The value of L was 150 cm, the approximate length of the proposed payload body.

Velocities in the range of 200 mph to 500 mph and densities in the range of 1×10^{-5} gm/cm^3 to 2×10^{-5} gm/cm^3 result in the following Reynolds numbers.

U in miles/hr	ρ in gm/cm^3	Re
200	1×10^{-5}	10,000
200	2×10^{-5}	20,000
500	2×10^{-5}	50,000

With Reynolds numbers in this range, the aerodynamic drag may be calculated using the expression applied for low Reynolds numbers:

Drag force = Drag coefficient x dynamic pressure x normal surface area (where dynamic pressure = $q = \frac{1}{2} \rho U^2$

U in miles/hr	ρ in gm/cm^3	q in dynes/cm^2
200	1×10^{-5}	810 (1.692 lbs/ft^2)
500	2×10^{-5}	5060 (10.57 lbs/ft^2)

A problem with wind tunnel testing is the density of the atmosphere in the tunnel being on the order of one hundred times greater

than that of the Martian atmosphere. To model the dynamic loading of the vehicle on Mars, much lower velocities will be required.

Once the form of the vehicle system has been established, the placement of subsystem components determines the final vehicle system. The subsystem constraints and requirements are not well defined, so that as additional information becomes available the payload design will be updated.

In placement of the subsystems there are three factors which must be considered: 1) the subsystem must perform its mission function without interferring with other systems, 2) the subsystem must fit inside the capsule, and 3) the composite vehicle system must have a center of gravity located within certain limits. It is also important that the subsystems be as flexible as possible, to permit altering of testing procedures as may become necessary or desired.

The maximum weight deliverable to Mars is restricted by the delivery system. It is therefore important that the vehicle structure weight be minimized to permit the largest payload fraction. A structural analysis is necessary to insure minimum vehicle structure weight.

Analysis of the composite vehicle system will be required in the areas of: vehicle dynamics; system operation and reliability; collapsability, landing and deployment; vehicle stability; and obstacle negotiation. Following the analysis, a comparison study will be made of the RPI MRV with the capabilities and deficiencies of other proposed Martian Roving Vehicle systems.

Task B. Systems Analysis

The objective of this task is to develop a framework within which vehicle design decisions involving conflicting requirements can be made. Efforts during the past period have been directed towards: optimization of the original system model, the effect of changing design-dependent assumptions on the system model, accessory optimal solutions for design parameter perturbations, and the on-board computer subsystem.

B.1. System Design Optimization for the Original System Model -

C. Pavarini, N. Vandenburg
Faculty Advisor: Prof. E. J. Smith

This task bases its work on the premise that the design for the Mars roving vehicle (MRV) can be characterized by a basic set of states and all the other factors which go into the design can be calculated from these states. The set of equations which describe how the other factors are calculated from the state variables is referred to as the original model. Presently these equations are basically the same as the equations in Ref. 9. However, through working with these equations it became apparent that some of them needed slight modification and so the original model was altered to include the improved equations for some of the subsystems for the MRV.

The reason for modeling the MRV on a total system basis is so that an optimal design can be found through the use of mathematical programming to search for locally optimal design over a properly limited region of state space. It should be noted that the state variables include both design and operational considerations since this design procedure considers the total system. The reason for the "locally" optimal design for the MRV is due to the search routine being able to only "see" locally and the nonlinear nature of the system evaluation function. It is believed that through the use of different starting points that global maximum of the system evaluation function, Ref. 9, can be found.

As mentioned above, this task has as its objective the optimization of the design of the original MRV model. The use of the nonlinear programming (NLP) techniques of extremizing a system evaluation function subject to various inequality constraints. In order to put the modeling equations of the original model into the proper form, extensive algebraic rearrangement was necessary. After rearrangement the system evaluation function had the form of one extremely nonlinear function in twelve variables. This function was to be maximized subject to various inequality constraints, that is constraints of the form $g_i(\underline{x}) \geq 0$, $i = 1,\ldots,m$. These include the trivial constraints, that is those which require the state variables to be positive, and various other factors which are calculated from the states to also be positive. For example, it is necessary that the weight of the communications system be positive. However, the weight of this system is a function of the state variables. In this case, it is a function of the power for communication and the area of the antenna.

The nonlinearity of the problem cannot be overemphasized. The system model has several nonlinear relationships inherent in the subsystems, notably the thermal control subsystem where thermal radiation introduces fourth order nonlinearities in several of the system equations for this subsystem. The communications subsystem introduces a mild nonlinearity due to the rate of communications being proportional to the product of the power for communications and the area of the antenna. The obstacle avoidance subsystem introduces several terms of exponential form. These and other nonlinearities combine to produce an extremely nonlinear system evaluation function.

This problem statement lends itself to a NLP procedure, Ref. 10, which will allow the programmer to include the inequality constraints quite easily. This procedure, Fiacco and McCormick's Sequential Unconstrained Minimization Technique (SUMT), was obtained early in the fall of 1971 and was installed upon RPI's IBM 360/50. The manner in which this very general technique is being used is as follows: The NLP problem is minimize $F(\underline{x})$ subject to $g_i(\underline{x}) \geq 0$, $i = 1,\ldots,m$. This problem is solved through the use of an interior penalty function method and a sequence of unconstrained problems is solved to arrive at the solution to the constrained problem. In particular, SUMT forms the function $P(\underline{x},r) = F(\underline{x}) - r\sum_{i=1}^{m} \ln[g_i(\underline{x})]$ and minimizes this function for a

decreasing sequence of r values. Note how the penalty term shapes the system evaluation function $F(\underline{x})$ so that there is a greater chance of converging to the dominate minimum and also note that the P function increases as a boundary is approached so that the sequence of minimizations stays inside the feasible region. There are some problems which this version of SUMT suffers from, notably the problem of convergence and some programming problems in the area of the numerical differencing used to determine the gradient at the various points.

There were many preliminary efforts into the area of programming the original system of equations for the model of the rover. After much rearrangement of the modeling equations and some simplification and correction of the modeling several locally optimal points were found for the original system model. These solutions were not very satisfactory and as a result the modeling for several of the subsystems was reexamined. In particular the manner of operation of the batteries was changed due to the problem of excessive time between recharges. The former assumption was that the batteries would be used right along as the rover was moving. The new assumption is that the batteries would only be used when the rover exceeds a particular design maximum (i.e. RTG power is sufficient for "normal" operation) and would otherwise be unused. The other subsystem which was reexamined was the thermal control subsystem. It was the thermal control subsystem which caused most of the problems in the preliminary efforts and it was this subsystem which had to be changed and simplified so that a solution to the optimization problem was possible. The modeling for the thermal control subsystem was reviewed and several new terms were added to the equations for this subsystem. Heat loss by convection and heat gain from infrared radiation from the surrounding atmosphere were the two major additional considerations. When these two additional considerations were included there were still problems with the thermal control subsystem which led to the reconsideration of the feasibility of the "heat pipes only" method of cooling. It was decided that the heat pipes did not provide enough cooling to meet the required internal temperature range requirement of between 290 and 310°K. Therefore the model was modified to include a compressor type system.

Some other constraints were added as a result of the preliminary efforts. It was noticed that there were insufficient constraints on the region of state space in which to search for an optimal design. In particular, the size of the antenna was quite large (2.9 m dia.) and the area of the outside skin was small ($\sim 5\ m^2$). As a result of the small surface area and poor thermal control modeling, the thermal insulation took up more volume than there was in the equipment package. This indicated a need for a constraint on the thickness of insulation and thus the volume of the equipment package was required to be positive. Other changes include the relinearization of the weight of the communicator function about a more reasonable design point and the reduction of the ratio of vehicle to instrument package weight from 2/3 to 1/2 to take into account new information provided by Task A. These and other minor changes in the values of constants bring the original model up to date.

The present effort lies in the area of reprogramming the original model so as to incorporate the changes listed above. Some very preliminary results indicate that a possible optimal design is one of large communications system (antenna $\curvearrowleft$ 1.7 m dia. i.e. maximum diameter allowed , power $\sim$ 150 watts, weight $\curvearrowright$ 163 Kg, data rate $\curvearrowleft$ 18931 bits/sec) and small science section (weight of science $\curvearrowleft$ 50 Kg i.e. smallest allowed). When compared with the rest of the design the power system is reasonable (energy of batteries $\curvearrowright$ 15 watt/hr., power of r.t.g.'s $\curvearrowleft$ 554). The constraints which were active as this point were:

total weight $\leq$ allowable launch weight (i.e. 570 Kg)

diameter of antenna $\leq \sqrt{3}$ m

velocity of motion $\leq$ 1.5 m

area of outside skin $\geq$ 8 m^2

weight of science $\geq$ 50 Kg

maximum design slope $\leq 20^{\circ}$

It should be noted that these results are preliminary and were obtained from an incomplete model since there was no real control on modeling of the thermal control system, namely the weight of the compressor as a function of the heat to be removed and the temperature gradient.

Future work involves using different starting points and modeling of the weight of the compressor. After this area of work is completed other models can be considered, notably those which result from the work of Task B.2.

B.2. Effect of Changing Design-Dependent Assumptions on the System Model

Lance Lieberman
Faculty Advisor: Prof. E. J. Smith

In formulating the system model for a semi-autonomous Mars roving vehicle, Ref. 7, it was necessary to make various assumptions in order to constrain the model for solution. Many of these assumptions merely entailed fixing parameters and constants at reasonable values; however, several were basic to the entire model, and a change in any one such important concept could necessitate remodeling whole subsystems and their governing equations. Since the assumptions employed were made on the basis of present available knowledge and expectations, there was no reason to believe that an alternate configuration or idea couldn't, or wouldn't, be embodied in the final design.

The objective of this subtask has been a consideration of alternate design assumptions; the model must be flexible enough to accept major changes in design-dependent assumptions. By remodeling the entire system of equations as necessary to represent a partially altered vehicle, the effect on the various parameters and the overall

changes in the model can be examined. A significant rise in the objective function, for example, could indicate a more efficient system and might be cause for further investigations in the same direction.

The first study performed was the addition of an active, stationary orbiter linking the rover with the earth ground station. In the original system model, Task B.1, a direct, two-way vehicle-earth communication link was assumed. The addition of an active, stationary relay orbiter at an approximate altitude of forty-thousand kilometers above the Martian surface has several immediately discernable advantages; not only does it cut down necessary communications power on-board the vehicle, allowing a decrease in necessary power allotment to the communications subsystem and/or a corresponding increase in the data rate, but it has the additional desirable advantage of allowing vehicle-orbiter communication at any time (continuous window), and subsequent relaying to earth during an increased time period.

A set of equations specifying the characteristics of the configuration was solved and led to the conclusion that the prime effect of introducing the orbiter link in the communication system was to remove any bounds on the data rate for the rover. In terms of the present system model, the effect was the removal of one equation, and the removal of several terms in various other equations which involved the data rate.

It should be noted that the determination of the orbiter specifications was not within the scope of this study -- rather, the question considered was given this additional link in the system, what will this alternate communication configuration buy in terms of vehicle performance efficiency. The answer is clearly an unrestricted data rate, at the expense of the design and orbiting of the relay. Further, the assumption regarding the stationarity of the orbiter may be removed without changing any of these results -- the only effect is the addition of a finite communications window.

A second study performed involved consideration of a change to a six-wheeled, triple compartment vehicle similar to that considered in Ref. 11. Such a vehicle, with two thermally controlled areas, as opposed to one for the originally modeled four-wheel rover, presented a new set of unique problems with regard to heating and cooling. It was assumed throughout that the first (forward) compartment contained the science experimental and electronics equipment, while the second (center) package contained all additional subsystem electronics, including the data processing unit; furthermore, both compartments were assumed to be of equal size and rectangular shape. Another primary assumption involved the placement of the radiating surfaces of the two forward compartments on the front and rear surfaces of each cubicle; while this was in agreement with present expectations and placement in the four-wheeled RPI MRV, it necessitated the addition of terms in the modeling equations for conduction between the adjacent radiators. It was determined that placing the radiators on the outer

(side) surfaces of the compartments eliminated the coupling between the two packages but increased the power required for thermal control due to smaller radiation surface areas on each compartment.

Because many changes were necessary in the thermal control subsystem of the vehicle, a new set of equations was derived using heat balances for the three major portions of the subsystem -- the body (compartment) skin, the radiators, and the internal region. By considering each of these regions individually, and each under 'day' and 'night' conditions, a set of fourteen equations in sixteen unknowns evolved. These were reduced to eight state variables in four equations, these being the 'day' and 'night' temperatures of the skin and radiators for each compartment. While the model could have been reduced to two states, fourth power radiation terms in the equations proved extremely difficult to handle in such a case.

Future work on this subtask should be aimed toward computer solutions for the entire model for each of these alternate configurations. The effect on the objective function is particularly important to determine the operational desirability of the changes in terms of the mission success criteria.

B.3. Accessory Optimal Solutions for Design Parameter Perturbations -
Carl Pavarini
Faculty Advisor: Prof. E. J. Smith

This section reports work accomplished for the period 1 July thru 31 December 1971. For the remainder of the period covered by the progress report, the author has been involved in work reported under Task B.1. A major reason for this allocation of effort is that the next logical step in continuing work with accessory optimal solutions (sensitivity analysis) requires at least partial completion of Task B.1. Specifically, an optimal design solution must be known before the method presented below can be utilized.

Consider the situation where an optimal design vector has been determined for a given mathematical model of a system (Task B.1.). Suppose that one (or more) of the components of the vector (i.e., one or more design parameters), must be adjusted. This may be due to factors not considered in the model:

a. Although the model equations are continuous, perhaps it is not feasible to design for the true optimal value of a parameter (e.g., if the optimal solution requires a communication data rate of 1.347 K, it may be more reasonable to use a 1.5 K value for hardware design)

b. Perhaps an outside constraint is added (e.g., the optimal solution requires the vehicle to climb slopes now considered too hazardous in terms of wheel slippage considerations)

c. It may be advantageous to use a certain piece of off-the-shelf-hardware, and its design values may not coincide with the determined optimal values.

In any of these cases, it would be desirable to know how to readjust the values of the design parameters that were unperturbed by the required change in order to maintain the optimal property of the solution.

The task of this sensitivity analysis, then, is to determine the optimal manner in which to adjust these design parameters relative to the initial perturbation. Work done to date considers the problem when one parameter undergoes a required perturbation by some "small" amount. Linearization techniques are employed to reduce the general nonlinear optimization problem to a set of linear inequalities, thus much reducing the complexity of the problem as compared to the original system optimization. The sensitivity approach has the advantage that it is no longer necessary to resolve the nonlinear optimization problem each time a design parameter (state) is perturbed.

Mathematical Analysis of the Problem

The original system design optimization problem has been cast in the form:

$$\max \quad f(x)$$

$$\text{subject to } g_i(x) \geq 0 \quad i=1,2,\ldots,r$$

$$h_j(x) = 0 \quad j=1,2,\ldots,s$$

where x is the n-dimensional vector of design parameters and f and all the g_i and h_j are, in general, nonlinear functions of the components of x.

The optimal solution (x^*) is known by solution of the original problem. Of the r inequality constraints one or more may be active (i.e., equal to zero) at x^*. Appending these to the s h_j's gives a set of m equality relations at x^*, where $m < n$, which now will be denoted $h_j, j=1,2,\ldots,m$.

A necessary condition at the optimal solution is the LaGrange condition

$$F(x^*) = \nabla f(x^*) + \nabla H^T(x^*)\lambda^* = 0$$

where

$$\nabla f_i = \frac{\partial f}{\partial x_i}$$

$$\nabla H_{ij} = \frac{\partial h_i}{\partial x_j}$$

∇H is an m x n matrix

and λ is an m vector of LaGrange multipliers.

Since x^* is known, the problem of finding the λ^* vector is the solution of n linear equalities. However, since x^* is found by iterative search, the LaGrange condition equations may not be accurately satisfied and it may be necessary to solve for λ^* in a least-squares sense.

If x_1 (the first component of x) is to be perturbed,

$$x_1' = x_1^* + \delta x_1 \ .$$

At the new optimal (x') the LaGrange condition must also hold:

$$F(x') = \nabla f(x') + \nabla H^T(x')\,\lambda' + \gamma \begin{pmatrix} 1 \\ 0 \\ \vdots \\ 0 \end{pmatrix} = 0$$

where γ is a new LaGrange multiplier, and the vector $\begin{pmatrix} 1 \\ 0 \\ \vdots \\ 0 \end{pmatrix}$ is the gradient of the new constraint on x_1.

A Taylor first-order expansion of F(x) about x^* yields

$$F(x') \approx F(x^*) + D\,F\,(x^*)(x' - x^*)$$

where DF denotes differentiation. Note that $x' - x^* = \delta x$. Expanding,

$$F(x') \approx F(x^*) + \left[\frac{\partial}{\partial x_i}\nabla f\right]^* \delta x + \nabla H^T(x^*)\left[\frac{\partial \lambda}{\partial x_i}\right]^* \delta x$$
$$+ \lambda^* \left[\frac{\partial}{\partial x_i}\nabla H\right]^* \delta x + \left(\frac{\partial \gamma}{\partial x_i}\right)\begin{pmatrix} 1 \\ 0 \\ \vdots \\ 0 \end{pmatrix}^T \delta x \qquad (1)$$

where the notation $\left[\frac{\partial}{\partial x_i}\right]$ is a gradient operation which transforms a vector to a matrix and a matrix to a three-dimensional array.

In (1), there are n equations. There are n unknowns in δx, nm unknowns in $\left[\frac{\partial \lambda}{\partial x_i}\right]$ and n unknowns in $\left(\frac{\partial \gamma}{\partial x_i}\right)$ for a total of n(m + 2) unknowns. However, solving for all of these unknowns is not necessary for determining the readjustments δx_i, i=2,...,n. Matrix algebra manipulation allows the following reductions:

$$\left[\frac{\partial \lambda}{\partial x_i}\right]\delta x \Longrightarrow \begin{pmatrix} \frac{\partial \lambda_1}{\partial x_1} \\ \vdots \\ \frac{\partial \lambda_m}{\partial x_1} \end{pmatrix} \delta x_1$$

$$\left(\frac{\partial \nu}{\partial x_i}\right)\begin{pmatrix} 1 \\ 0 \\ \vdots \\ 0 \end{pmatrix}^T \Longrightarrow \left(\frac{d\gamma}{dx_1}\right)\begin{pmatrix} 1 \\ 0 \\ \vdots \\ 0 \end{pmatrix} \delta x_1$$

Since interest is in the n-1 readjustments, define

$$\eta = \begin{pmatrix} 1 \\ \eta_2 \\ \vdots \\ \eta_n \end{pmatrix} \qquad \text{so that} \quad \delta x = \eta \, \delta x_1$$

and equation (1) becomes

$$\left[\frac{\partial}{\partial x_i} \nabla f\right]^* \eta + \nabla H^T(x^*) \frac{\partial \lambda}{\partial x_1} + \lambda^* \left[\frac{\partial}{\partial x_i} \nabla H\right]^* \eta + \frac{d r}{\partial x_1} \begin{pmatrix} 1 \\ 0 \\ \vdots \\ 0 \end{pmatrix} = 0 \tag{2}$$

where $$\left\{ \lambda^T \left[\frac{\partial}{\partial x_i} \nabla H\right] \right\}_{ij} = \sum_{k=1}^{m} \lambda_k \frac{\partial^2 h_k}{\partial x_i \partial x_j}$$

There remain n linear equations, and there are n+m unknowns ((n-1) η's, m from $\frac{\partial \lambda}{\partial x_1}$, and $\frac{dr}{dx_1}$, a scalar).

Another m equations can be obtained from the linearized constraints

$$\nabla H(x^*) \eta = 0 \tag{3}$$

which requires that the new optimal point satisfies a linear approximation to the constraints about the original optimal solution. The readjustments are calculated from

$$\delta x_i = \eta_i \, \delta x_1$$

Results Obtained

Because the technique of the previous section utilizes linear approximations both to the LaGrange condition and the constraint equalities, and because the solution x^* may be only an approximation to the actual solution to the original problem, the values of the readjusting parameters η_i, i=2,...,n are only estimates. However, it is hypothesized that since the system model itself is by nature inexact, the values of η obtained will give a good "feel" as to the sensitivities of the design parameters to a change in any one of them. This remains to be demonstrated for the actual system model, although it has been true for various smaller-dimensional test problems.

The method requires that all constraints be considered as strict

equalities. When an active inequality is treated as a strict equality for purposes of analysis, this, in effect, requires the inequality to also be active at the new solution, x'. This assumption may not be valid, especially when two or more inequalities are active at x^*. Therefore, as a check, it is advisable to treat different combinations of the active inequalities as equalities for several runs of the problem. In addition, if the new solution x violates any inequality that was not treated as active at the adjusted solution, that inequality should be treated as active, and the problem resolved.

For simple problems (those where the true solution is observable, and calculations can be done by hand) the method has been effective in finding the readjustment parameters accurately.

Extension of the present effort will be in the following areas:

a. testing of the method with more complex problems (saddle points, ridges, linearly dependent constraints, higher dimensionality, extremely nonlinear functions)

b. investigation of the inequality problem to attempt to determine a better way to resolve the active-inactive problem

c. establishing sufficiency conditions for the method

d. allowing more than one parameter to be initially varied.

B.4. On-Board Computer Subsystem - D. Meagher, C. Boroughs, F. Samuel
Faculty Advisor: Prof. E. J. Smith

The objectives of this task are:

1. investigation of alternative internal structures (architectures) for the Mars Roving Vehicle on-board computer

2. establishment of a device to be used to test both alternative architectures and the operation of either models of subsystems or actual subsystem hardware

3. to use the results of 1) and 2) to draw conclusions about the optimal design of the on-board computer and the applicability of existing computing units.

The term 'on-board computer' is used to refer to the central processing unit and its peripheral equipment (I/O devices, memory, special processing devices, etc.). The question of on-board computer architecture relates to the internal organization of computer components, and the master control program, written to enable the computer hardware to perform specified operations.

Because the MRV must operate semi-autonomously, and because the vehicle system is by nature complex, the computer must be a highly specialized machine. How the processor should be structured, and how it should interface with its peripheral devices as well as the other vehicle subsystems are architectural considerations that can only be answered in the context of the functions that will be required of the computer.

One approach is the development of an architecture simulator, a device that allows the user to operate a general purpose computer (in this case a GEPAC - 30) as if it had a very specific and specialized hardware. This simulator has been constructed and operates in real-time in an interactive mode with the user. It provides facilities for modifying the architecture as well as the capability to simulate the operation of any vehicle subsystem and its interaction with the computer. In addition, a simulated I/O bus, interfaced through A/D and D/A converters provides the capability of actually placing hardware under the direct control of the simulation of the on-board computer.

The initial effort was directed toward reviewing the past work done on the MRV and its subsystems. A particular emphasis was placed on vehicle objectives and operational considerations in order to gain insight into the demands to be placed on the computer subsystem. A comprehensive list of the computer functions required by each of the subsystems was generated.

The next step in the design was to relate the vehicle data processing requirements to existing computer technology in an attempt to design the computer architecture. In trying to select an architecture, it was decided that a simulator would be a necessary tool. It would enable the designers of the architecture to model different architectures and to make changes in existing ones. In addition, it would allow other groups to model their subsystem, to find out its relation to the vehicle and computer subsystem.

In designing the simulator, three requirements were defined:

1. Ease and versatility for the user
2. Enable different architectures to be modeled and tested
3. Test the different subsystems using the simulator

Upon conclusion of the design effort, work on the simulator was started and completed.

The simulator package was broken up into two sections. They are the interaction control and the execution control. The interaction control section was designed for communications with the user. It accepts commands from the user enabling him to make changes to his models and to obtain information on its operation. This section is broken up into three parts. The first part receives input from a teletype and treats it appropriately as either data or

control information. The second part determines the actual command and then executes it. The third part handles all input-output (I/O) operations for all devices attached to the computer.

The execution control section performs two operations. The first is the execution of user programs. These are the programs that would control the vehicle or test the various subsystems. The second part establishes an interface with the subsystem. This can either be a computer program or an actual hardware device.

With the simulator completed future work will be towards a more complete architecture and the building of models for the various subsystems.

The proposed architecture includes a powerful instruction set. This set is capable of performing all arithmetic functions. Included are floating point operations. It also has logical operations and instructions for efficient high speed I/O operations. When vehicle system operation has been modeled to the stage where the models can be interfaced with the computer, this architecture will be tested on the simulator. At present, there are also plans to place the vehicle prototype developed at Rensselaer under direct computer control.

Task C. Navigation, Terrain Modeling and Path Selection

The mission plan to undertake a systematic exploration of Mars requires that the roving vehicle can be instructed to proceed under remote control from its landing site to a succession of desired locations. This objective requires that the vehicle possess the capabilities: of sensing and interpreting the terrain to provide the information required by a path selection system, of selecting paths with due regard to safety and other considerations, and of knowing its location and that of its destination. The task relating to the use of an orbiting satell te-vehicle navigation system was completed as of February, 1972 and the detailed progress report presented in the previous project progress report will not be repeated herein. A final report covering this task is in progress. Emphasis has been directed to the subtasks of: range measurement using lasers, discrete obstacle detection, obstacle detection systems, terrain modeling, and path selection systems evaluation. Details of the progress made are provided below.

C.1.a. Range Measurement - Gerald Zuraski
Faculty Advisor: Prof. C. N. Shen

The objective of this subtask is a preliminary design for a range measurement system to sense terrain ahead of the Martian roving vehicle. Instrumentation for a mid-range path selection and obstacle avoidance system has been investigated. A laser rangefinder is to be used to sense terrain three to thirty meters ahead of the Mars roving vehicle. The major components of the system are (1) the laser, (2) the photodetector and (3) the scanning system. The parameters of these components have been estimated as a function of the terrain reflectivity, the range to be

covered, algorithm to be used, some algorithms requiring more data than others. The 'best' system would minimize power and weight, while adequately defining terrain to ensure vehicle safety.

Range Measurement Errors

The range error is of considerable importance in evaluating the performance of navigation schemes. Various schemes have been proposed which use combinations of angle and range measurements or range measurements alone. The final choice of a particular scheme will depend heavily upon the range accuracies that can be achieved. What follows is a detailed discussion of the range error.

The range is determined by transmitting a pulse of laser light to the Martian surface and measuring the light reflected back to the vehicle. Two photodectors are employed, one senses the light emitted from the laser and the other senses the light reflected from the surface. The signal outputs of the two detectors are used to control the operation of a time interval meter. The errors involved in the measurement of the time interval arise from two distinct sources, noise and quantization.

The quantization process is shown in Figure 23. The time interval meter consists of three basic elements, (1) a square wave oscillator or 'clock', (2) a counter, and (3) a gating circuit. The error involved with the generation of the triggering waveform will be considered later. The triggering waveform initiates and stops the count. The true time interval (to wihin the accuracy of the triggering waveform) is given by $t = t_2 - t_1$. The recorded time interval is $NT = t_2' - t_1')$. The net error is the difference $e = t - NT = (t_2 - t_2') - (t_1 - t_1')$. If we denote $t_1 - t_1'$ by y and $t_2 - t_2'$ by x, the total error is $e = x - y$. x and y can be considered as independent random variables since they arise from physically independent sources. Also, for $N \gg 1$, x and y will have uniform probability densities over the interval 0 to T. The probability density of the total quantization error can be found by convolving the density functions of x and y since x and y are independent. The resulting density function is shown in Figure 24. The total quantization error is seen to have zero mean and variance given by $\sigma_e^2 = \frac{T^2}{6}$. Note also that the maximum error is $\pm T$. The range error can be related to the time error by $\sigma_R = \frac{c\sigma_e}{2}$, where σ_R = standard deviation of range error, c = speed of light, σ_e = standard deviation of time error. Thus, a $\frac{1}{4}$ nanosecond clock will produce a standard deviation in range of about 1.5 cm. Note also that the same clock will produce a maximum range error of $\pm$ 3.75 cm.

The accuracy of the triggering waveform has been estimated for one particular method of thresholding. The error involved in generating the start pulse at t_1 can be assumed to be negligible compared

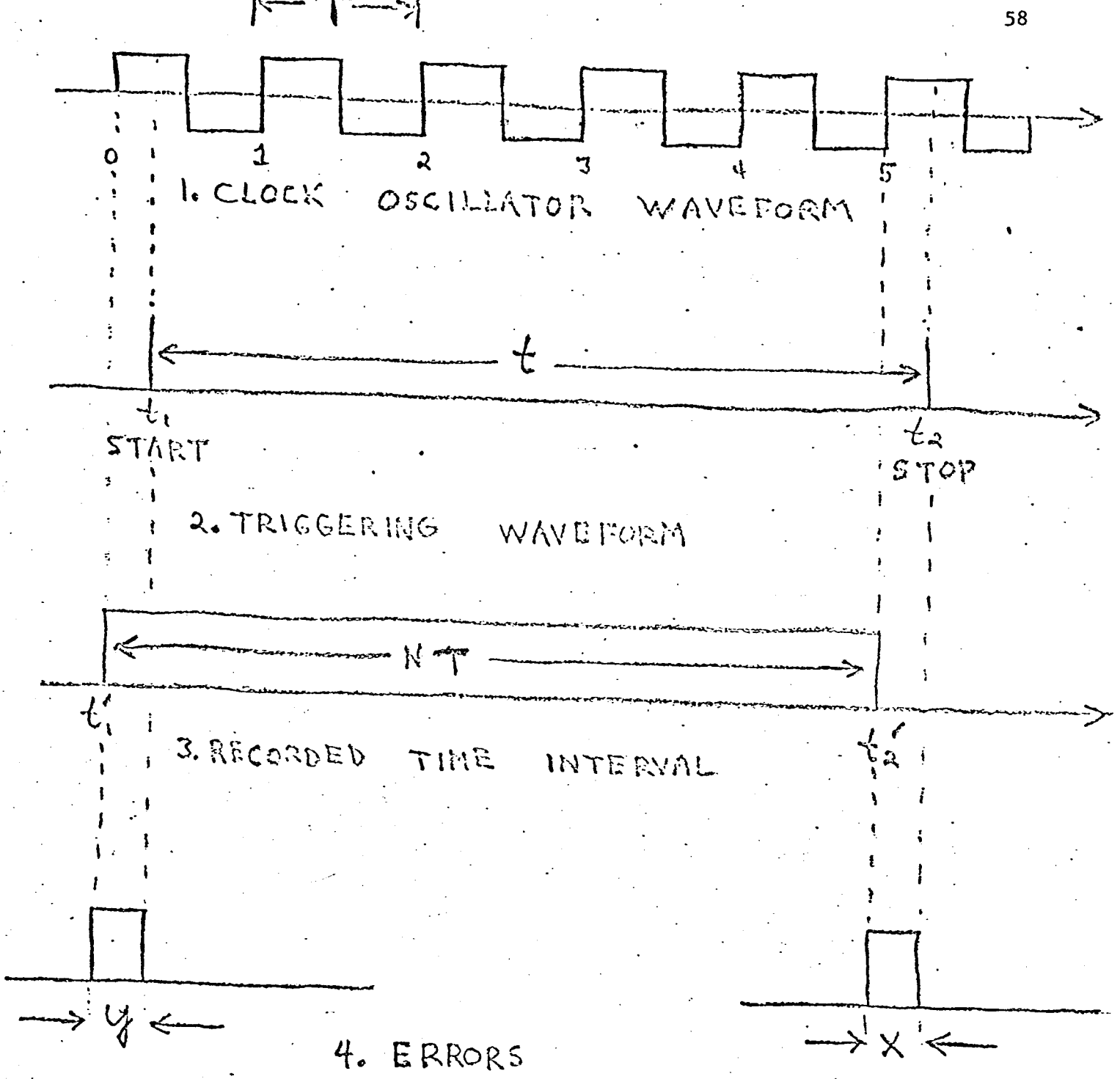

FIGURE 23. QUANTIZATION

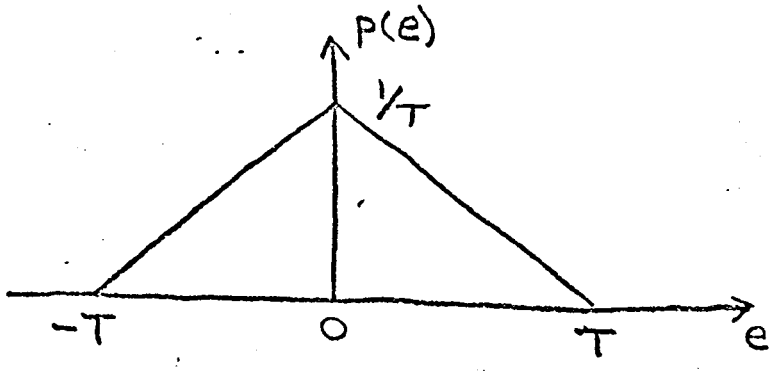

FIGURE 24. PROB. DENSITY OF ERROR

to the error involved in generating the stop pulse at t_2 since the signal-to-noise ratio will generally be much greater at t_1 than at t_2. An upper bound on the error can be derived in terms of the average slope of the transmitted pulse and the signal-to-noise ratio. The received pulse is shown in Figure 25. The average slope of the 'noiseless' signal is given by $m = \frac{2S}{\tau}$, where S is the maximum amplitude of the signal and τ is the signal duration. The pulse shape is assumed to be symmetric. If no noise is present, the thresholding device will generate a triggering pulse when the signal reaches one half of its maximum value or any other preset percentage of its maximum value. The same procedure is used to generate the start and stop triggering pulses. When there is no noise present, the only error will be the quantization error of the counter. When noise is present, it will cause an error in the generation of the stop pulse. If we denote this error by Δt, from Figure 25, the magnitude of the error is $|\Delta t| \leq \frac{N}{m}$, where N is the noise amplitude and m is the average slope of the transmitted signal. Thus, $|\Delta t| \leq \frac{\tau}{2}\left(\frac{1}{S/N}\right)$. From this equation we can draw two conclusions. First, it is desirable to have as narrow a pulse width as possible, and second, the signal-to-noise ratio should be as high as possible. The range error associated with a pulse width of 10 nanoseconds and a signal-to-noise ratio of 20 is 3.75 cm. It should also be noted that the timing error is minimized if the threshold point is placed at the point of steepest slope on the transmitted signal.

Target Cross Section

The power requirements of the laser are highly dependent upon the reflectivity of the terrain. A rough estimate of the peak transmitter power can be made by assuming the terrain to be an ideal diffuse surface (Lambert model). Snow is an example of such a surface. If the receiver field of view is greater than the target area, $P_t = \frac{2\pi R^2}{A_D \cos\theta} P_r$ where

P_t = transmitted power
P_r = received power
A_D = detector area
R = range
θ = angle between surface normal and receiver

If absorbtion of light by the surface is taken into account this equation becomes

$$P_t = \frac{2\pi R^2}{nA_D \cos\theta} P_r$$ where n = target reflectivity.

This equation was evaluated at several points to illustrate the magnitude of the different parameters. The results shown in Table 3 are for $A_D = 1$ cm^2, $P_r = 10^{-8}$ watt and $\theta = 0$. The $P_r = 10^{-8}$ watt corresponds to a signal-to-noise ratio of about 10, Ref. 12. Note

that more power is required than is shown in the table if the receiver is not perpendicular to the surface.

TABLE 3. Peak Transmitted Power (watts)

n	R = 7 m	R = 14 m	R = 28 m
.1%	30 w	120 w	480 w
1%	3 w	12 w	48 w
10%	.3 w	1.2 w	4.8 w

Experimental evidence, Re. 13, has shown that the Lambert model is approached with increasing surface roughness only when the incident light arrives in a near-normal direction. Since the measurement schemes considered for use on the rover require the incident beam to arrive at shallow angles, a better model is needed. Such a model has been developed by Torrance and Sparrow, Ref. 13. The major features of the model are (1) small random mirror like facets, (2) multiple reflection, (3) internal scattering, (4) shadowing, and (5) masking. The model generally applies when the root-mean-square surface roughness is greater than the wavelength of the light used.

The reflectance distribution is specified in terms of a normalized bidirectional reflectance.

$$\frac{P(\psi;\theta,\phi)}{P(\psi;\psi,0^\circ)} \quad \frac{g F(\psi,\hat{n})[G(\psi_p,\theta_p)/\cos\theta]\exp(-C^2\alpha^2)+\cos\psi}{g[F(\psi,\hat{n})/\cos\psi]+\cos\psi}$$

The angles ψ, θ and ϕ are shown in Figure 26. The Fresnel reflectance $F(\psi,\hat{n})$ is a strong function of ψ for $60^\circ < \psi < 90^\circ$, which is the range of angle that must be used in the rangefinding system. As an example, the Fresnel reflectance for magnesium oxide varies from .1 to 1 over the range of ψ cited. The Fresnel reflectance also varies widely with material. The shape of the Fresnel curves differ markedly for metals and nonmetals.

The factor $G(\psi_p,\theta_p)$ takes into account the geometry of a rough surface (a V groove model is used). C and α define the distribution of facet slopes about the mean-surface plane. g is an arbitrary scale factor used to fit the model to experimental data. Typical curves for the bidirectional reflectance ratio are shown in Figure 27. The dashed line represents the Lambert model. Note that peaks in the distribution occur at angles greater than the specular angle. These off-specular peaks are caused by the factor $G/\cos\theta$ in Equation (1). It should be noted that $G/\cos\theta$ is strictly geometrical, and thus all materials will exhibit the off-specular peaking.

Since the actual magnitude of the bidirectional reflectance

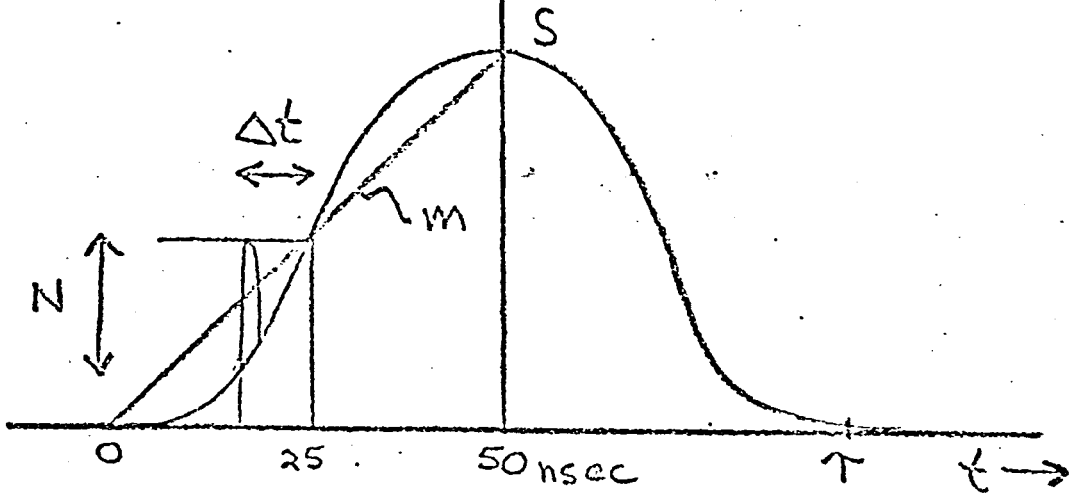

FIGURE 25. RECEIVED PULSE

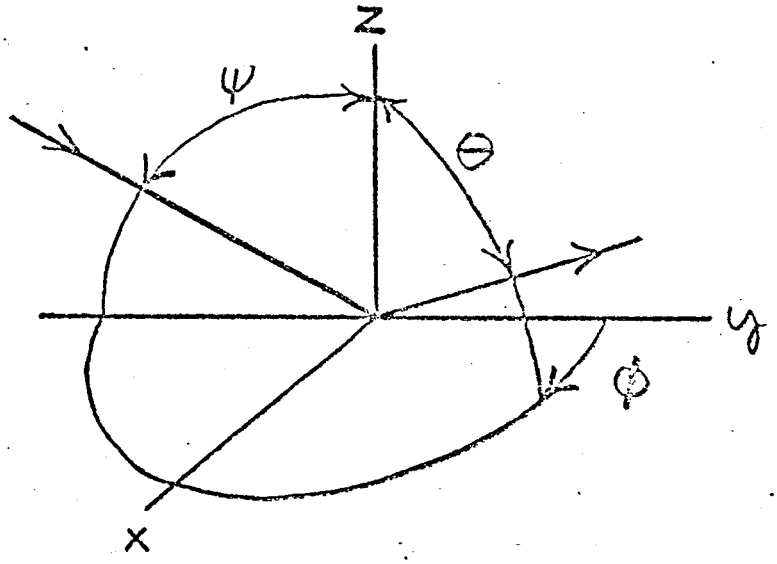

FIGURE 26. Ψ, Θ, Φ

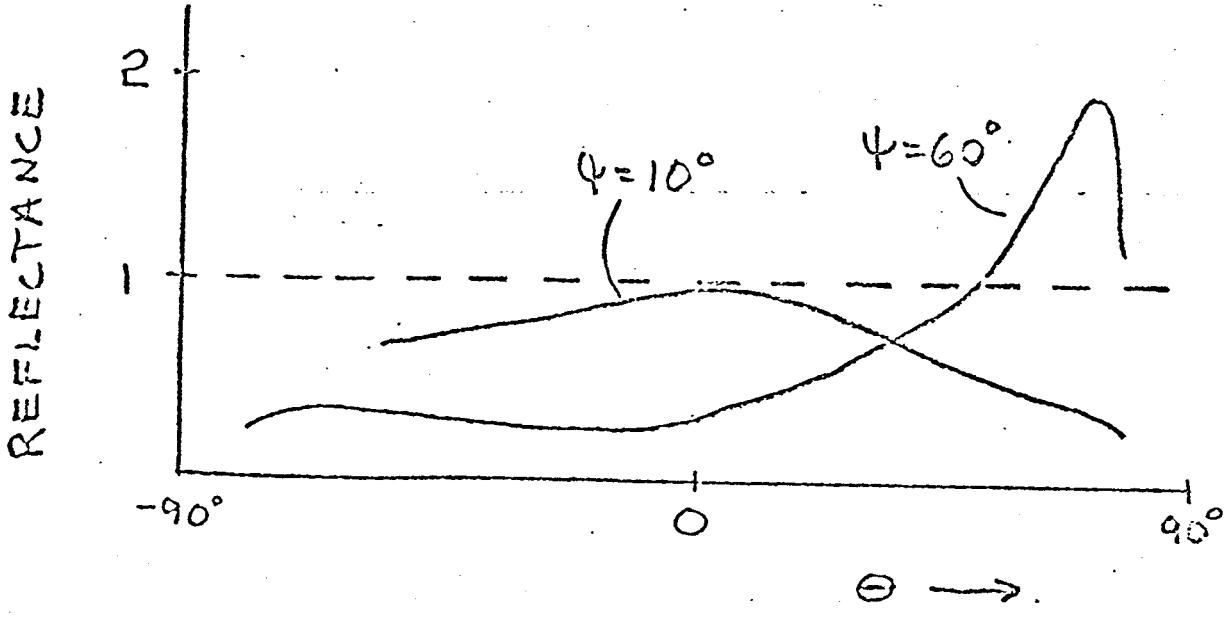

FIGURE 27. BIDIRECTIONAL REFLECTANCE

ratio is almost impossible to predict, an experiment is recommended for future work in this area. The primary objective of the experiment would be to determine the dynamic range of the reflectivity. Samples used in the experiment should be of varying degrees of roughness and material composition and measurements taken over a wide range of angles relative to the mean surface normal. The results of such an experiment could then be used to determine if controlled power output of the laser is necessary in order to prevent detector damage or detector saturation.

The spectral reflectance of two types of surfaces, Ref. 14, is shown in Figure 28. The reflectance is assumed to be measured normal to the surface although the reference did not explicitly state how the measurement was made. In any case, it is important to note that the reflectivity increases as wavelength increases. The near infrared part of the spectrum is therefore a better choice than the visible part of the spectrum.

Detectors

Consideration must be given to the protection of the detector from intense radiation when the vehicle gets close to a specular surface. Under such conditions, almost the entire output of the laser could be focused upon the detector. As an example, consider a typical PbS detector, Ref. 15, whose damage threshold is 0.32 J/cm^2. A fast rise time detector, Ref. 16, has an active area of approximately $2x10^{-5}$ cm^2. Thus, the maximum input energy per pulse is $0.32x2(10)^{-5} = 6.4x10^{-6}$ Joules. If we consider a laser with a pulse width of 50 nsec, the damage threshold in terms of peak output power of the laser would be $6.4(10)^{-6}/50(10)^{-9}$ = 130 Watts. If the laser's output is restricted to be less than 130 Watts peak, no damage will occur for this particular detector. Similar calculations could be made to determine the damage threshold in terms of peak power output of the laser for other detectors.

Another problem relating to excess radiation is saturation. The larger the input energy, the longer it will take for the detector to recover. This is due to the finite charge carrier lifetimes of semi-conductor materials. Recovery time can be as long as several milliseconds, Ref. 15, which could restrict the maximum scan rate. In view of this, it is desirable to operate a detector with the lowest input that will produce a reasonable signal-to-noise ratio. This is also consistent with minimum laser power.

TABLE 4. Photodiode Characteristics

Diode	Wavelength Range (μm)	Peak Efficiency (%)	Sensitive Area $(cm)^2$	Capacitance (pF)	Series Resistance (Ω)	Response Time (sec)	Dark Current (A)
Silicon n+-p	0.4-1	40	$2x10^{-5}$	0.8	6	$1.3x10^{-10}$	$5x10^{-11}$
Silicon p-i-n	0.6328	90	$2x10^{-5}$	1	1	$1x10^{-10}$	10^{-9}
Silicon p-i-n	0.4-1.2	90 @0.9 μm	$5x10^{-2}$	3	1	$7x10^{-9}$	$2x10^{-7}$
Ge n+-p	0.4-1.55	50	$2x10^{-5}$	0.8	10	$1.2x10^{-11}$	$2x10^{-8}$

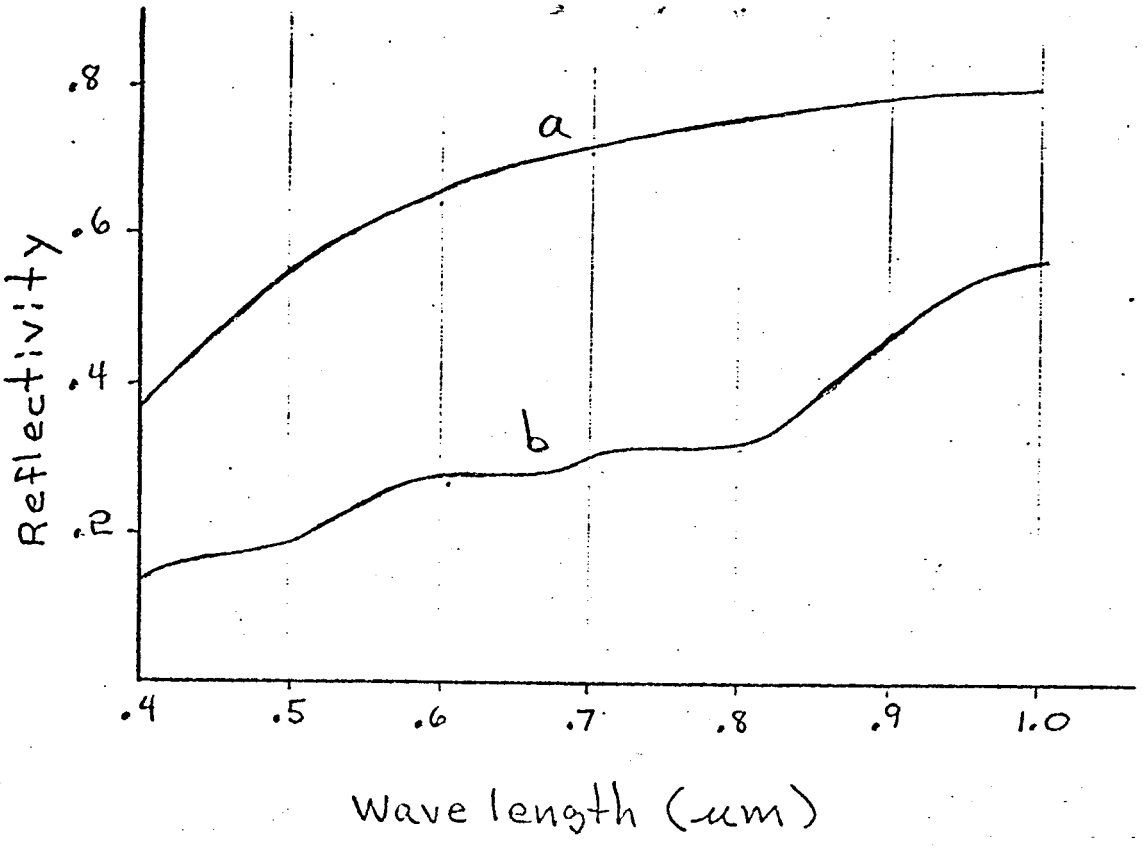

(a) limestone, clay, & similar bright objects
(b) sands and bare areas in the desert

Figure 28. Spectral Reflectance

Characteristics of several high speed photodiodes are given in Table 4, Ref. 16. It can be seen that there is a tradeoff between response time and peak efficiency. A diode with a response time of 0.13 nsec has an efficiency of 40% whereas a similar diode with a response time of 7 nsec has an efficiency of 90%. Note also that the slower diodes have larger sensitive areas. All of the photodiodes listed in Table 4 operate at room temperature ($300^{o}K$).

The Laser

A semiconductor laser is probably the most likely candidate for use in the ranging system because of its small size. The spectral range of several semiconductor lasers is given in Table 5, Ref. 17. Those may be operated in pulsed mode at room temperature.

TABLE 5. Semiconductor Lasers

Material	(m)
$Al_{1-x}Ga_xAs$	.63-.90
$GaAs_{1-x}P_x$	.61-.90
GaAs	.83-.91

A variety of GaAs lasers are available, Ref. 18, with an energy conversion efficiency of about 4%. The nominal wavelength is 9050 A with a drift rate of 2.5 $A/^{o}C$. The duty cycle of these devices is 0.1% for units with a peak power output of 10 Watts or less. For output powers up to 300 Watts, the duty cycle is 0.02%. If we assume a 50 nsec pulse, the repetition rate for the lower power devices is 20,000 pulses per second and for the high power devices is 4,000 pulses per second. Thus 1,000 range measurements per second is a conservative estimate of the capability of the laser. Since the wavelength shifts with temperature, the spectral filter at the detector must be broad enough to accommodate this shift. A spectral filter with an optical bandwidth of 100 A can tolerate a $40^{o}C$ temperature shift. Consideration should be given to minimizing the temperature rise of the GaAs laser (i.e. by heat sinking) since the power output may decrease and a wide spectral filter will be required thus degrading the signal-to-noise performance of the system.

Scanners

An electronic scanning system is thought to be more desirable than a mechanical scanning system from the standpoint of reliability, weight and power. Thre is a wide range of electronicly controller scanners presently available, Ref. 19. These include piezoelectric devices, bender bimorphs, bimetallic strips and electro-optic crystals. Of these the piezo-electric laminated bimorph looks very promising. Power requirements are very small (milliwatts) and units with scan rates of 0.2 msec with a 6^{o} angular scan are commercially available, Ref. 20. Acousto-Optic deflectors using lead-molybdate, Ref. 21, can achieve scan rates of 300 kHz but the angular scan is reduced to $\pm$ 2.5 milliradians. The total angular scan can be increased by using

a lense, however the angular resolution will remain equal to that of the scanning device. Resolution varies, typically 100 to 400 elements. A two dimensional scan can be achieved by using two scanning devices placed so that one scans perpendicular to the other. A possible scanning system is illustrated in Figure 29. An advantage of this configuration is that the transmitter and receiver use the same beam steering devices, thereby providing automatic tracking.

Conclusion

A reasonable rangefinding system can be constructed from presently available components. A Gallium Arsenide injection laser operating at 9000 A°can be used for the transmitter. A silicon p-i-n photodiode can be used as the receiver. The beam scanning can be accomplished electronically by means of electro-optic beam deflectors. Present day technology can provide the fast risetimes necessary to achieve a range error on the order of 5 cm. The components chosen are small, lightweight, and do not require high operating voltages, nor large amounts of power. Thus, the feasibility of using a gallium arsenide laser, a silicon p-i-n photodiode, and electronic scanning has been established. The terrain reflectivity is known only approximately at present. The dynamic range of the reflectivity must be investigated further. If the dynamic range is large, it may be necessary to control the power output of the laser as well as using automatic gain control at the receiver. There are three major areas to be investigated in future work. First, an experiment to estimate the range of terrain reflectivity should be undertaken. The data obtained from this experiment should be compared to the theoretical model presented in this paper. Second, the circuitry of the rangefinding system should be investigated. Third, the optics of the scanning system should be investigated to determine how wide a scan can be achieved. After this work has been accomplished it will be possible to accurately determine the weight and power requirements of the entire system.

C.1.b. Discrete Obstacle Detection - William Mounce
Faculty Advisor: Prof. C. N. Shen

A problem crucial to the autonomy of a Martian roving vehicle is the detection, identification, and avoidance of obstacles and terrain dangerous to the vehicle's safety. The problem may be divided into two parts: discrete obstacles such as rocks, craters, crevasses, and slope obstacles which would waste power, cause sliding, or possibly overturn the vehicle. This project is concerned with the design and analysis of a split-beam discrete obstacle detection system for possible use on the Martian rover. The system is based on the comparison of the return times of the two parts of a split laser pulse reflected off the surface in from of the vehicle. A discrete obstacle causes a large variation of this time difference from that expected if the terrain were flat, thus indicating an obstacle.

The system described above has been analyzed for a variety of rover and terrain conditions to determine its feasibility, and the necessary design considerations. One of the more important areas of

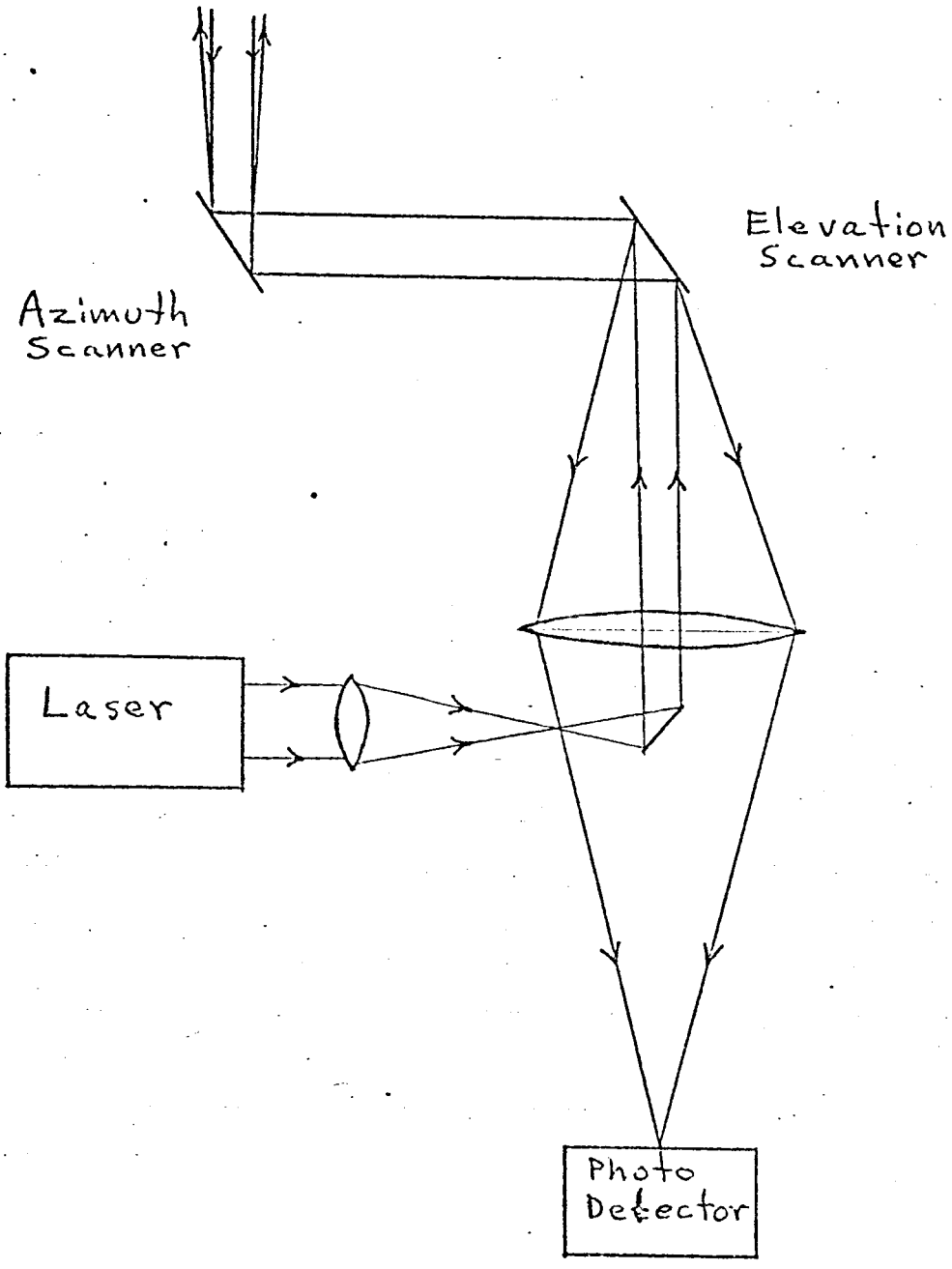

Figure 29. Scanning System

study was the effect of rover motion on this system. It employs a point by point comparison only. The fixed base for taking data needed for a complete terrain map, Ref. 22, 23, is not required and a working system, while the rover is in motion, may be available. The results of the analysis show that if the scan distance is kept within about 10 m. from the vehicle, this system could very well handle this problem. Also, the possibilities for instrumentation were explored with several options presented and the best scanning scheme and decision algorithms were described.

A positive discrete obstacle may be defined by a vertical height, h, and the incident slope, m, in the forward path of the rover, since these are the parameters encountered. Both parameters must be considered to judge a possible obstacle's danger; for example, a mound and a step of the same height do not pose equal hazard.

A negative obstacle is a more difficult problem due to the hidden region behind its rim; thus the in-path slope loses its meaning and only the depth may be considered. Any obstacle detection system must consider the height and slope or depth of obstacles to the vehicle's capabilities to find a safe path. Past work on the problem at Rensselaer required a stationary rover and included large instrument errors, Ref. 24. Thus, another method was chosen.

The split-beam obstacle detector shown in Fig. 30 has a single laser pulse emanating from a fixed height sensor, A, which is split so as to illuminate the surface in front of the rover at two distinct points. The first point is designed to be a fixed distance, x, from the rover when it is on a plane surface. Because the ideal geometry is fixed, the return time difference between the two parts of the pulse may be determined from the system and obstacle parameters and the speed of light, c;

$$\Delta tf = 2/c \left(A\sqrt{1+\left(\frac{x+h\cot(m)}{A-h}\right)^2} - \sqrt{A^2+x^2}\right) \quad (1)$$

For obstacle detection, the actual return time difference Δt is compared to Δtf and if the difference is great enough, as determined by set thresholds, an obstacle is indicated. Mathematically, if Δtd is the set threshold, an obstacle is indicated when $\Delta t > \Delta tf + \Delta td$ or $\Delta t < \Delta tf - \Delta td$ as shown in Fig. 31. The threshold is, in terms of system parameters:

$$\Delta td = 2/c \left(h\sqrt{1 + \left(\frac{x+h\cot(m)}{A-h}\right)^2}\right) \quad (2)$$

and the critical points in time are

$$\Delta tf - \Delta td = 2/c \left[(A-h)\sqrt{1+\left(\frac{x+h\cot(m)}{A-h}\right)^2} - \sqrt{A^2+x^2}\right] \quad (3)$$

$$= 2/c \left[\sqrt{(A-h)^2 + (x+h\cot(m))^2} - \sqrt{A^2+x^2}\right] \quad (4)$$

$$\Delta tf + \Delta td = 2/c \left[(A+h)\sqrt{1+\left(\frac{x+h\cot(m)}{A-h}\right)^2} - \sqrt{A^2+x^2}\right] \quad (5)$$

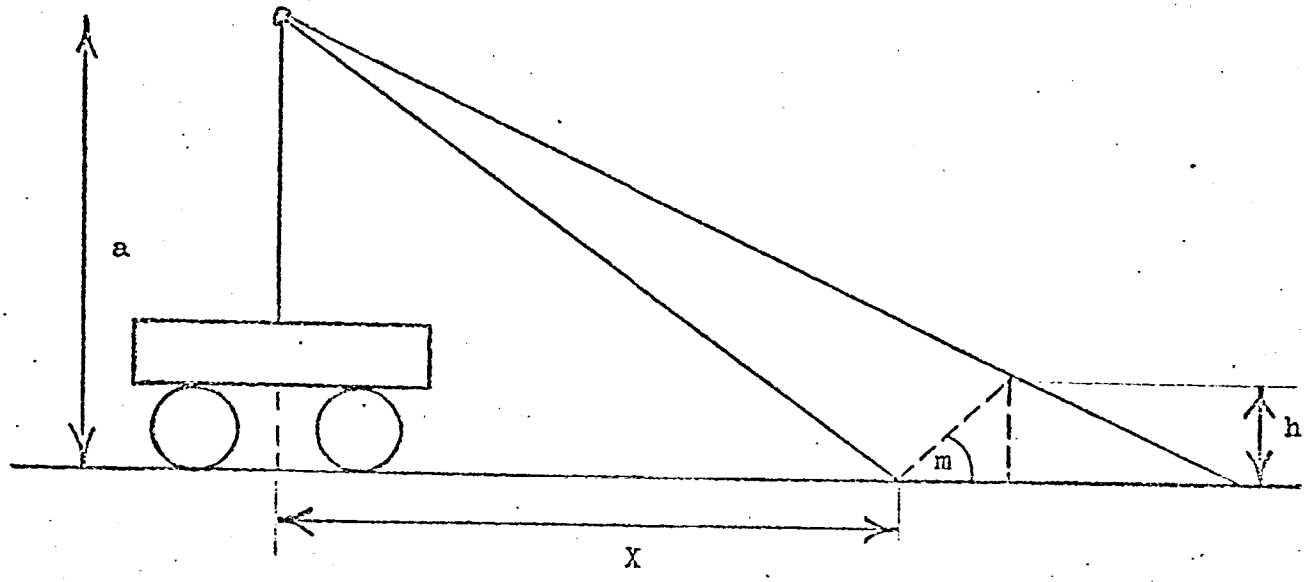

Figure 30. Measurement Geometry

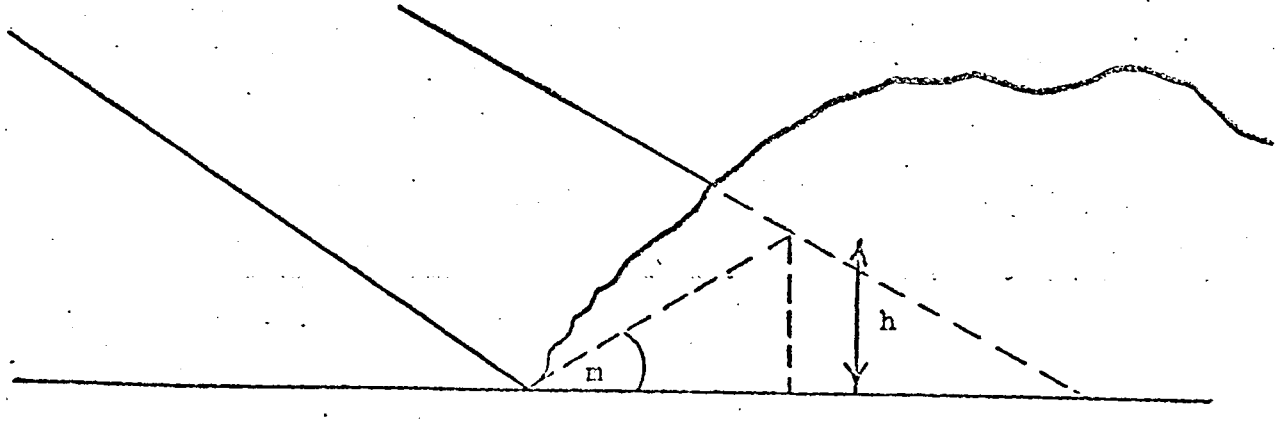

Figure 31. Positive Obstacle Detection

For the analysis of this system, the following cases were considered for their effect on the system; the rover tilted up over a rock or down into a crater (Figs. 32 and 33) and the lower beam of the split pulse incident on terrain is not the same height as the plane formed by the rover's wheels, such as a rock or a crater in its path. Fig. 34 shows the first problem, the degradation of the critical height and slope parameters as the rover tilts to 10^{o}, depending upon the original scan distance, x, set for the system. As the tilt gets larger, the height, h, considered an obstacle, becomes larger than the design h of 1/2 meter, taken as wheel radius of RPI MRV. This clearly shows that the closer the scan is to the rover, the more insensitive the detection scheme is to tilts. If the rover is level, but the lower beam is not hitting the rover plane, an error is also introduced as shown in Figs. 35 and 36, where the worst case is a 1/2 m object. The maximum error here is .09 m, which is not large. Another factor, visibility into craters is also determined by scan distance, and favors a close scan. For example, at x = 10 m, the smallest 1/2 m deep crater detected is 1.6 m wide, which could be dangerous. All of these considerations favor a scan as close to the rover as possible, but this distance must also be chosen in the light of the vehicle's stopping distance and turning radius. Thus the optimum scan distance would be 5-10 m from the vehicle. To minimize detection errors due to the rover tilting with respect to the plane of the obstacle, the distance between the sensor and the incidental terrain along one of the parts of the split beam could be measured roughly to determine if the length is considerably longer or shorter than designed; thus invalidating the readings at that point. For example, a scan set at 7 m impinges at 11 m with a 7^{o} rover tilt and the critical height becomes .8 m instead of .5 m. If the worst case error is set at .7 m, then any tilt above 5^{o} gives invalid data and should be ignored. (For a 4 m long rover and a .5 m maximum step, the worst tilt is 7^{o}).

The scanning scheme in the horizontal plan for the split beam, Fig. 37, must "blanket" the surface so that no obstacles go undetected. It is assumed that the rover has a speed of about 2 km/hr, Ref. 24. and an arc covering about two rover widths on either side of the line of travel. To provide covered turning space, a terrain coverage by a .1 m by .1 m grid of data points would require 600 pulses per second, which is far exceeded by present laser technology, Ref. 25 and 26. The scanning may be accomplished by a carefully timed spinning mirror or one of the new electro-optic devices now appearing, Ref. 25. One problem not considered by this scheme is the cross path slope danger. How bad this is may be calculated by considering the rover width against the worst "safe" terrain. The greatest cross path slope occurs when a depression not quite .5 m deep is beside a rock not quite .5 m high with one wheel of the rover resting on each. (Greater rocks and craters are detected obstacles). The resulting tilt is 30^{o}, which must be compared to vehicle capabilities.

The decision algorithm can be as sophisticated or as simple as desired. In its simplest form, a go no-go decision at each scan point determines directions to be avoided, weighted, of course, by the desired heading. This could be improved by correlating adjacent data points to override poor or erroneous data, or more completely define obstacles. For example, a crevasse smaller than one detected by two

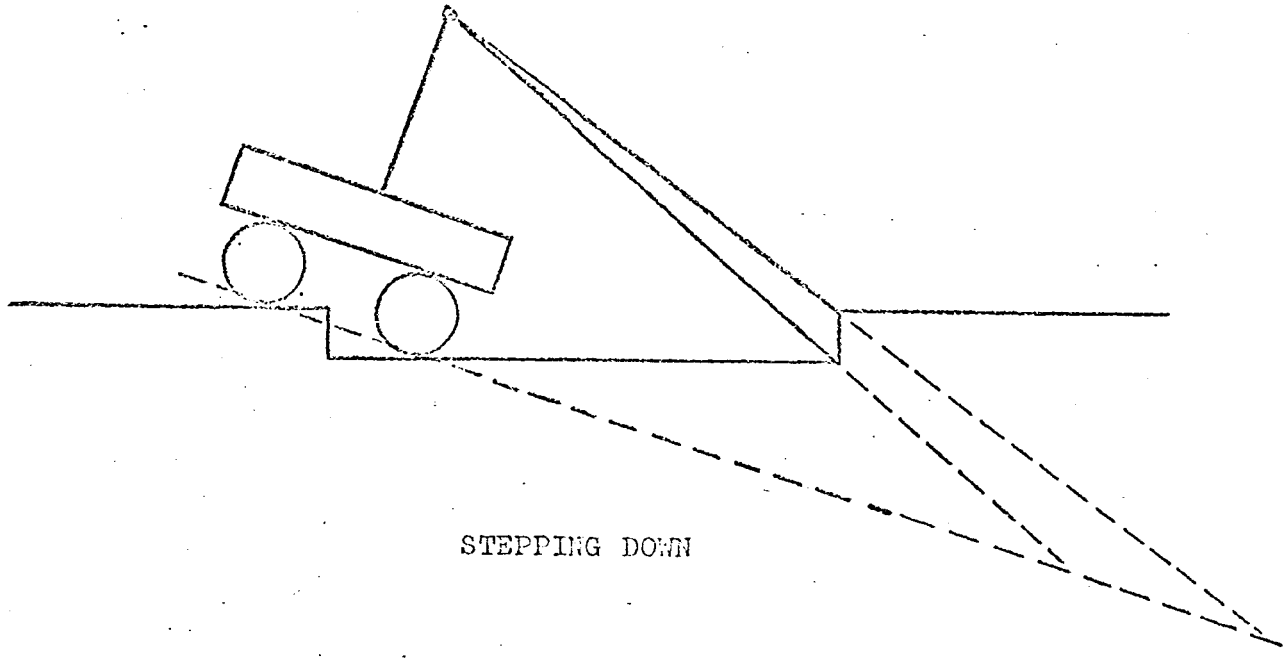

Figure 32. Detection Errors

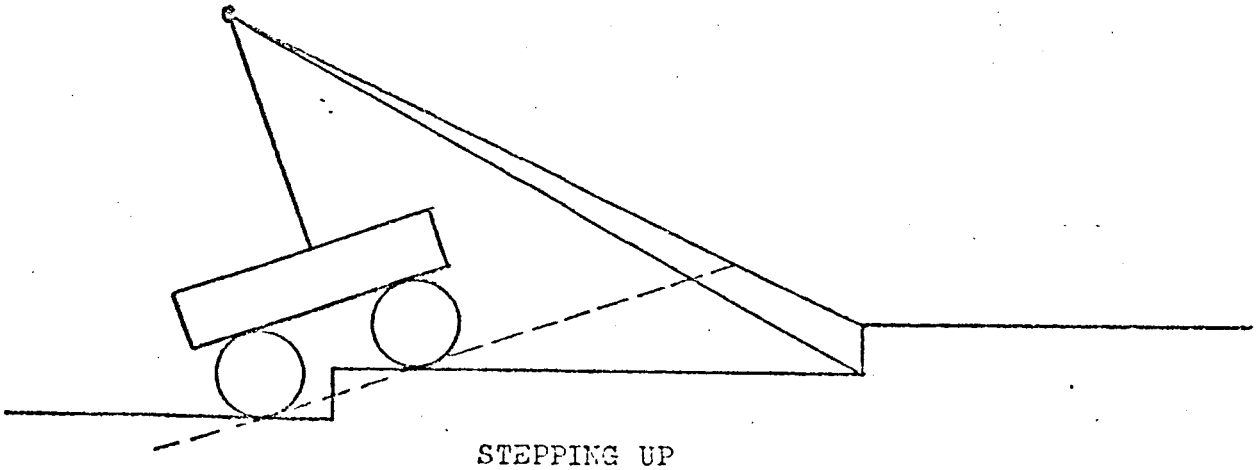

Figure 33. Stepping up

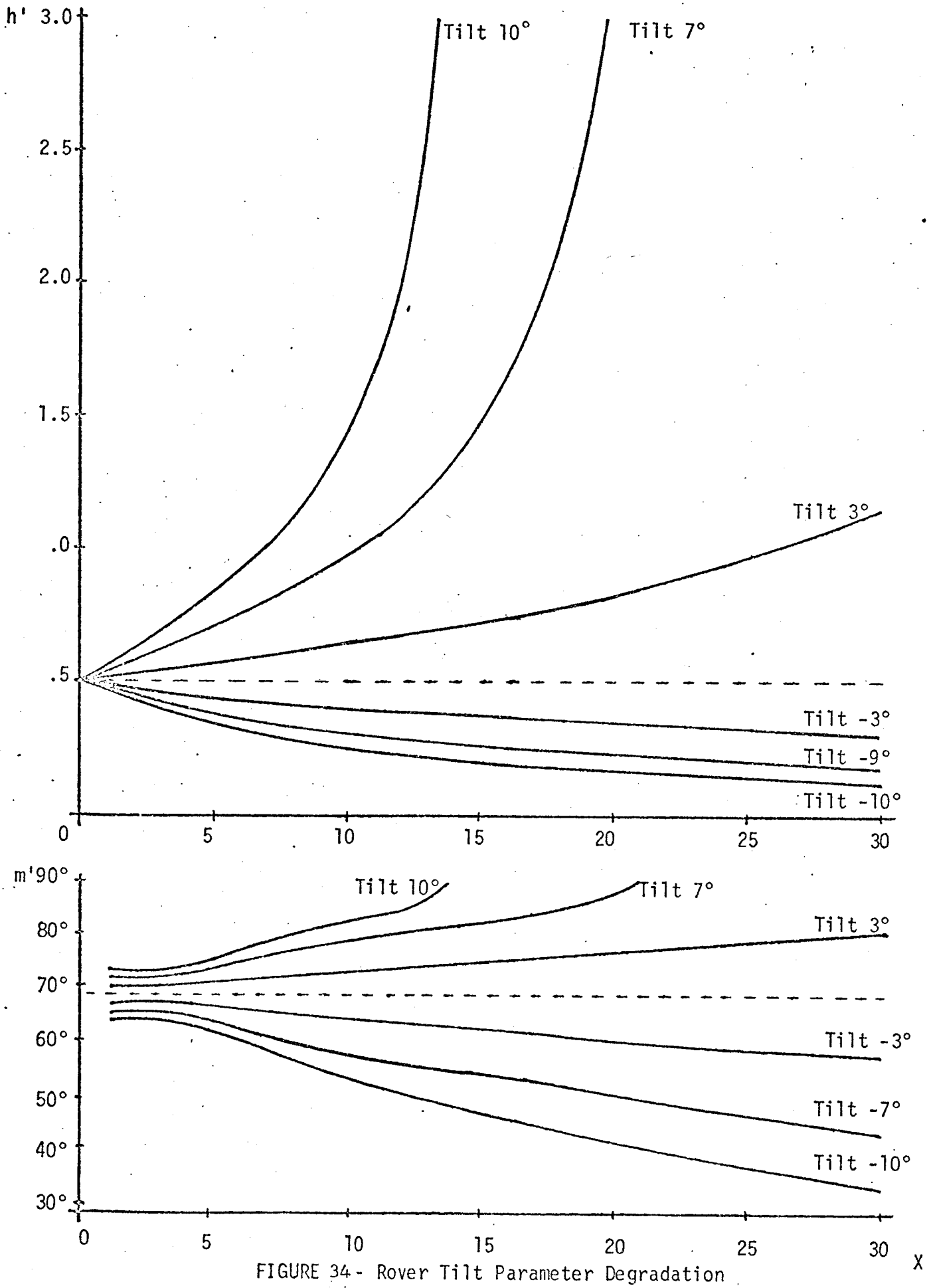

FIGURE 34 - Rover Tilt Parameter Degradation

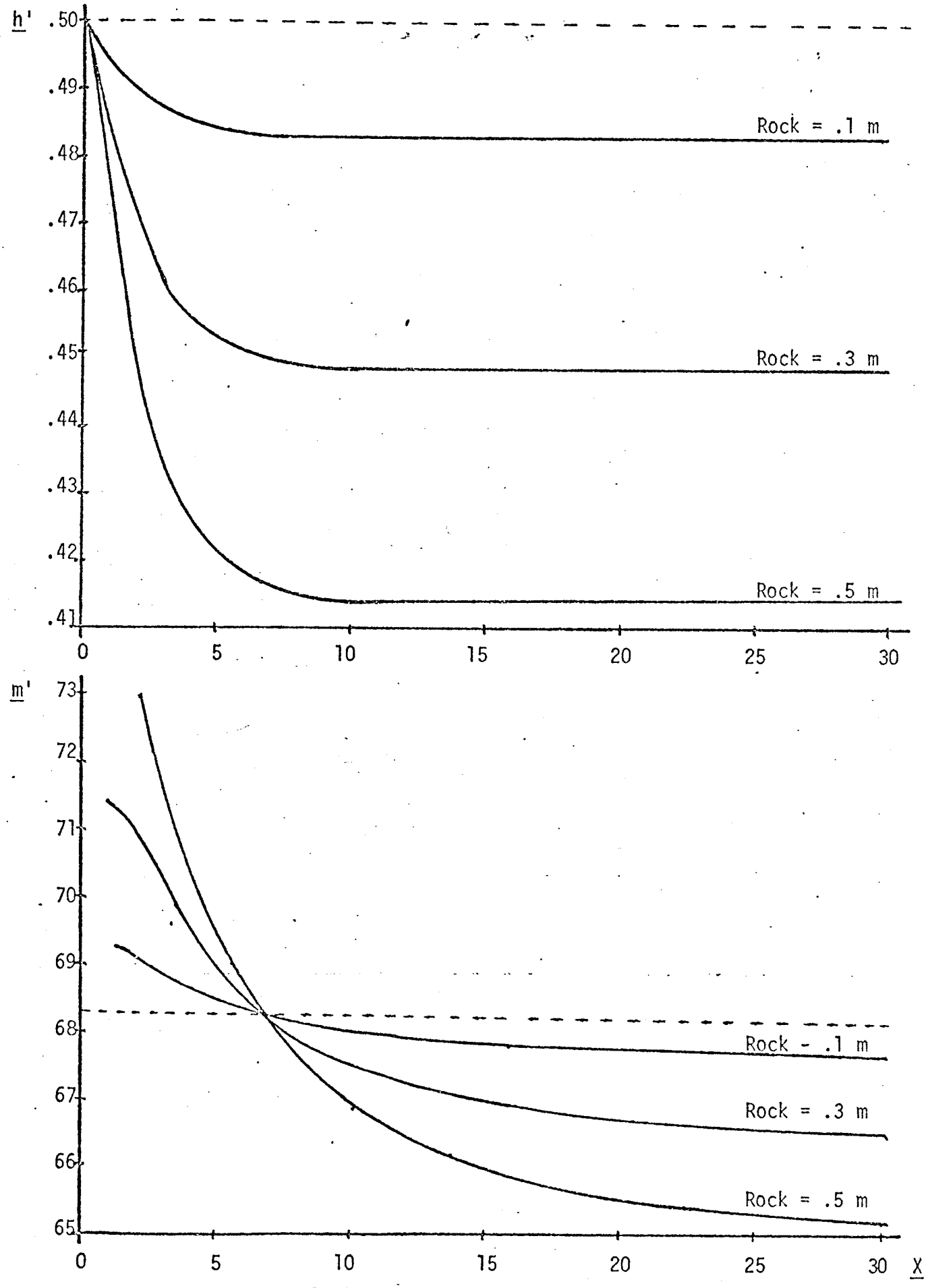

FIGURE 35. Rock in Lower Beam

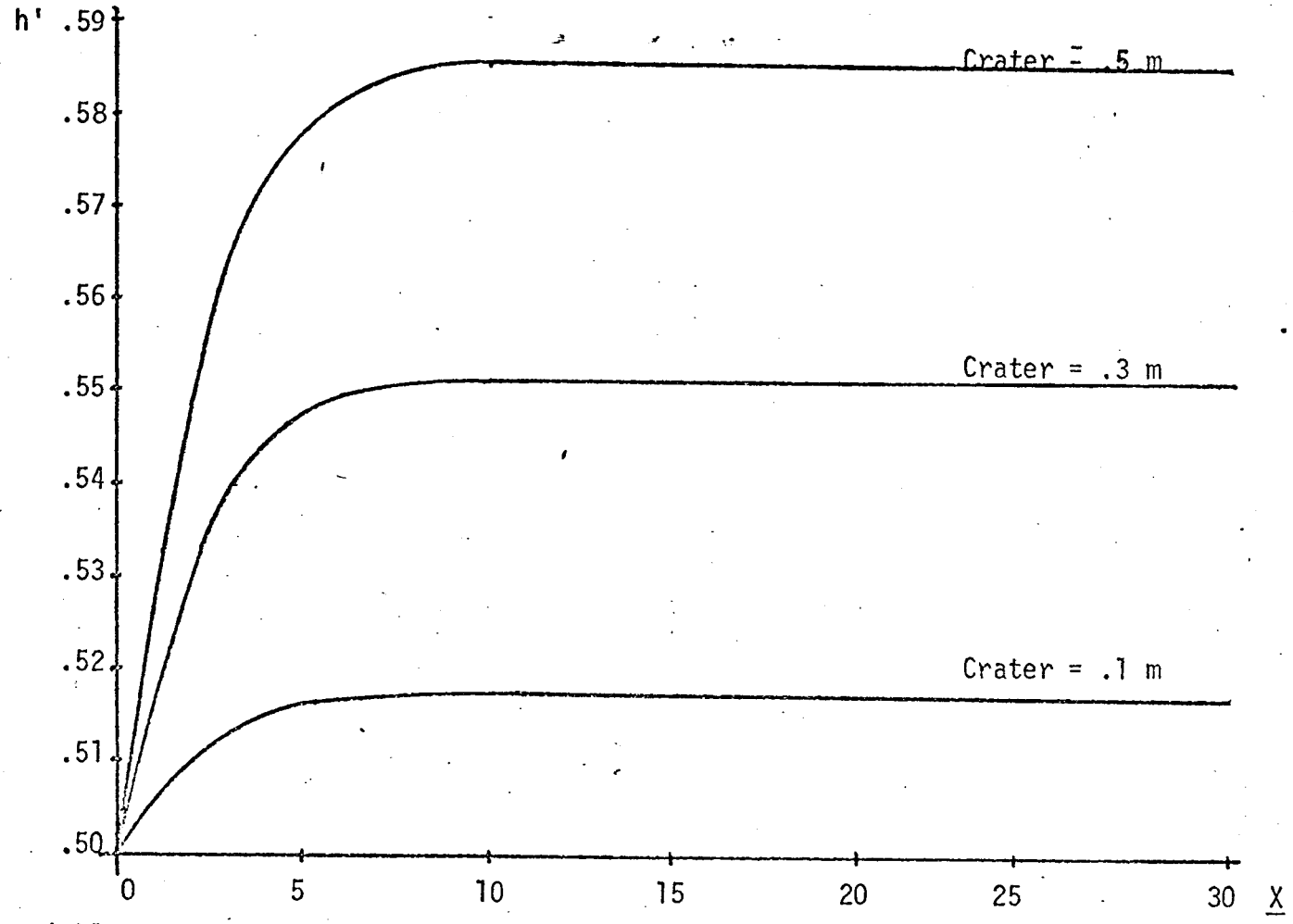

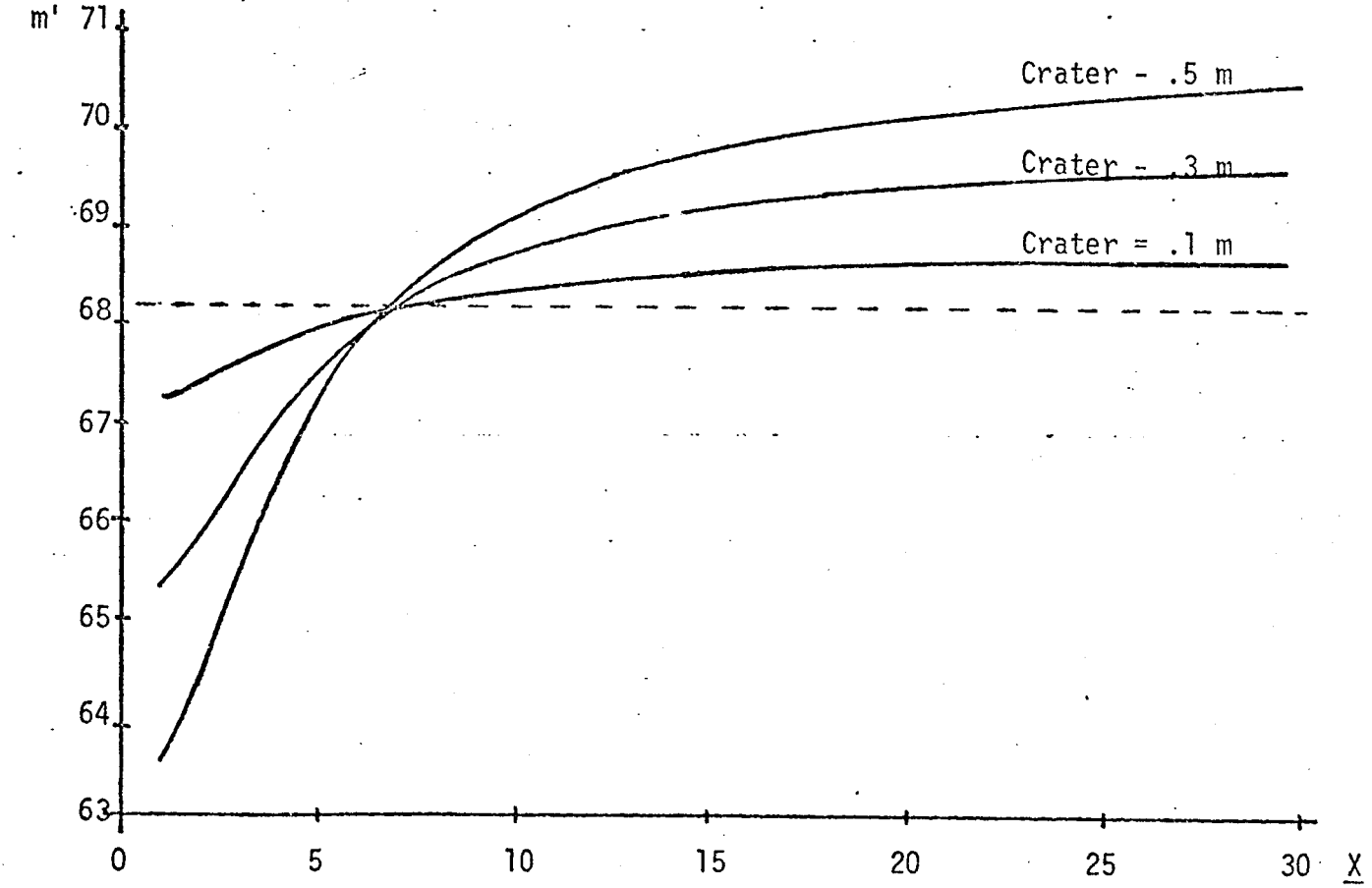

FIGURE 36.- 1/2 m Crater in Lower Beam

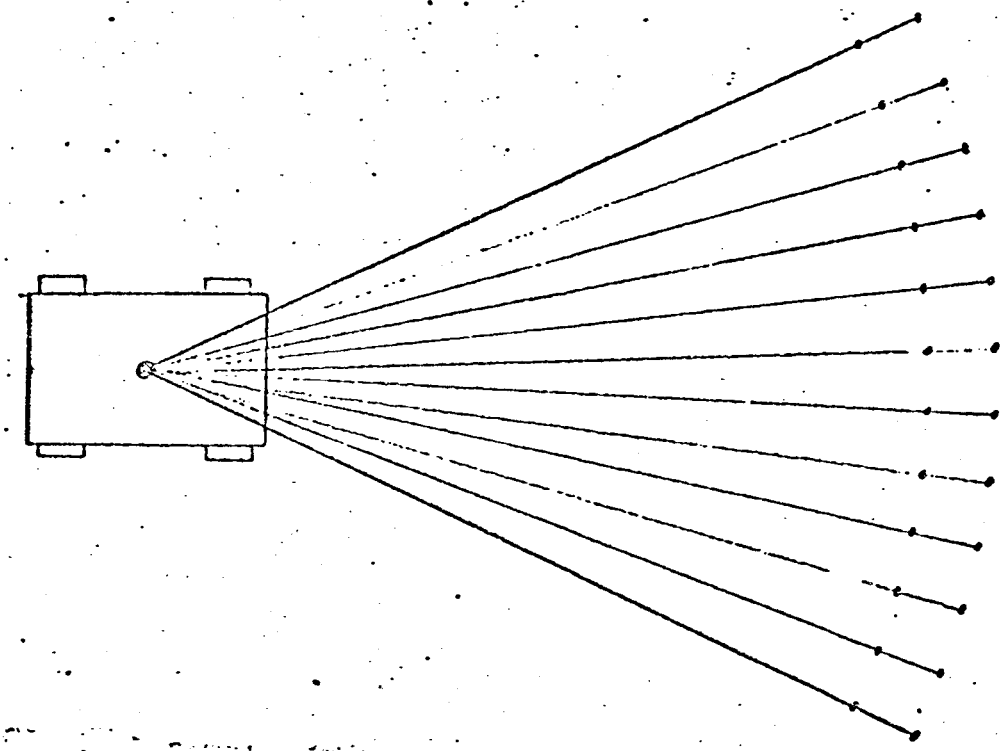

Figure 37. Scan Pattern

adjacent beams is of no danger if the spacing is .1 m. A more complex scheme using scans at two different ranges is also possible; a far warning and a closer insurance scan to give the best vehicle safety. The end result depends on computer, power, and accuracy requirements.

Splitting the output beam of a laser is on the surface a very simple task employing either a half-silvered mirror or an electrified double prism intersecting half the beam, Ref. 27. The problem is that under certain terrain configurations, the ambiguity in which part of the beam returns first may result in a misclassification of unsafe terrain. There are several possible solutions depending on the frequency, pulse width, and power consumption desired, and the final choice would probably depend on experimental results. The best possibility from a system viewpoint would be a laser which transmits at two distinct frequencies which could be split by a prism and detected by two frequency selection dectectors. Unfortunately, the gas and solid lasers which have this property, transmit more than two frequencies and require large amounts of power, Ref. 27. The neodymium laser is possible with a visable center frequency and a strong infrared harmonic. For energy efficiency, the semi-conductor lasers are best with specially doped gallium-arsenide lasers operating in the green and red regions, monochromatically, Ref. 26. To avoid the ambiguity using these, a single beam may be split and one part delayed by fiber optics or mirros, or two separate lasers at different frequencies could be used. The problem with two lasers is the inaccuracy in the time the pulse starts. These possibilities and new advances in the state of the art should be explored to find the best available system.

Future work should involve finding the best split beam laser, and actually testing the system on various terrains. Most of the sources of error have been theoretically analyzed, but only under test will all the problems and inherent inaccuracies become apparent.

C.1.c. Obstacle Detection System - John Golden
Faculty Advisor: Prof. C. N. Shen

The objective of this task is to develop a design for the short range obstacle detection system of the Mars rover, amenable to the characteristics of the RPI Mars Roving Vehicle (MRV). The design is an autonomous system using range-finder data to model the terrain in terms of its height and slope characteristics. Basic to the system is the laser/detector investigated under Task C.1.a., Ref. 28, and capable of restricting range error (standard deviation) to 5 cm. The system is defined in the following sections under obstacle definition, data acquisition method, and path selection. System operation and analysis, especially as to data error, are also explained.

Obstacle Definition

A first step to detecting obstacles on the unknown Martian terrain is approximating this terrain by discrete obstacles, i.e., the entire terrain is flat except for discontinuous obstacles-both positive and negative obstacles. A method of navigating through such terrain involves measuring the height of all terrain, then rejecting

as unpassable any heights above .44 m or below - .44 m, as shown in Table 6.

TABLE 6. RPI MRV Parameters

Maximum Step Navigable	.44 m	= Radius of Rover wheel
Maximum Negative Step	-.44 m	= Radius of Rover wheel
Widest Crevice Fordable	.66 m	= 3/4 Diameter of Rover Wheel
Maximum Slope Climbable	$\pm 25^{o}$	
Rover Speed	5 miles per hour, maximum	
Rover Width	3 meters	
Rover Stopping Distance	<1.5 meters	

Such a system is capable of directing rover safely, because it eliminates all unsafe terrain. Some of the terrain eliminated, however, is actually passable because a gradual slope precedes an excessive height. Figures 37 and 38 show situations where height or depths are excessive but the terrain is still passable because of the gradual slope or minimal extent of negative obstacles. Thus, the system eliminates too much passable terrain, causing rover to turn too often, therefore wasting energy in turns and in the extreme, eliminating all the terrain so that rover cannot move. To eliminate these failings, the system with step heights is supplemented by slope data. Now an obstacle exists only if its height magnitude is over .44 m and if the slope magnitude preceding it is more than 25 degrees, (see Table 6).

Method of Data Acquisition - Type of Data

For the normal, non-stereo mode, range and angle measurements are made, as in Fig. 37. These measurements, along with the known deviation of sensor staff from the local vertical, allow the system to compute base b and height h of the terrain. These values in turn allow the computation of slope: $S = (h_2-h_1)/(b_2-b_1)$. Different points in the terrain are investigated by using a laser/detector which rotates about a vertical axis and sends out discrete scans in azimuth directions.

Scanning Rates: Such a discrete scanning technique introduces some unknown terrain between data points. Now, below .66 m of unknown terrain, the rover can ford over an undetected crevice. Therefore, the scan must be made fast enough to insure a maximum of 0.66 m between in-path points for all situations. Worst case situation is depicted in Fig. 39 in which the rover tries to see over the crest of a hill. Were the system to fix the speed of scan of this worst case situation, the rover would be taking data every few centimeters -- which is a gross waste of laser power when navigating level terrain and slows down rover motion unnecessarily. To rectify the problem, a variable scan rate is employed, or the vehicle is simply driven more slowly uphill. A typical scan rate for level terrain, at rover velocity of 1 meter/second is .66 seconds per scan: or a scan rate of about 2Hz.

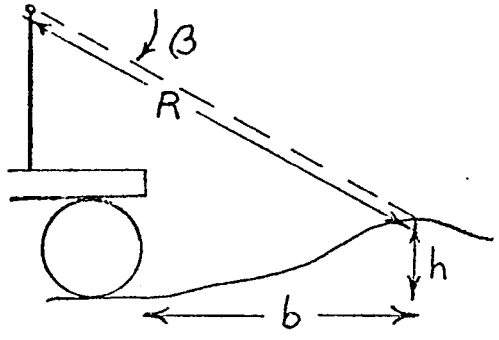

Figure 37
Positive Features
and
Data Acquisition

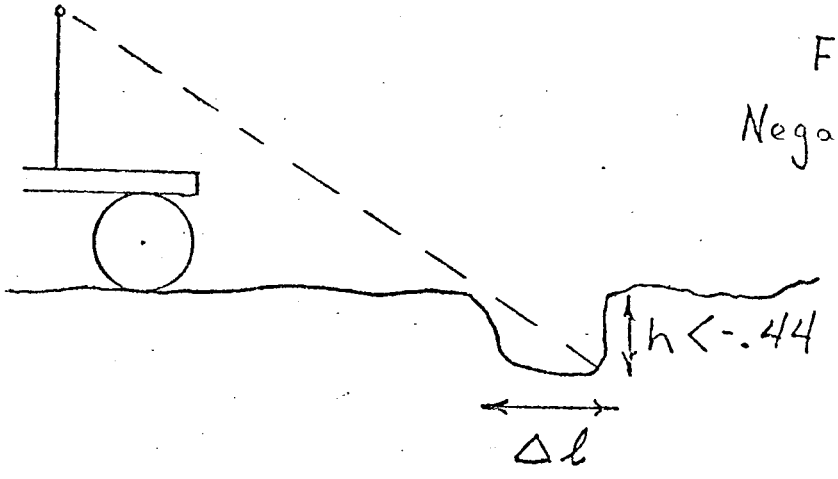

Figure 38
Negative Feature

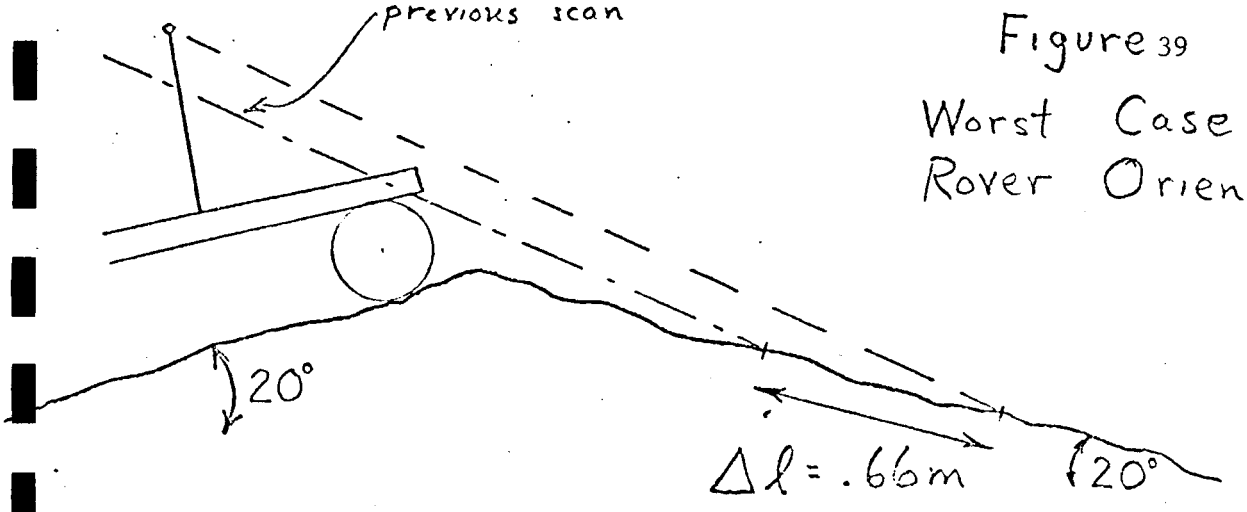

Figure 39
Worst Case
Rover Orientation

An electronic beam deflector, Ref. 28, is capable of sweeping very accurately at 5kHz.

Choice of Incident Angle β: The range of interest in short range navigation is 3 to 30 meters. Certainly it would be beneficial were we able to extract terrain data from 30 m away. This would facilitate terrain modeling so that we could slowly steer around obstacles instead of having to make the hard turns which are necessary because we have knowledge of terrain only 3 m away. Nevertheless, this system's choice for the range of data is 4 meters because the RPI MRV's wheelbase of 3 meters causes safe turns to be managed only with knowledge of terrain 4 meters or more away (including a margin of safety). Furthermore, terrain information is obtained much more easily at 4 meters than 30 meters because: (a) with reference to Fig. 39, higher incident angle β means less terrain information lost when navigating hills and (b) ability to investigate craters is increased. We choose sensor height D - 3 meters also to enhance these two considerations. Note also that the 4 meter range minimizes laser power and that the RPI MRV is very capable of making the necessary sharp turns and fast stops, Table 6.

Mechanical design has reached no final decision at this date, but it appears likely that the sensor package on RPI's MRV will be located over the rear wheels -- 3 meters back of front. A sensor staff reaching 3 meters above ground is feasible from the mechanical viewpoint. With these values, the proper choice for β is 23.2 degrees.

Path Selection

Once the rover has sensed the terrain and decided whether an obstacle exists it must decide what to do with that information. That is, a path selection decision must be made. Two possibilities immediately appear:

(a) a GO/NO-GO decision rule, and

(b) a Weighted Feature decision rule,

involving more sophisticated terrain modeling.

The first decision rule, GO/NO-GO, responds to the yes or no proposition: does an obstacle exist which the rover would encounter by continuing its present course? Thus, the laser scan should extend just enough in azimuth ($=76^{o}$) to insure a safe traveling width for the rover. If no obstacle exists within this region, the decision is GO; continue motion in the same direction (towards the mission goal). If an obstacle does exist within this region, the direction of motion is changed, and another scan made for new obstacles. It is noted that the safe traveling width includes a turning margin so that the rover may turn safely into a known terrain.

The second decision rule, using weighted terrain features, utilizes not only data on existence of obstacles, but on the magnitude of the terrain (i.e., relative height and slope of terrain). Thus, a decision is made among several navigable paths on the basis of which

is easiest to climb, therefore uses the least energy. The difference between the two decision rules may be observed by referring to Fig. 40 where the height of terrain is plotted versus azimuth angle for one scan. Here the GO/NO-GO rule would choose 0 degrees as the direction, and it certainly is a navigable path. However, the weighted feature rule would find an even better path -- that requiring less climbing power. This advantage is not at some cost, because the weighted feature rule requires a scan wider than before to enhance its capability of comparing several paths. Also, the GO/NO-GO rule can be used for systems in which only the existence of obstacles is known and not the magnitude of terrain, whereas the weighted feature rule requires such knowledge in the form of quantitative values for base, height and slope. It is noted that the system proposed in this report does measure the magnitude of terrain. Furthermore, it seems that such information may be obtained from the terrain at no cost in data error, and therefore magnitude of terrain data should be used in the path selection rule. The determination of which path selection rule is best will not be made here, since it appears that such a determination can best be made with the help of simulation programs for each decision rule, (see Task C.2.).

System Operation

The flow diagram of Figure 41 illustrates how the range and angle measurements, and knowledge of sensor orientation facilitate the operation of the system using the GO/NO-GO decision rule as an example. First, the base and height (magnitude of terrain) data are computed, then the system investigates whether a discrete obstacle exists. If not, the decision rule say GO (continue motion in some direction). If height is excessive, then it is determined if a gradual slope preceding that point allows that path to be navigable, Fig. 37. This investigation is carried out by using the computer-stored data from several previous scans to generate a stochastic fit, (see Task C.1.d.) to approximate the slope. Another situation in which an obstacle of excessive height may be navigable terrain is depicted in Fig. 38. For this case, the crevice is deep but short in duration -- and rover can roll over negative obstacles less than .66 m. The procedure for this case is to first discover that $h < -.44$ m and the slope is less than negative 25 degrees. This direction is not rejected yet, but the rover continues motion until more scans allow the system to determine the extent of the negative feature. If the extent is less than .66 m, the feature is still regarded as navigable. Note here that the ability of the RPI MRV to turn rapidly allows the rover to continue motion in this way and still be able to turn away should the negative feature extend more than .66 m.

As far as the weighted feature decision rule is concerned, a similar flow diagram could be invented to represent its operation. Terrain measurements would be combined by an index of performance such as $y = K_1 h + K_2 S$. This index y would be multiplied by a directional weighting function designed to give preference to directions towards mission goal.

Figure 40

SYSTEM OPERATION

in GO/NO-GO mode

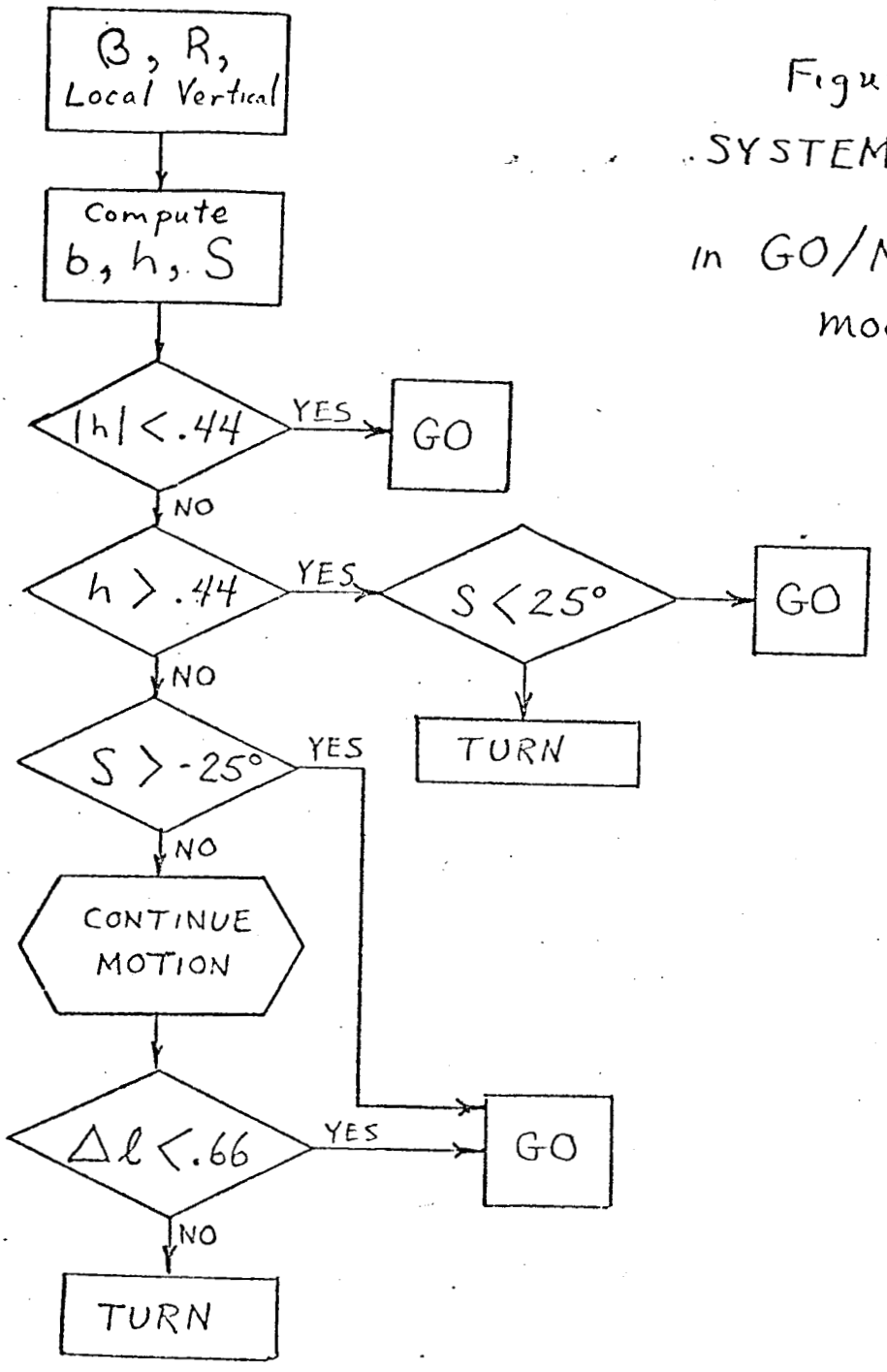

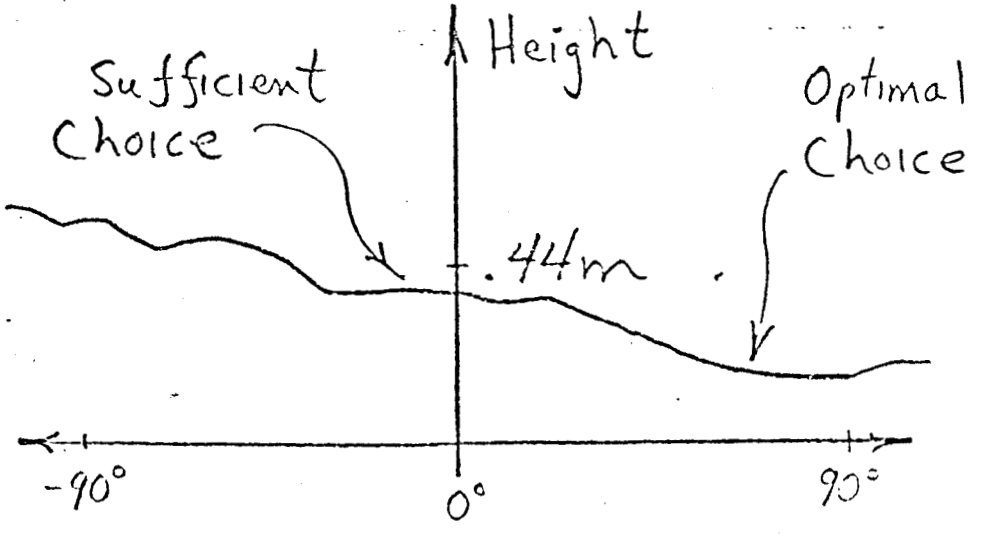

Fig 41
Path Selection
Differences

Sensitivity and Other Analysis

The system operation presented above should function properly, characterizing terrain as unpassable if and only if it exhibits excessive height and excessive slope and is long enough in extent to be dangerous. Some possible failings are:

a. The discrete scanning process creates unknown regions which must be rendered small enough for all situations so that the unknown regions cannot represent dangerous regions. Sufficiently rapid scanning should eliminate this problem.

b. The time required for scanning must be reasonably small. In fact, a laser scheme was ruled out previously because "the amount of time required to determine where the obstacles are located is too large...due to mechanical scanning". However, an electronic beam deflector could be used for scanning to eliminate this problem.

c. The determination of data must be accurate enough to be meaningful. What follows is a sensitivity analysis to determine accuracy of data, and some methods to further enhance measurement data.

First, the knowledge of angle and range errors is required. The variance of range data is 25×10^{-4} m^2, based on a standard deviation of 5 cm, Ref. 28. Angle error is due to beam divergence ($=10^{-3}$ radians) and local vertical error ($=10^{-2}$ rad.). Therefore the variance of angle data is 10^{-4} radian^2.

Now, referring to Fig. 39, the accuracy of discrete data (base and height) is analyzed -- assuming, for geometric simplicity, that the sensor staff is vertical.

$$h = D - R \sin\beta \tag{1}$$

$$b = R \cos\beta \tag{2}$$

The expected values of the variance of height is computed, using the expected parameters: $h = 0$, $b = 7$ m

$$\begin{aligned} \text{Var } h &= (R^2\cos^2\beta)(\text{Var}\,\beta) + (\sin^2\beta)(\text{Var } R) \\ &= \left(\frac{\delta b}{\delta \beta}\right)^2 (10^{-4}) + \left(\frac{\delta h}{\delta R}\right)^2 (25 \times 10^{-4}) \\ &= 49 \times 10^{-4} + 3.9 \times 10^{-4} \\ &= 54 \times 10^{-4} \end{aligned} \tag{3}$$

Therefore:

σ_h = 7.35 centimeters, a value low enough to allow meaningful terrain data.

As for slope data:

$$S = (h_2 - h_1)(b_2 - b_1) = \frac{\Delta h}{\Delta b} \tag{4}$$

$$dS = \frac{d(\Delta h)}{\Delta b} - \frac{d(\Delta b)}{(\Delta b)^2}\ \Delta h \qquad (5)$$

The expected value of the variance of the slope is computed, for which the expected parameters are h = 0, b = 7 m.

$$\text{Var } S = \frac{1}{(\Delta b)^2}\ (2R^2\cos^2\beta)(\text{Var}\beta)+(2\sin^2\beta)(\text{VarR}) \qquad (6)$$

$$= 2\ (\frac{\delta S}{\delta\beta})^2\ 10^{-4} + 2\ (\frac{\delta S}{\delta R})^2\ (25 \times 10^{-4})$$

$$= 225 \times 10^{-4} + 17.8 \times 10^{-4}$$

$$= 243 \times 10^{-4}$$

Therefore $\sigma_S = 15.6 \times 10^{-2} = 8.9$ degrees

Again, the low error permits accurate data. A stochastic fit, using several points, can decrease error further.

Stereo methods have been investigated to attempt in reducing the data error. The stereo concept involves the use of triangulation to eliminate either the angle measurement or the range measurement and rely on two range measurements or two angle measurements, respectively. As example, the range stero is presented, Fig. 42, for which the systems equations with vertical sensor staff are:

$$h = \frac{D+d}{2} + \frac{(R^2-r^2)}{4L} \qquad (7)$$

$$b = 1/2R^2 + 1/2r^2 - L^2 - \frac{1}{16L^2}\ (R^4+r^4-2r^2R^2)$$

$$S = \frac{\Delta h}{\Delta b}$$

Such a system is seen as an advantage in cases where, for the example of slope data, the first term of equation (6) is significantly smaller than the second term. In the range stereo system, $\frac{\delta S}{\delta\beta} = 0$ but $\frac{\delta S}{\delta R}$ is larger than the non-stereo case. For the present values of range and angle errors, stereo schemes are not appropriate, because errors due to range or angle are fairly close. But should instrumentations create a disparity between range and angle errors, then certainly stero methods could be used to good advantage. In fact calculations show that a system with range error (standard deviation) of .8 cm or less would constitute a situation in which stereo methods could enhance data accuracy.

Figure 43 shows how system accuracy varies with incident angle, for various measurement errors. Note that stereo has no advantage if angle error can be restricted to $\sim 3^o$.

Conclusions

The best range at which to take data has been determined to be 7 meters from the sensor. The detection scheme utilizes slope data, which has been shown to be accurate as is the height data. A stereo

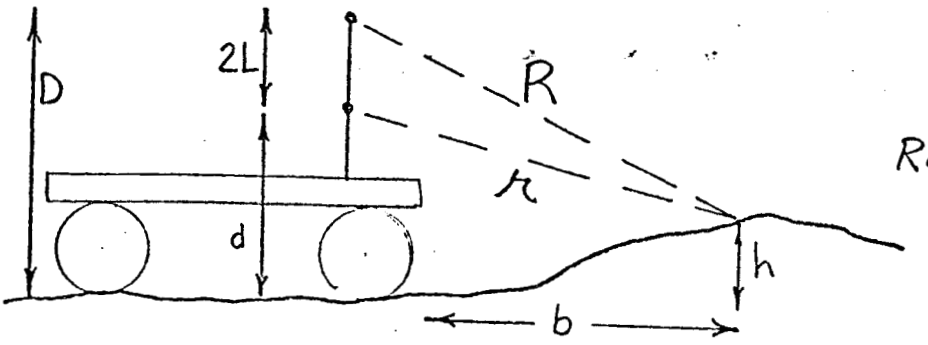

Figure 42

Range Stereo

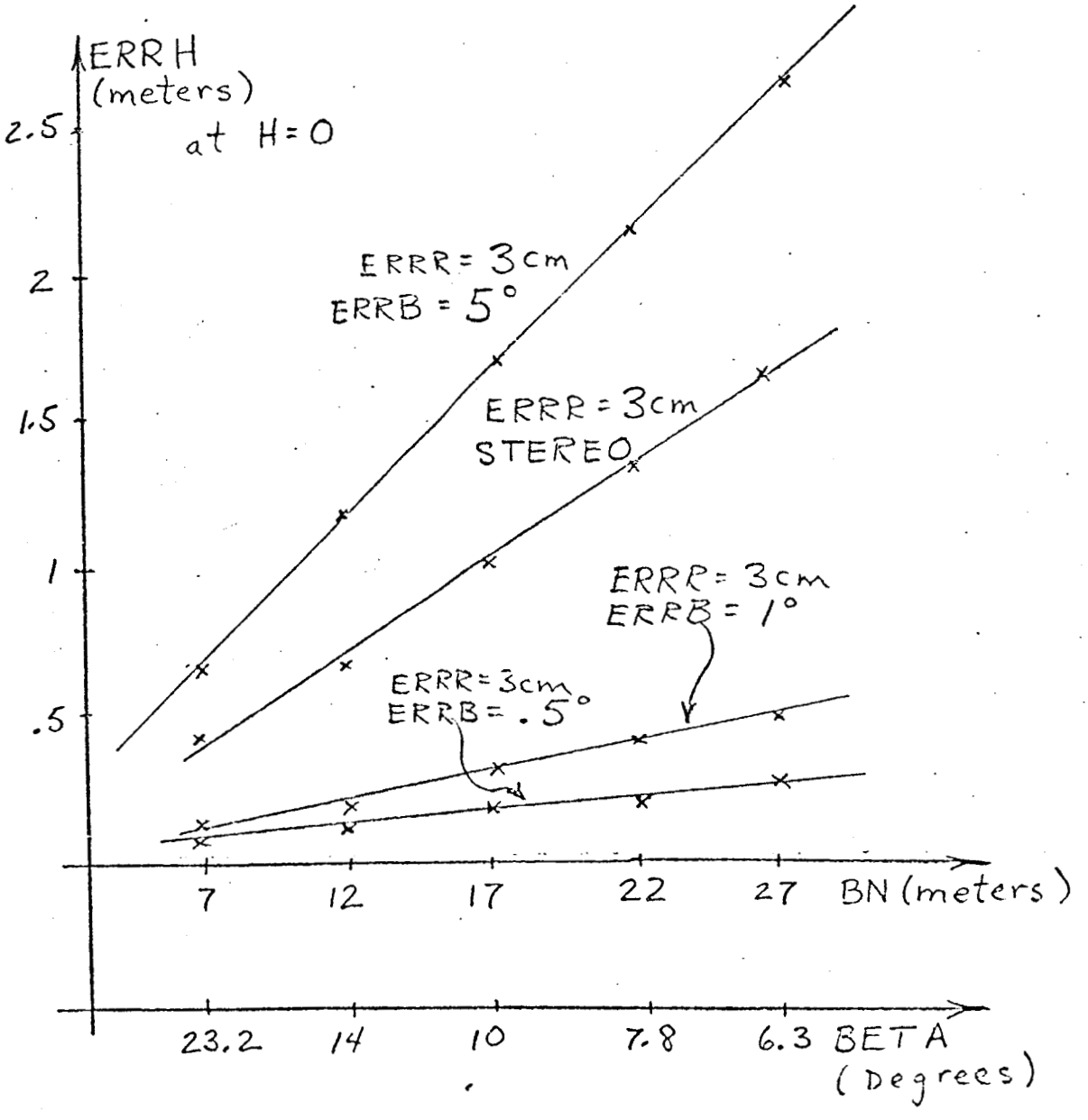

HEIGHT ERROR vs. INCIDENT ANGLE
for various MEASUREMENT ERRORS

Figure 43

method of data-gathering was formulated but found inferior to the normal mode for present values of measurement errors. A flow chart defining system operation based on height, slope and extent of negative terrain has been formulated. Investigation of the scan rate indicates that the rate is best varied from 2Hz to 5kHz depending on the rover's orientation from 0 to 25°.

For future work, a simulation study is recommended to determine the superior decision rule: GO/NO-GO or a weighted feature decision. Also, an effort should be made to insure that angle error is below .5 degrees or that range error is below .8 centimeters, which would facilitate stero methods.

C.1.d. Terrain Modeling- Edward Schoen
Faculty Advisor: Prof. C. N. Shen

The problem of deriving a path selection algorithm which will allow the rover vehicle to traverse the surface of Mars safely can be divided into two main areas of study. The first area constitutes the collection of data necessary to determine the Martian surface features. The second area of study is the interpretation of the data, and the decision policy used, once a valid representation of the surface is obtained. This report will concern itself with the latter area with emphasis placed on interpretation of data.

It is assumed that a means of collecting data, whether radar, sonar, or laser, is available. The data available from the sensor will be a range measurement, R, from the transmitter to the point on the terrain, a heading angle, θ, which is measured with respect to the heading angle of the vehicle, and an elevation angle β, which is measured with respect to a horizontal plane fixed to the vehicle. These angles are shown in Fig. 44 and represent positive values. The coordinate axes is fixed to the vehicle. It is assumed a reference

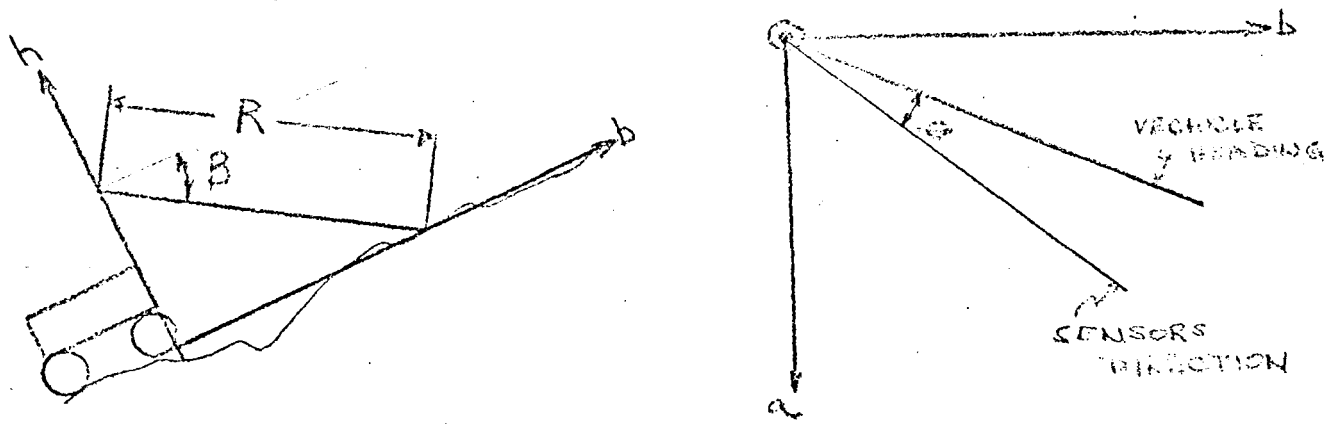

SIDE VIEW TOP VIEW

FIGURE 44

VECHICLE COORDINATE AXES

to the local vertical is known at all times. It is possible to model part of the terrain as a plane defined by the following equation:

$$h = aX_1 + bX_2 + X_3 \tag{1}$$

Once the plane is known, the slope of the terrain is given by

$$S_G = (X_1^2 + X_2^2)^{\frac{1}{2}} \tag{2}$$

where $X_1 = \frac{\partial h}{\partial a}$ = Cross path slope (3)

and $X_2 = \frac{\partial h}{\partial b}$ = In path slope (Ref. 22 and 23) (4)

If the terrain slope, S_G, is less then a predetermined criterion the path is considered to be safe for the vehicle.

To determine the equation of the plane four measurement points are taken. These measurements contain errors from two sources. One source is the range error from the sensor. The other source of error arises from errors in angle measurements. It is important to know how these measurement errors will effect the approximation of the plane. For this reason an error analysis will be done in the next section.

Each measurement consists of a range return and two angles, θ and β. With these three quantities the three coordinates h, a, and b of the terrain point can be determined. Taking four measurement points a stochastic fit can be made to approximate a plane that represents the actual terrain. The geometry of the problem showing h, a, and b is given in Fig. 45. A sensor height of 3.0 meters is assumed.

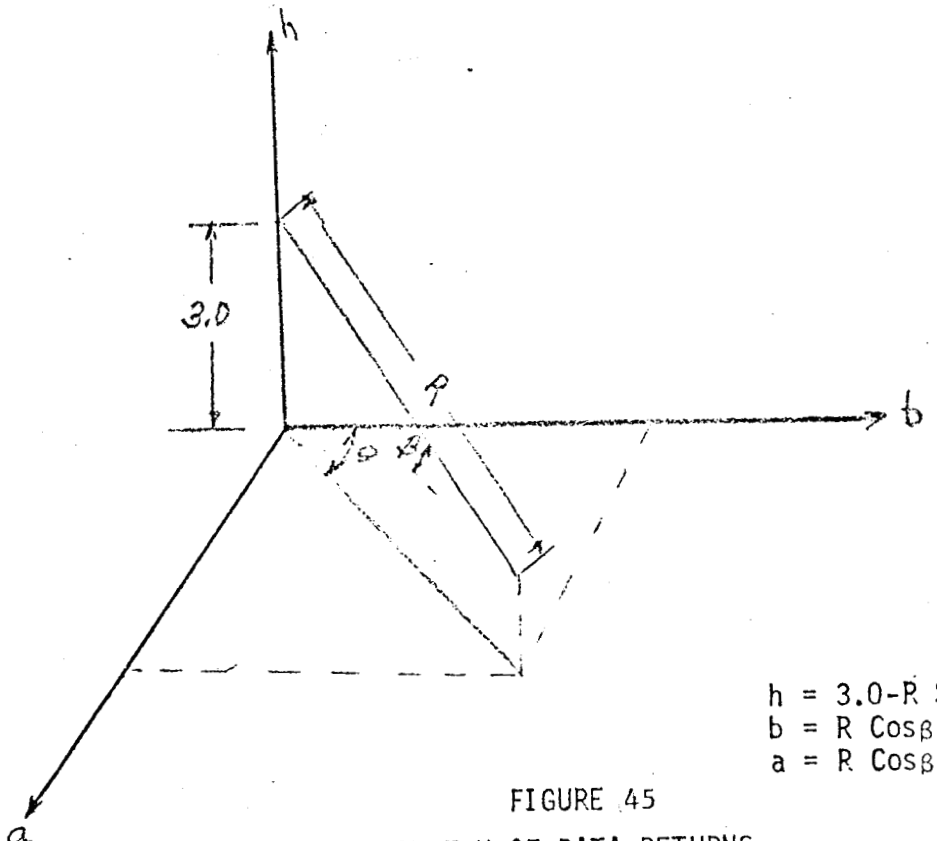

$h = 3.0 - R \sin\beta$
$b = R \cos\beta \cos\theta$
$a = R \cos\beta \sin\theta$

FIGURE 45

GEOMETRY OF DATA RETURNS

The type of stochastic fit used was a weighted least square fit on the variable h. This type of fit, Ref. 29 and 30, assumes no errors in the variables a and b. We are interested in determining the random variables Δb, Δh, and Δa in terms of the errors $\Delta\beta$, $\Delta\theta$ and ΔR. It is assumed that β, θ, and R are zero mean gaussian variables.

Equations 5, 6, and 7 show these relationships

$$\Delta b = \cos\bar{\beta}\cos\bar{\theta}\,\Delta R - \bar{R}\sin\bar{\beta}\cos\bar{\theta} - \cos\bar{\beta}\sin\bar{\theta}\,\Delta\theta \tag{5}$$

$$\Delta h = -(\bar{R}\cos\beta\Delta\beta + \sin\bar{\beta}\,\Delta R) \tag{6}$$

$$\Delta a = \cos\bar{\beta}\cos\bar{\theta}\,\Delta R + \bar{R}\sin\bar{\beta}\sin\bar{\theta}\Delta\beta - \bar{R}\cos\bar{\beta}\cos\bar{\theta}\,\Delta\theta \tag{7}$$

where $\bar{\beta}$, $\bar{\theta}$ and $\bar{R}$ are the true values.

Knowing the probability of error in our measurements we would now like to know the probability of error in our model.

If we had an errorless sensor the four return points, not exactly in a plane, $(\bar{a}_1, \bar{b}_1, \bar{h}_1)$, $(\bar{a}_2, \bar{b}_2, \bar{h}_2)$ $\ldots(\bar{a}_4, \bar{b}_4, \bar{h}_4)$ could be used to form a plane defined by

$$\hat{h}_1 = \bar{a}_1\hat{X}_1 + \bar{b}_1\hat{X}_2 + \hat{X}_3$$

The estimated parameters $\hat{X}_1$, $\hat{X}_2$, $\hat{X}_3$ minimizes the following error:

$$\text{ERROR:} = \sum_{i=1}^{4}(\tilde{h}_i - \hat{h}_i)^2$$

where $\hat{h}$ is the corresponding height in the plane

Using matrix notation

$$\bar{A}\,\underline{\hat{X}} = \underline{\hat{h}}$$

where $\bar{A} = \begin{pmatrix} \bar{a}_1 & \bar{b}_1 & 1 \\ \bar{a}_2 & \bar{b}_2 & 1 \\ \bar{a}_3 & \bar{b}_3 & 1 \\ \bar{a}_4 & \bar{b}_4 & 1 \end{pmatrix}$ $\hat{X}_1 = \begin{pmatrix} \hat{X}_1 \\ \hat{X}_2 \\ \hat{X}_3 \end{pmatrix}$ $\underline{\hat{h}} = \begin{pmatrix} \hat{h}_1 \\ \hat{h}_2 \\ \hat{h}_3 \\ \hat{h}_4 \end{pmatrix}$ $\underline{\tilde{h}} = \begin{pmatrix} \tilde{h}_1 \\ \tilde{h}_2 \\ \tilde{h}_3 \\ \tilde{h}_4 \end{pmatrix}$

The values of X are given by equation (8)

$$\hat{X} = (\bar{A}^T\bar{A})^{-1}\bar{A}^T\underline{\tilde{h}} \tag{8}$$

The same procedure can be followed for the measurements (a_1, b_1, h_1)---(a_4, b_4, h_4). These measurements define a plane, $\tilde{h} = a\tilde{X}_1 + b\tilde{X}_2 + \tilde{X}_3$

The estimated parameters $\tilde{X}_1, \tilde{X}_2$ and $\tilde{X}_3$ minimizes the error

$$\text{ERROR} = \sum_{i=1}^{4} (h_i - \tilde{h}_i)^2$$

where $\tilde{h}_i$ is the corresponding height in the plane.

Thus $A \underline{\tilde{X}} = \underline{\tilde{h}}$

$$\text{where } A = \begin{pmatrix} a_1 & b_1 & 1 \\ a_2 & b_2 & 1 \\ a_3 & b_3 & 1 \\ a_4 & b_4 & 1 \end{pmatrix} \qquad \tilde{X} = \begin{pmatrix} \tilde{X}_1 \\ \tilde{X}_2 \\ \tilde{X}_3 \end{pmatrix} \qquad \underline{\tilde{h}} = \begin{pmatrix} \tilde{h}_1 \\ \tilde{h}_2 \\ \tilde{h}_3 \\ \tilde{h}_4 \end{pmatrix}$$

$$\underline{\tilde{X}} = (A^T R^{-1} A)^{-1} A^T R^{-1} \underline{h}$$

$$\text{where } b = \begin{pmatrix} h_1 \\ h_2 \\ h_3 \\ h_4 \end{pmatrix} \qquad R = \begin{pmatrix} \sigma_1^2 & 0 & 0 & 0 \\ 0 & \sigma_2^2 & 0 & 0 \\ 0 & 0 & \sigma_3^2 & 0 \\ 0 & 0 & 0 & \sigma_4^2 \end{pmatrix}$$

σ_i^2 = variance of h on ith measurement

To determine the allowable errors in range and angle measurements a number of different planes were identified using the stochastic fit of the previous section for a number of different standard deviations of the range and angle measurement errors.

Each plane was examined using a 1, 5, and 10 cm. standard deviation on the range error. For each of the above range standard deviations, an angle standard deviation in β and Θ of one to five milliradians in increments of one milliradian was used. The standard deviations of β and θ were assumed equal for each case.

Original measurements were taken at angles of β = .1 and .095 milliradians and Θ =0 and .02 milliradians for each β. The point of intersection of the plane to be modeled and the sensor signal was calculated. The calculation yields h, a, and b. The range from the transmitter to the terrain point is then calculated. The range return and the two angle measurements are then perturbed plus or minus one standard deviation. Using Eq. (1), the measurement points are determined. The final step is to use the measured terrain points in the stochastic fit and determine the approximation to the model.

The original measurements were taken such that if the terrain were a horizontal plane with h=0, the sensor beam would intercept the terrain about thirty meters in front of the vehicle. The four measurements were separated to form a rectangle that was approximately 1.5 meters long and 1.0 meters wide.

To minimize errors due to the rocking and rolling of the vehicle while data is being collected, it is assumed the sensor can be positioned, via a crystal focusing system in one or two milliseconds.

Tables 7 and 8 show the various results of the approximation to the plane defined by:

$$h = .25a + .2b - 4.0$$

The first table is for a one centimeter standard deviation in the range return data. The second table is for a five centimeter standard deviation in the range measurements. Results using a ten centimeter standard deviation for the range are approximately the same as those for a five centimeter standard deviation. For this reason, those results are omitted.

The standard deviations used for the angle measurements are shown in the first column of the tables. The resulting models are shown in column two. The error for the cross-path and in-path slopes are found in the last two columns respectively.

Figure 46 is a set of graphs of the error in the in-path and cross-path slopes as a function of various standard deviations of the angle measurements. The graph at the top of Fig. 46 is for a range standard deviation of one centimeter. The bottom graph is for a five centimeter standard deviation. The in-path slope is shown as a dashed line. The solid line represents the cross-path slope.

Figure 47 shows the effects on the error in the slope measurements when six data points are used for the stochastic fit instead of four. The graphs are for a standard deviation of five centimeters in the range return.

TABLE 7
EFFECT OF RANGE ERROR OF 0.01 METER ON
IN-PATH AND CROSS-PATH SLOPES

Plane to be modeled: h = .25a + .2b - 4.0
actual cross-path slope = 14.036°
actual in-path slope = 11.21°

ΔB RAD	MODEL	ERROR X_1 DEG	ERROR X_2 DEG
.001	$h = .237a + .161b - 3.074$	.669	2.186
.002	$h = .139a + .073b - 1.0111$	6.117	7.149
.003	$h = .049a - .032b + 2.479$	11.226	13.194
.004	$h = .0099a - .077b + 2.531$	13.465	15.757
.005	$h = .0014a - .092b + 2.862$	13.953	16.562

TABLE 8
EFFECT OF RANGE ERROR OF 0.05 METER ON
IN-PATH AND CROSS-PATH SLOPES

ΔB_{RAD}	MODEL	ERROR X_1 DEG	ERROR X_2 DEG
.001	$h = .273a + .161b - 3.095$	-1.24	2.162
.002	$h = .174a + .073b - 1.012$	4.185	7.152
.003	$h = .057a + .033b + 1.482$	10.791	13.21
.004	$h = .014a - .078b + 2.536$	13.24	15.77
.005	$h = .0023a - .092b + 2.857$	13.91	16.57

Conclusions

1. For a given angle deviation, the errors in the in-path (X_2) and the cross-path (X_1) slopes are approximately the same for the three range deviations.

2. Angle deviations are dominant over range deviations from one to ten cm.

3. Errors in the in-path and cross-path slopes increase linearly as angle deviations increase from one to four milliradians.

   Errors in the slopes reach a steady state value as the angle deviations approach ten miliradians.

4. Four point fits gave better results than a three point fit.

5. Six point fits gave better results than a four point fit except when measuring a negative cross-path slope. This might be due to the closeness of the measurement.

6. Even for a one milliradian standard deviations on β and Θ, errors in cross-path slopes were as high as three to five degrees. An algorithm which is not dependent on angle measurements might yield better results.

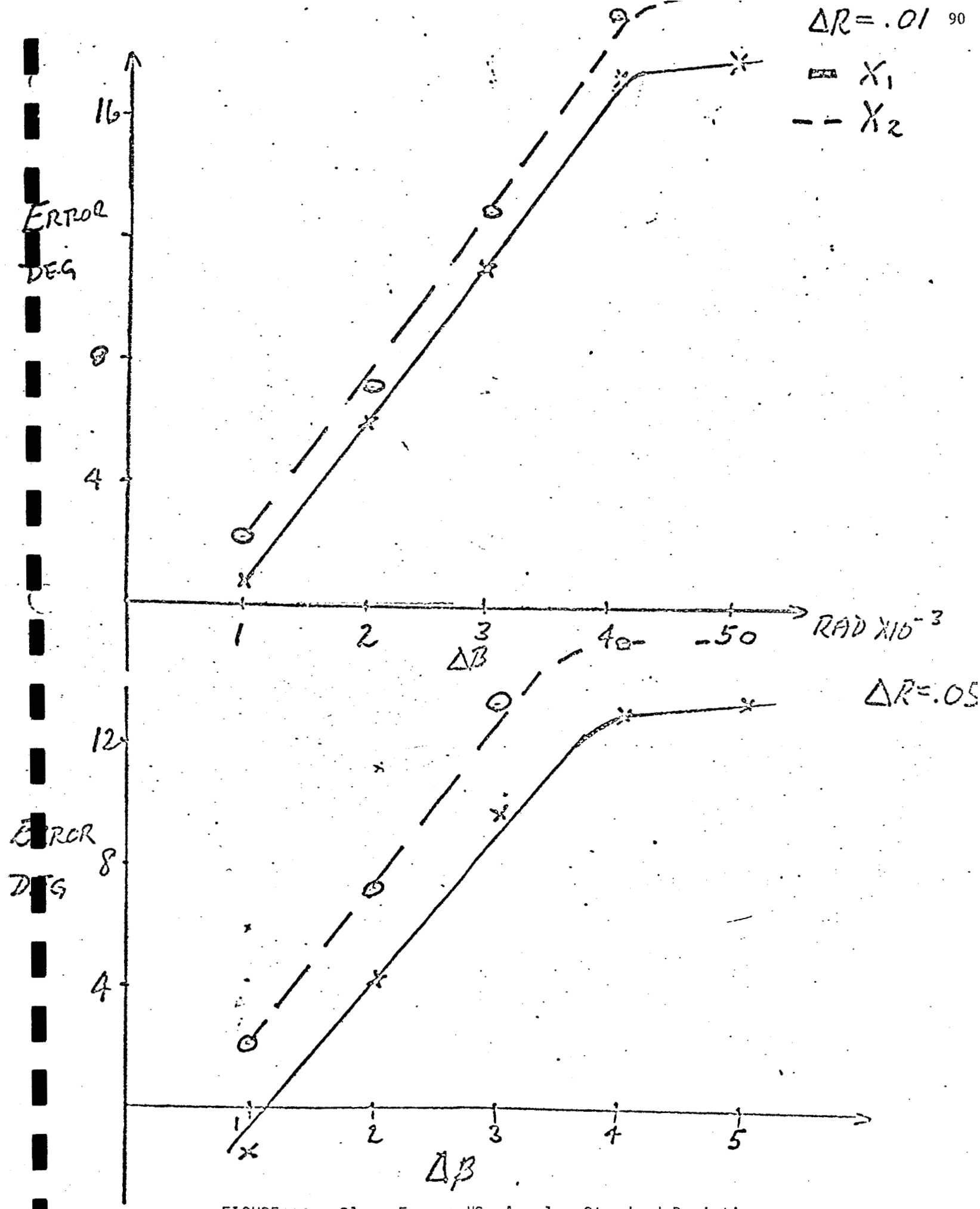

FIGURE 46- Slope Errors VS. Angular Standard Deviations

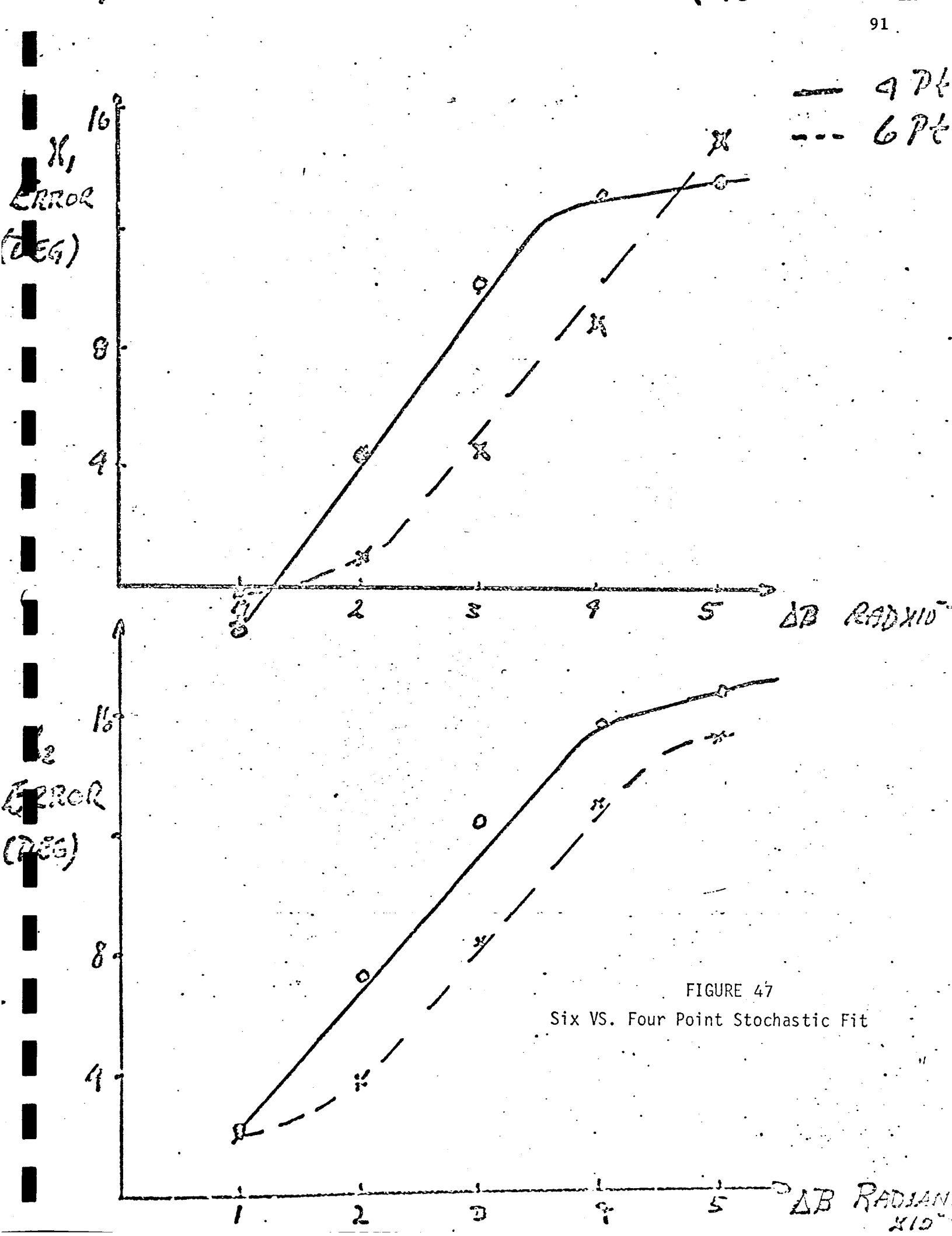

FIGURE 47
Six VS. Four Point Stochastic Fit

C.2. Path Selection System Evaluation - S. Boheim, W. Purdon
Faculty Advisor: Prof. D. K. Frederick

The objective of the present effort is twofold. The first is the development of a computer package which will provide the capability of dynamically simulating a wide variety of sensor, terrain modeling, and path-selection algorithm combinations. The second is the generation of criteria for the quantitative evaluation and comparison of the system's performance. It is anticipated that the development of a realistic simulation capability is a necessary condition for the establishment of meaningful performance criteria.

Previous efforts in the area of path selection systems have concentrated upon the development of a terrain modeling system, including analysis of the effects of sensor error on the model, and upon studies of path-selection algorithm characteristics. One such study did involve the integration of terrain modeling and path-selection systems for the purpose of algorithm performance evaluation, Ref. 22. However, these works have been mainly applicable to a long-range obstacle detection system, e.g., sensor ranges of 50 to 1500 meters, and have not included quantitative criteria for performance evaluation.

Here, attention has been directed at mid-range applications, assumed to be 3 to 30 meters, as distinct from short-range applications using a tactile sensor and the previously studied long-range system.

The progress in the two areas of study is discussed below, followed by a statement of future work.

C.2.a. Computer Simulation Package

The computer simulation package is a self-contained unit. Not only does it simulate the functions of a terrain sensor and modeler, contain a path selection algorithm, and simulate the vehicle's motion dynamics, but it also includes a mathematical description of a terrain and evaluates system performance using the criteria established for this purpose. The inclusion of the latter two items in the package reduces error-prone handwork and extends considerably the scope of the simulation's evaluation capabilities.

There were two major considerations taken into account during the computer package design. First, the flexibility of the simulation is of primary importance. For example, the substitution of alternate path-selection algorithms and sensor schemes based upon conclusions from simulated runs must be conducted with a minimum of reprogramming. Inputing of terrain data must be flexible enough to allow for the evaluation of system performance over a variety of terrain types.

As a second consideration, it must be possible to incorporate non-ideal features which will tend to degrade vehicle performance. Such additions will enhance the realism of the simulation and improve resultant reliability. Examples of non-ideal features are vehicle bounce, the slope of terrain at the vehicle's location, and sensor-reading uncertainty.

The areas of program development in which the efforts have been made to date are discussed below.

Program Structure

In establishing the computer simulation package structure, the approach taken has been to separate logical functions into individual blocks as much as possible. The structure of the package is shown in Fig. 48, where the lines between the blocks indicate information flow. The blocks may be grouped into the following three categories: path selection system, simulation environment, and evaluation and display.

To date, development has proceeded to software implementation of these three categories, as described below:

Path Selection System

(i) Sensor Simulator Block - The scheme chosen for an initial development of this block involves a laser beam scanner with zero beamwidth. The vehicle is assumed to be stationary for each scan and there is a uniform time (T) between scans. A single beam is swept horizontally and discrete samples are taken during each scan. The beam has a fixed attitude with respect to the planet's true vertical.

The block simulates the motion of the beam scan and the impingement of the beam on the terrain. Values for the x and y coordinates along the beam are supplied to the terrain characterization block which in turn generates a value of the altitude of the terrain (z) at the point x,y. The value of z is compared with the altitude of the beam (z*) at the same x,y coordinates. The process is continued until z* is sufficiently close to z, Fig. 49. Then this value of z is taken to be the altitude of the terrain at the point of beam impingement, and the range from the sensor to the impingement point is calculated.

The output of the block includes the azimuth and elevation angles and range from the sensor to each of the points of impingement along the beam scan. The block also has the capability of simulating more than one beam scan from the vehicle location, so as to satisfy the information requirements of more sophisticated terrain models. Noise may be added to the elevation angle and range measurements of the sensor to simulate the effect of a moving, bouncing vehicle.

(ii) Terrain Modeling and Path-Selection Algorithm Blocks - These two blocks simulate the calculations which must be performed by the on-board computer in order to generate a steering command for the vehicle to execute. The terrain modeling block uses the simulated sensor measurements to construct a model of the terrain that

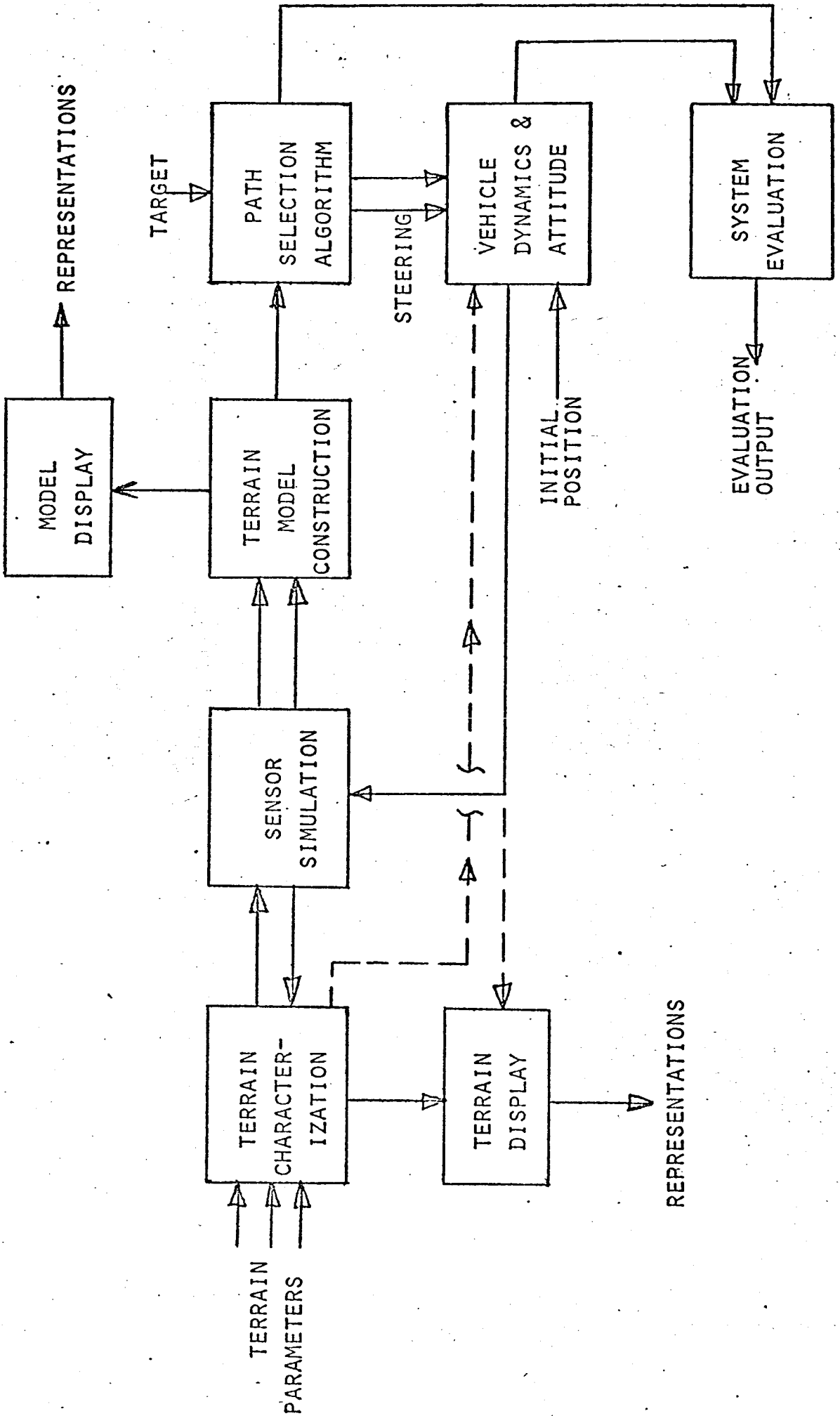

Figure 48. Simulation Structure

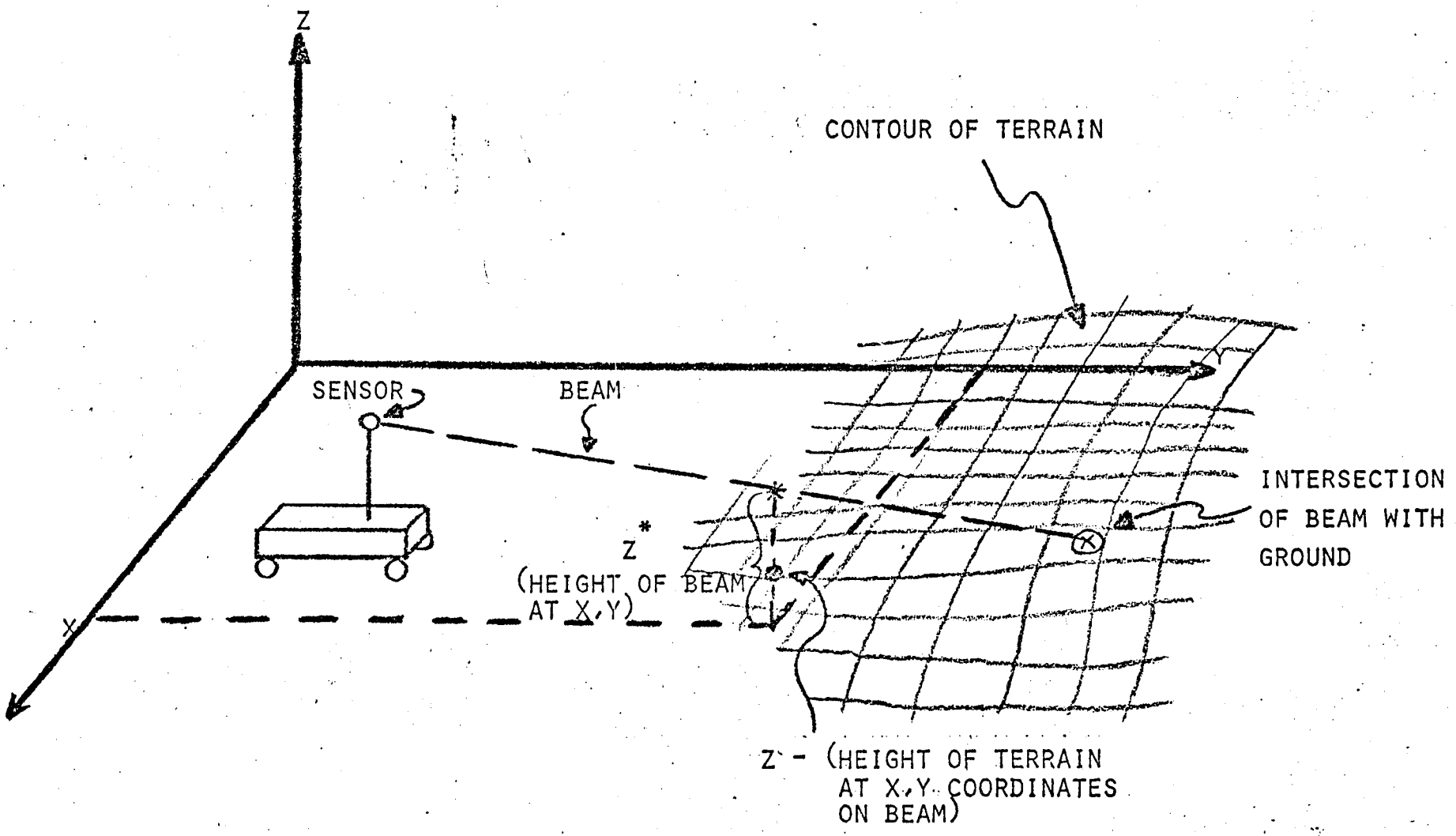

Figure 49. Geometry of Beam Impingement Calculation

has been scanned by the mid-range sensor. The path-selection algorithm block uses the terrain model to select a desired vehicle path. The output of the path-selection algorithm block is a steering command which will move the vehicle in the desired location.

A more detailed description of the development of these path-selection system blocks, and the terrain characterization block (see below), can be found in Ref. 31.

Simulation Environment

The blocks in this category set up and conduct the actual simulation. The terrain characterization block contains the mathematical description of the surface on which the vehicle is to travel, and the vehicle dynamics and attitude block moves the vehicle on this surface.

(i) Terrain Characterization Block - The initial investigation for the design of this block involved studies of various mathematical approaches to terrain description. The approach settled upon involves utilizing a polynomial (in the two independent variables x and y) representation and building Gaussian distributions upon this base. These descriptions are used to convey low frequency features. In addition, a special-features input allows for boulders and crevasses (high frequency components). The block will read in data conveying each of the mathematical characterizations of the terrain, and will store that information. Once the simulation of a path selection process begins, the block provides the value of the altitude of the surface at any given x,y location, using all of the terrain features specified.

The software development has been completed for a polynomial and a special-feature terrain description. The polynomial may vary in complexity from zero to ninth order. The special feature description allows the user to add boulders, crevasses, cliffs, and craters, and to specify the size, shape, and location of any of these terrain features. The Gaussian feature description has been left for future work.

(ii) Vehicle Dynamics and Attitude Block - The purpose of this block is to simulate the motion of the vehicle and to provide the systems evaluation block with the necessary information for analysis of the vehicle's motion. Its output includes such information as the velocity, location, and the direction of the vehicle at the next mid-range sensor scan time, as well as the information mentioned earlier that is being passed to the systems evaluation block. To date, software implementation has been completed in the following areas:

Vehicle Response Time - Provisions have been made so that the vehicle can turn only at a specific rate and so that the travel of the vehicle during very slow sensor scans and/or very slow computer calculations can be simulated. These provisions are optional and the user can assume ideal conditions, if desired.

Downhill Acceleration - When the vehicle is on a positive slope, a potential energy formula, derived in Ref. 22 is used to calculate power requirements and the velocity of the vehicle. When the vehicle is on a negative slope, the vehicle's motors are turned off and the vehicle is accelerated by gravity only. Regenerative breaking is assumed so that the vehicle will not travel faster than a velocity specified by the user.

Random Disturbances - Noise of two types may be added to the measurements of the mid-range sensor and/or to other parameters of the path selection system. The noise, simulating random effects due to the bouncing of the vehicle as it moves, may be either filtered or unfiltered white noise. If the former is desired, a second-order filter is used which has the same damping factor and natural frequency as the vehicle's dominant mode.

Short Range Sensor - An ideal mechanical sensor simulator is available. Since a short-range mechanical sensor may interfere with science operations, this simulation provision is optional and is controlled by the user.

Evaluation and Display

These blocks provide intermediate simulation information, graphical displays, and an evaluation of the performance of the path selection system for the user.

(i) Systems Evaluation Block - This block evaluates the performance of a path selection system using the evaluation criteria established in Task C.2.b. below. Software implementation of this block has been completed.

(ii) Terrain Display Block - This block presents the user with a contour map of the surface contained in the terrain characterization block. An example of such a map is given in Fig. 50. The vehicle paths shown on this figure have been superimposed by hand and will be discussed later. Each band on the map indicates a difference in elevation of 0.5 meters. The map shows an area of about 900 square meters.

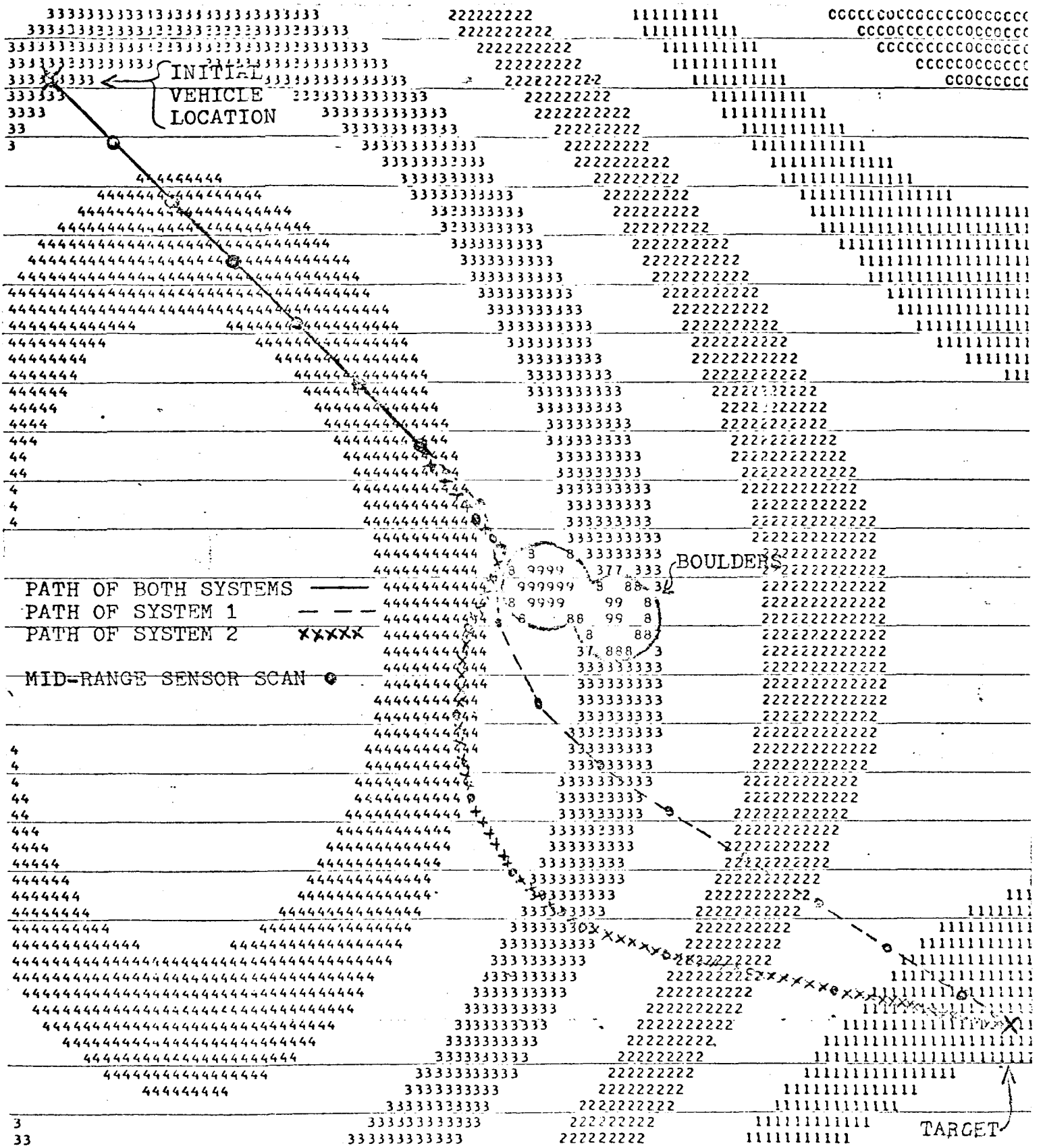

Figure 50. Terrain Contour Map with Vehicle Paths Superimposed

(iii) Model Display Block - This block will provide the user with a representation of the terrain model computed by the path selection system, but has not yet been implemented.

C.2.b. System Evaluation

To develop an effective means for evaluating the performance of the vehicle for various path selection systems, both quantitative and heuristic methods of evaluation have been employed.

Quantitative Evaluation

It is desired to describe mathematically as many important features of the path selection system as possible so as to minimize the need for subjective evaluations. The following formula has been postulated so that important characteristics of a system and their relative importance can be stated analytically:

$$D = \sum_{i=1}^{3} W_i F_i$$

where D is the figure of merit or measure of desirability of the system,

F_i are indexes that represent the important characteristics, or features, of the system,

W_i represent the weights of the corresponding indexes.

Numerically, the indexes are numbers ranging between zero (worst case) and unity, (optimum value), the weights range between zero (least important) and unity, (most important), and the figure of merit ranges between zero (least desirable) and unity, (most desirable).

If the weights and indexes are appropriately chosen, then the system which generates the highest value of D, when the above formula is applied, would be the most desirable system. Assuming that the indexes chosen adequately describe the system's performance, there still remains the selection of the values of the weights. At this point in time, the weights have been selected so that all performance indexes are assumed to be equally important. Adjustment of these weights for performance indexes not equally important has been left for future work.

The actual mechanics of each index must now be considered. Tentatively, it has been decided that three indexes sufficiently describe vehicle performance, and, if certain conditions are set, the number of indexes may be reduced to two. The three indexes are:

(i) Path Length - If D_m is the distance between the starting point and the target, and D_e+D_m is the length of the path chosen by the vehicle, then

the index

$$F_1 = \frac{D_m}{D_e+D_m}$$

is defined.

(ii) Battery Time - If the total time taken by the vehicle to reach its target is called T_e+T_m, and the time that the vehicle uses its batteries is called T_b, then the index

$$F_2 = \frac{T_e+T_m-T_b}{T_e+T_m}$$

is defined.

(iii) Traverse Time - If D_m is the distance between the vehicle and the target, and the maximum velocity of the vehicle is V_m, then the minimum time required to reach the target is $T_m=D_m/V_m$, and the index

$$F_3 = \frac{T_m}{T_e+T_m}$$

is defined.

The first index penalizes long and/or wandering paths while the second penalizes the selection of paths that contain steep slopes, thereby forcing the vehicle to rely on its batteries as well as its radioactive thermal generators (RTGs). If the vehicle must slow down for other reasons besides steep slopes (e.g., tactile sensor contact), then the system will be penalized for this loss of time through the third index.

Heuristic Evaluation

Some important characteristics of a system are not easily described in quantitative form, and yet these characteristics seem to require evaluation. The following two features fit into this category:

(i) Safety of Path Selected - Although the safety of the vehicle is of primary importance, it is difficult to analytically describe the inherent danger to the vehicle present in a selected path. What is hoped to be an indication of safety has been implemented by counting the number of times the tactile sensor indicates the vehicle is about to encounter an obstacle.

(ii) Correct Performance - Situations may arise where the vehicle is called upon to 'not succeed'. For example, if the target is surrounded by an untraversable crevasse, then it would be better for the vehicle to get 'close', rather than attempt to reach the exact target. This

feature is a purely heuristic characteristic, and any evaluation in this area would be performed by humans.

Comparison of Two Path Selection Systems

To demonstrate the use and simulation capabilities of the computer simulation package, the comparison of two different path selection systems will be presented. The comparison is not meant to say which system is 'good', or 'bad'. Rather, it is to demonstrate which system performs better for the particular set of conditions provided in this simulation. Both systems below arrived on-target, but in a different manner. The two systems are described, the simulation situation is presented, and then the performance of the two systems is shown and evaluated.

(i) Path Selection System #1 - The sensor used in this system is mounted on an ideal platform so that elevation angles are always measured with respect to the planet's true vertical, not the local surface vertical. The sensor makes 17 equally spaced range measurements in a 40° horizontal scan in front of the vehicle. The elevation angle is fixed for each measurement at 82.4° from the vertical. The terrain model builds a 17 element go/no-go map corresponding to the 17 possible paths in front of the vehicle by assuming that the terrain is linear from the vehicle to the range measurement impingement point, and then computing the slope of this 'linear' terrain segment. If the slope exceeds a certain threshold value, then a no-go condition exists. The normal mode of the path-selection algorithm determines which of the 17 paths will move the vehicle toward the target in the straightest line. If an obstacle lies in this path, then the first path to the right is inspected, then the first path to the left is inspected, then the second path to the right, etc., until a path is found in which no obstacle exists. A steering command is then generated to move the vehicle on the appropriate path. If all 17 paths contain obstacles, then the vehicle stops, rotates 30° clockwise, and scans new terrain for a path to follow. This alternate scheme is the algorithm's emergency mode.

(ii) Path Selection System #2 - The sensor in this system is also mounted on an ideal platform, as in System #1. The sensor makes 17 equally spaced sets of range measurements in a 40° horizontal scan in front of the vehicle. Each set of range measurements is made at elevation angles of 66.8° and 70.85°. The terrain model builds a 17 element go/no-go map, corresponding to the 17 possible paths in front of the vehicle, by subtracting one of the range measurements in a set from the other and comparing the difference to a threshold value. If this value is exceeded, then a no-go condition exists. This terrain model is developed in greater detail in Ref. 32. The normal and emergency modes of the path-selection algorithm are the same as those used in System #1.

The simulation situation is shown in Fig. 49. Two boulders 5 meters in diameter were placed on a straight line between the vehicle's initial position and its target. The mid-range sensor was used once every 3 seconds, and the vehicle was initially pointed directly at the target.

The performance of the two systems is shown in Fig. 50 and Table 9. System #1 did not use its emergency mode as often as System #2 because the slope method of terrain modeling is effective at any range, whereas the range difference method fails if the vehicle is too close to the obstacle. On the other hand, System #1 never saw the obstacle and ran into it. System #2 saw the obstacle, but in steering around it the system failed to maintain a safe distance. As a result, System #2 lost sight of the boulder and ran into it. Finally, if no emergency mode were available, both systems would have been unable to negotiate the obstacle once they had run into it, and the vehicle would stop moving.

Summary

A computer simulation package has been developed which simulates and evaluates the performance of path selection systems. The package has been designed to be both realistic and flexible. The evaluation criteria developed encompass both heuristic and quantitative methods to insure meaningful evaluation results. Finally, a comparison of two typical path selection systems has been included to demonstrate the capabilities of the computer simulation package.

Future Work

Future work is planned in the following three areas:

(i) Continued Software Development - Work will include software implementation of the model display block, the Gaussian terrain feature capability in the terrain characterization block, and the expansion of the capabilities of the vehicle dynamics and attitude block, such as the software implementation of vehicle slippage.

(ii) Refinement of Evaluation Criteria - The weights in the figure of merit formula will be adjusted so as to reflect the relative importance of the performance indexes to each other. Also, new performance indexes will be considered in order to obtain more accurate evaluation of path selection systems.

(iii) Software Implementation of Path Selection Systems - Implementation of systems already available is a logical extension of research in this area. Finally, using the computer simulation package as a tool, more complicated and/or sophisticated path selection systems may be produced and evaluated.

TABLE 9

SYSTEM COMPARISON

	System 1	System 2
Path Length(meters) -	78.00	83.00
Traverse Time(seconds) -	52.00	55.34
Battery Time(seconds) -	1.34	1.34
Figure of Merit -	0.972	0.934
Use of Emergency Mode -	2	7

Task D. Chemical Analysis of Specimens

One important phase of the initial missions to Mars is the search for organic matter and living organisms on the martian surface. The present concept for attaining this objective consists of subjecting samples of the atmosphere and surface material to certain chemical and biochemical reactions and thereafter analyzing the products produced, probably in a combination gas chromatograph/mass spectrometer (GC/MS). The gas chromatograph is proposed for separating complex mixtures evolved from the experiments into small groups of similar chemical species. Chemical analysis of these groups would be accomplished in the mass spectrometer.

Most of the previous effort has involved the systems analysis of the gas chromatograph using simulation, Ref. 33, 34. This technique uses mathematical models, which incorporate fundamental parameters evaluated from reported experiments, to explore various concepts and to direct further experimental research. Application of prior work to multicomponent chemical systems and improvement of the mathematical model are currently being studied.

The objectives of the task have been extended to include preliminary studies of the entire chemical analysis system. System topics being considered include carrier gas generation and removal, sample size and component detectability limits, and limitations imposed by and upon the mass spectrometer.

The task problems are being attacked by a five-member team, each of whom is pursuing a specific assignment:

1. Mass spectrometer system characteristics.
2. Carrier gas generation and removal.
3. Chromatograph model evaluation using multicomponent chemical systems.
4. Improvement of the mathematical model of the chromatograph.
5. Estimation of chromatograph column parameters which appear as constants in the mathematical models.

D.1. GC/MS System Concepts

a. Mass Spectrometer System Characteristics - M.P.Badawy

b. Carrier Gas Generation and Removal - C.W.Jarva
Faculty Advisor: Professor P.K. Lashmet

The overall concept of the chemical analysis system is shown schematically in Fig. 51. The idea of the combined gas chromatograph/mass spectrometer for use in detecting life on other planets has been described by others, Ref. 35, 36, 37. The design of such a system to function in a hostile atmosphere represents a formidable problem which is suitably handled by system modeling and simulation by computer. For simulation to be effective, it is necessary to uniquely describe the important characteristics of the entire system by a minimum number of variables and equations. The development of the governing relations for the system components excluding the gas chromatograph is the initial

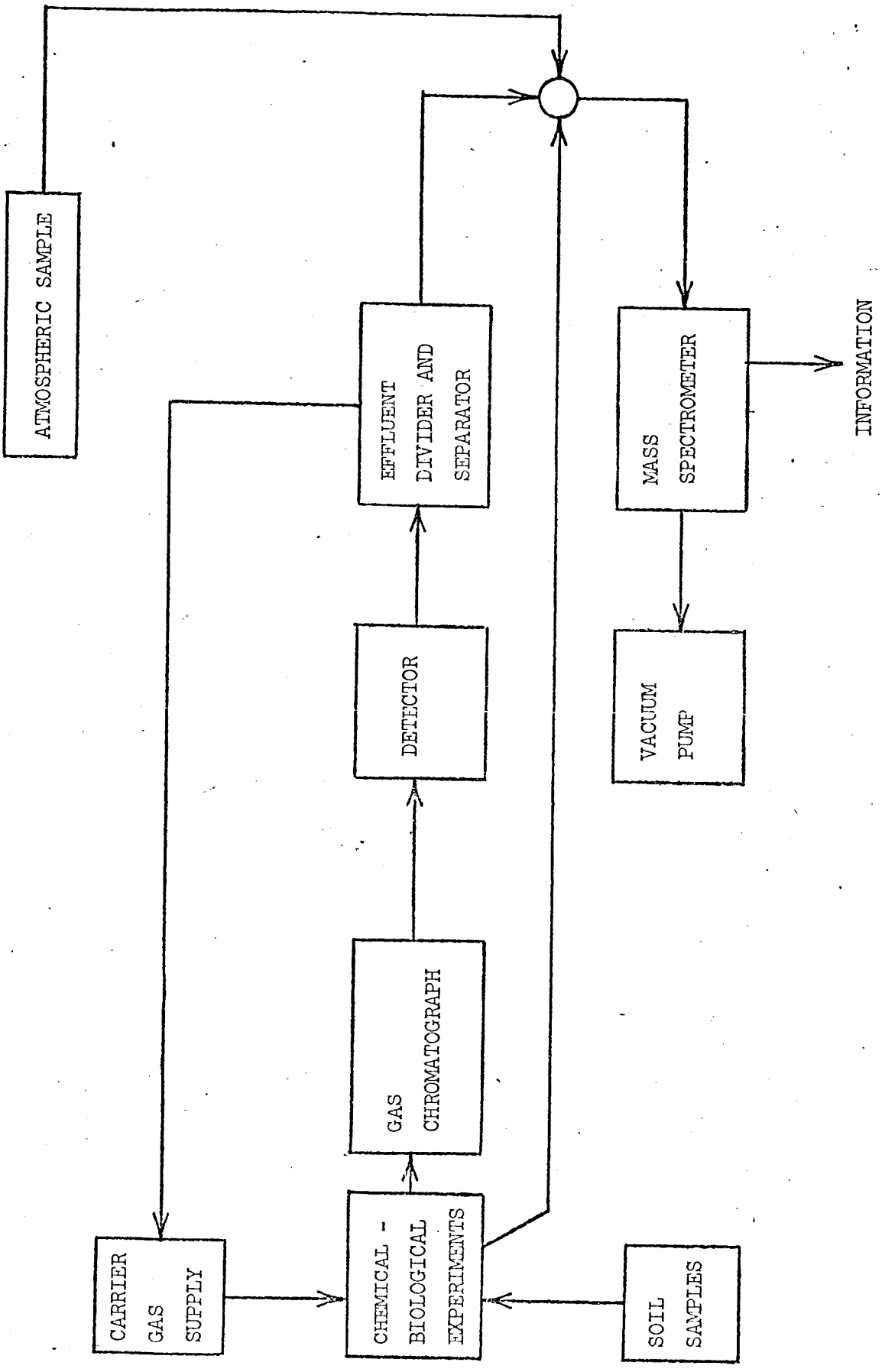

Fig. 51: Process Schematic of Gas Chromatograph - Mass Spectrometer System

objective of this subtask.

It is the purpose of the mass spectrometer to provide mass spectra from three different inputs: effluents from the gas chromatograph; direct samples from the life-determining experiments; and samples of the atmosphere. Functional requirements for the Viking mass spectrometer have been defined previously, Ref. 37, 38 and typical specifications appear in Table 10.

Small mass spectrometers suitable for adaptation to the Mars roving lander have been under development, Ref. 35, 38, 39, 40, and prior work is being reviewed to quantitatively represent the various characteristics and limitations of the instrument. Specific topics include the following:

1. Mass range and resolution as affected by magnetic field and accelerating voltage.
2. Scan rate as affected by scan method.
3. Effect of operating pressure (vacuum) upon system performance.
4. Power requirements as affected by system parameters.
5. Weight and volume as affected by system parameters.

From the literature, it is evident that the instrument may be multifunctional. For example, McMurray and Green, Ref. 49, report that fast scan rates are not required for high resolution mass spectra whereas low resolution data from fast scan rates may be satisfactory in certain instances. Miniaturization and the resulting problems with the power supply and voltage level are not trivial considerations, judging from the reported catastrophic failure of one instrument under development, Ref. 39. These studies and development programs provide physical limitations of the equipment, a necessary input for proper system analysis.

Mathematical modeling of the gross characteristics of the mass spectrometer has been initiated, based on prior reports, Ref. 38, 42. The basic relation between the mass range, accelerating voltage, and magnetic field is shown in Fig. 52 for a single focusing instrument having a radius of curvature of 3.8 cm. The desired mass range of 20-200 AMU corresponds to m/e shown in Fig. 52 of 0.05 to 0.5.

Current work involves the relations between required input energy and the various system parameters and operating mode. The processes occurring in the ionization chamber are being investigated to relate ion current to sample flow rate, vacuum, and accelerating potential. A study of the energy requirements for maintaining the magnetic field will result in less power and less severe levels for the operating parameters. This concept will be considered in these studies.

The major equations for modeling for spectrometer are expected by the end of the summer. Component (mass spectrometer) and system (GC/MS) simulation will be initiated in September 1972, and major results

TABLE 10

TYPICAL DESIGN SPECIFICATIONS: MINIATURIZED MASS SPECTROMETER

Mass range	12-200 atomic mass units (AMU)
Mass resolution	$(M/\triangle M)_{10\% \text{ valley}} = 140$; 12-140 AMU
	$(M/\triangle M)_{20\% \text{ valley}} = 200$; 140-200 AMU
Sensitivity	2.5×10^{-8} amp/(nanogram/sec) at 200 AMU
Minimum detectable output current	1.0×10^{-11} amp
Dynamic range (maximum peak/minimum peak)	10^5
Maximum ion source pressure	10^{-4} torr
Mass scan rate	5.3 seconds for 12-200 AMU

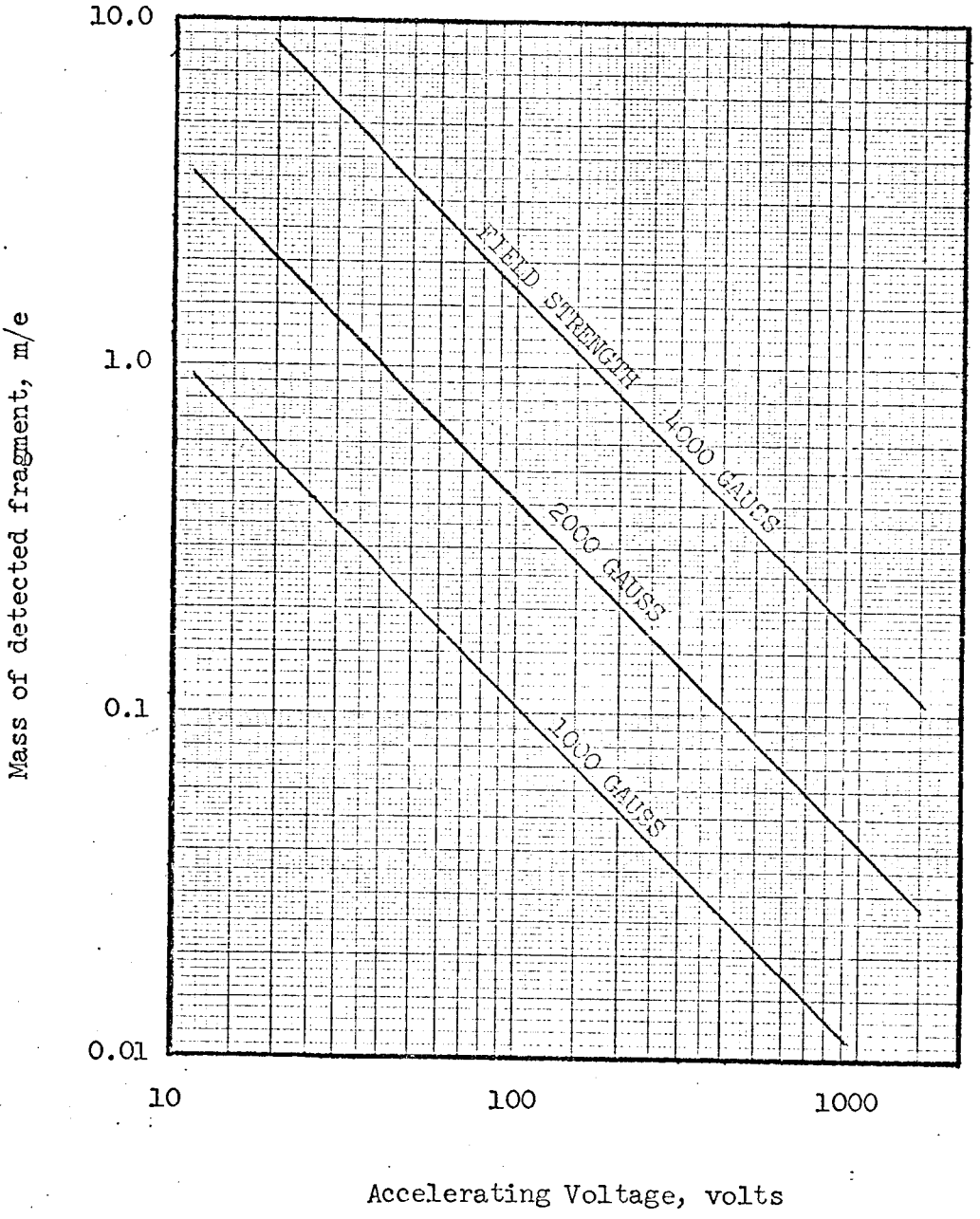

Fig. 52: Effect of Field Strength and Accelerating Voltage on Mass Detected in Typical Mass Spectrometer.

for use in the system design and the overall system analysis, Task B, should be available by March, 1973.

Carrier gas, which is relatively inert with respect to the samples being analyzed and which must be in supply for an appreciable part of the mission, is required to propel minute samples through the column of the gas chromatograph, Ref. 33. On arriving at the mass spectrometer, which operates at a low pressure ($< 10^{-4}$ torr), the major portion of this carrier gas must be separated from the sample and must be removed from the system. Thus the systems for generating, separating, and removing the carrier gas are important to overall system design and operation. It is the objective of this subtask to generate the basic characteristics and limitations of the more promising concepts to aid in the design of the final overall system.

The quantity of carrier gas available on the lander depends upon the frequency and time of operation of the chromatograph. For short periods of operation, simple high-pressure gas storage with discharge to the atmosphere after separation from the samples prior to entering the mass spectrometer may be adequate. For more frequent or longer periods of operation, a recycling or regeneration technique may be advantageous.

Because of its simplicity and inherent reliability, the high-pressure gas storage concept was considered initially. Figure 53 shows the estimated vessel size as a function of charge pressure and several operating times for a typical chromatographic system. Estimates of the minimum thickness for the vessel wall are shown in Fig. 54. These estimates assume fiber-reinforced, spherical construction having an allowable working stress of about 10^5 psi, Ref. 43. Based on preliminary estimates of the weight of the composite vessel, the storage vessel concept appears promising, so the calculations are being refined by considering the following:

1. Hydrogen is permeable to most metals considered for the vessel skin. Permeability rates have been reported, Ref. 44, so this effect on gas storage requirements can be considered.

2. Welds, valves, and other closures have a small but finite leakage rate which will affect the gas storage requirements. Maximum rates based on helium leak detection limits, Ref. 45, will provide a basis for determining the severity of this effect.

3. Better working stress-density information for the fiber reinforced metallic vessel must be obtained for a reliable estimate of the vessel weight. NASA-sponsored work in the area, Ref. 43, may be helpful.

A carrier gas removal system must be considered because the operating pressure of the mass spectrometer is about 10^{-7} times the pressure expected in the chromatograph, Ref. 46. Also, in order to maintain an adequate amount of sample for analysis by the mass spectrometer, a

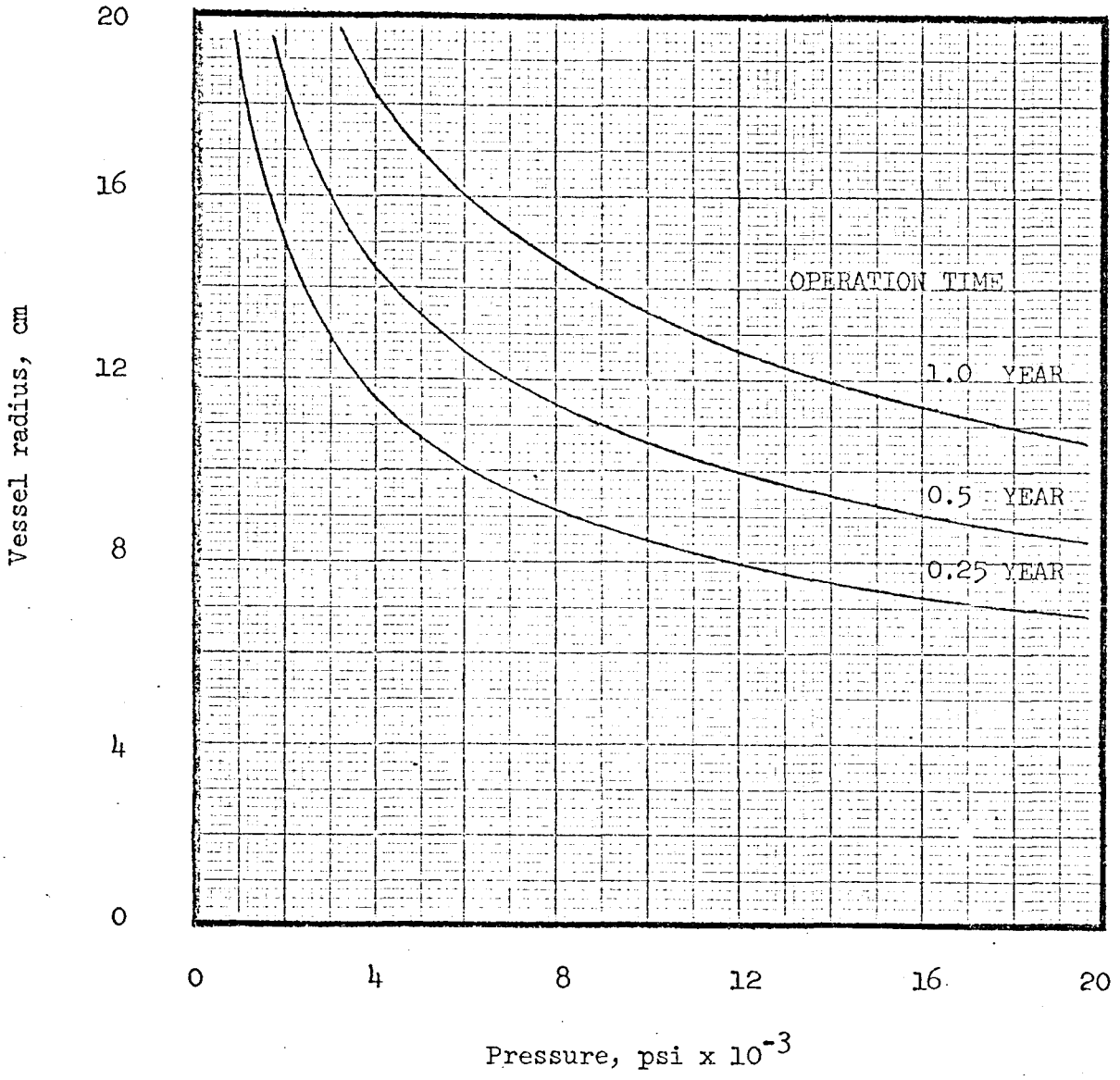

Fig.53 : Effect of Charge Pressure and Operation Time on Size of Carrier Gas Sphere.

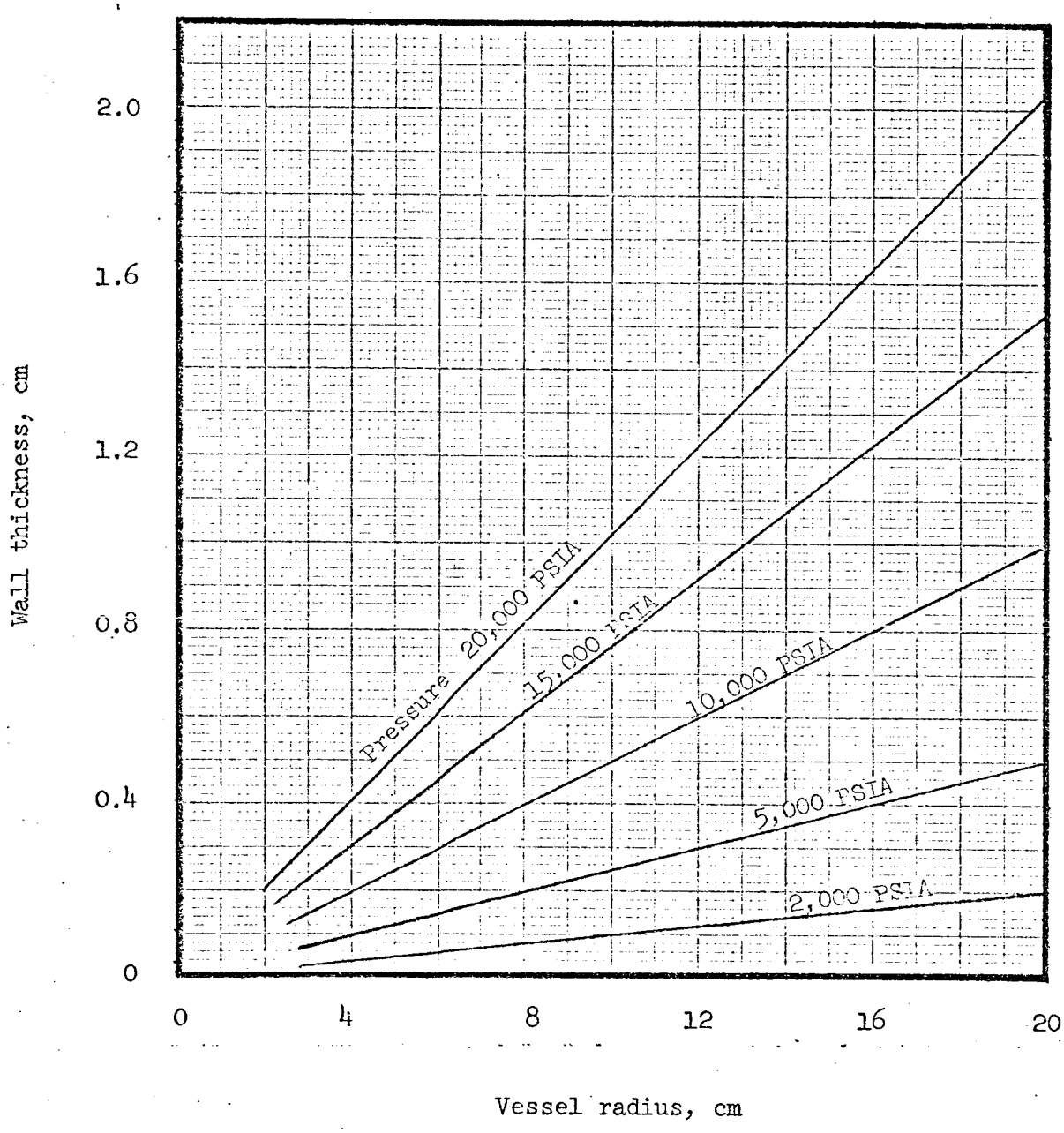

Fig. 54: Estimated Wall Thickness of Carrier Gas Sphere for Various Charge Pressures and Vessel Sizes

technique for concentrating the sample must be provided, Ref. 47, 48, 49. Among the most promising separators, if hydrogen is to be used as a carrier gas, is the palladium-silver alloy membrane to maintain hydrogen flow, Ref. 51. This might be accomplished by reacting the effluent hydrogen with oxygen and removing the resulting water vapor by adsorption or by ejection to the atmosphere, Ref. 48. Use of the palladium-silver alloy as the cathode and anode in a fuel cell offers an interesting possibility. Hydrogen for carrier gas usage may be generated by water electrolysis and then be recovered via membrane diffusion and reaction with hydroxyl ions in the fuel cell electrolyte as water which can be re-electrolyzed, Ref. 58, 52.

Although these systems are promising, problems arise because of the structural breakdown of the palladium during temperature and pressure recycling, Ref. 53. Furthermore, contamination by halogens and other chemicals reduce the effectiveness of the membranes, Ref. 52. Other separating techniques such as semipermeable silicone rubber membranes and supersonic (Ryhage) separators possibly have merit.

Upon completion of the gas storage study, a review of the carrier gas removal system will be initiated. This study will yield the gross characteristics and limitations of proposed systems and will provide a basis for conducting overall system studies. It is expected that the gas storage study will be completed in December, 1972 and gross characteristics of the carrier gas system will be available in May, 1973.

D.2. Chromatographic Model Evaluation Using Multicomponent Chemical Systems - P.S. Keba
Faculty Advisor: Professor P.K. Lashmet

A mathematical model composed of a system of partial differential equations was developed earlier to represent the chromatographic column behavior, Ref. 33. Solutions to linearized approximations of the differential equations obtained by classical techniques have been reported, Ref. 54, 55. Because of their complexity, the equations were solved by assuming the sample to be injected as an impulse. Using data obtained from a specially constructed chromatographic test facility, Ref. 56, Benoit showed that convolution of the input data with the theoretical impulse response gave a reasonable representation for a single component in the system, Ref. 34. It is the objective of this subtask to experimentally verify the mathematical model for multicomponent chemical systems using superposition of single component data. Specifically, the simplified equilibrium adsorption model, Ref. 55, is being considered:

$$Y(\theta) = \sqrt{\beta Pe/4\pi\theta^3} \quad \exp\left[-(Pe/4\beta\theta)(\theta-\beta)^2\right]$$

where

β = $1 + (1/mR_0)$

θ = dimensionless time = vt/L

v = carrier gas velocity

t = time

L = column length

Pe = the Peclet number, a dimensionless measure of sample diffusion in the carrier gas

mR_0 = a thermodynamic parameter, specific to the chemical system considered

Y = composition response to a unit impulse

This model assumes the gas at each point to be in equilibrium with the solid adsorbent; i.e., the column is very long. The Peclet number is predictable since it depends only upon the system configuration and fluid mechanics. The thermodynamic parameter mR_0 is specific to the system used and is determined from the system data using a curve fitting technique.

Prior to the experimentation, modifications to the test facility were made to provide more accurate measurement of the carrier gas flow rate and the gas pressure within the chromatographic column. In addition, the equilibrium adsorption model above was re-evaluated with the single component data of Benoit, Ref. 34, using a more acceptable correlation for the Peclet number (see Task D.4.). Basic conclusions about the adequateness of the model remained unchanged (see Task D.2 for quantitative aspects). This preliminary work has been documented in a recent report, Ref. 57.

Initial studies of multicomponent chemical systems involved the binary system n-pentane/n-heptane which is representative of a heavy organic system. A Chromosorb 102 column, described in Table 11, was used, and the mixture was vaporized prior to entering the column. Chromatographic data were obtained at 150 and 200°C. The composition of the sample was varied from an excess of one component to an excess of the other. The following pentane compositions (by weight) were used: 100%, 99%, 75%, 50%, 25%, 1%, 0%.

Figure 55 shows typical chromatographic data for the binary system (50% by weight pentane) at 200°C. Superimposed on the data are the chromatograms as predicted from the equilibrium adsorption model using pure component data (superposition) and the convolution procedure of Benoit, Ref. 34. It is apparent that the actual data lags the predicted data in time. This trend is observed for both compounds over the entire composition range as shown in Table 12. It is evident that as the component composition in the sample becomes less, the time lag becomes greater. This occurs for both pentane and heptane. Data at 150°C show the same trends, the deviations from superposition being more pronounced.

Earlier work, Ref. 55, showed the parameter mR_0 is the primary factor affecting the time when the maximum composition appears. The fact that the peak occurs at a different time for each sample composition suggests that mR_0 is a function of composition which decreases as

TABLE 11

CHROMATOGRAPHIC COLUMN CHARACTERISTICS

Designation	Chromosorb 102	Molecular Sieve 5A	Carbowax 1500/ Chromosorb P
Composition	Microporous styrene divinyl - benzene polymers	Synthetic zeolite	Polyethylene glycol (20% by weight) on diatomaceous earth
Temperature range	to 250°C	to 350°C	to 225°C
Application	Separation of low molecular weight highly polar substances	Separation of light gases	Separation of high boiling, polar compounds

Length - 100 cm; outside diameter - 0.32 cm; inside diameter - 0.22 cm; particle size - 0.025/0.018 cm

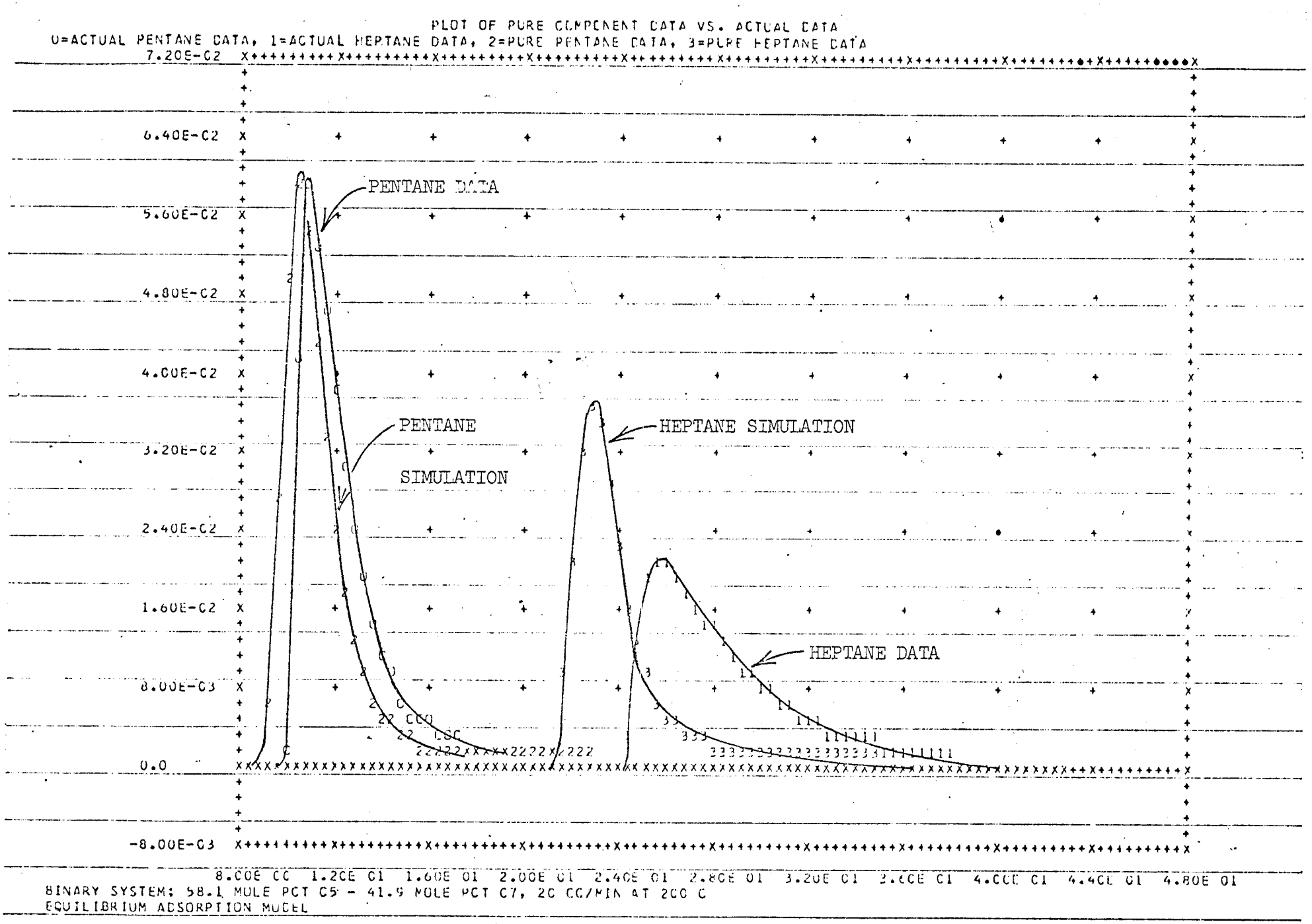

Fig. 55: Comparison of Predicted and Actual Chromatograms for Pentane-Heptane System on Chromosorb 102 at 200°C

TABLE 12

EVALUATION OF SUPERPOSITION

Pentane - Heptane System on Chromosorb 102 Column at 200°C

Pentane Composition weight percent	Pentane Peak seconds	Heptane Peak seconds
0	—	85.0
1	43.0	86.5
25	41.0	89.0
50	39.5	94.5
75	39.0	102.0
99	38.5	110.0
100	38.5	—

the composition of the component decreases (or as the composition of the other component increases). This is not surprising considering the physical processes involved during the adsorption step. Adsorbent surface coverage is an important factor in processes involving the adsorption phenomena such as catalysis, and must be considered.

In summary, it appears that superposition of the basic equations is an idealization, at least for the specific system studies, but it offers a first-order approximation to system behavior. In the immediate future, additional data for the pentane-heptane system will be obtained on the Chromosorb 102 adsorbent at other temperatures in the range of 50 to 200°C. In addition, the behavior of this system with the Carbowax 1500 adsorbent described in Table 11 will be studied. This column is fundamentally different from the Chromasorb 102 adsorbent (see Task D.3 for further discussion), and is believed better represented by the system equations currently being studied. These studies will provide data to investigate compositional effects on the term mR_0 and will guide further theoretical work. The experimental work should be completed in December, 1972, and final analysis and evaluation is expected by May, 1973.

D.3. Chromatograph Model Improvement - P.T.Woodrow
Faculty Advisor: Prof. P.K. Lashmet

In previous work, Benoit, Ref. 34, showed that for certain systems, the equilibrium adsorption model represented fairly well single component data provided the input pulse was considered through a convolution procedure. In other instances, however, agreement between the theoretical prediction and experimental data was not as satisfactory. Dispersion in the gas composition existing the chromatographic column was observed greater than that predicted by the model. It is the objective of this subtask to investigate methods for improving the predictive capability of the model.

A less restrictive solution to the system of partial differential equations was reported earlier, Ref. 58, and was adapted for use in the chromatographic system studies, Ref. 54. This solution does not assume equilibrium adsorption and introduces a dimensionless mass transfer parameter N_{tOG}. This model, summarized in Table 13, was developed before the data reduction program and convolution procedure, Ref. 34, were available. Although preliminary analysis showed the model to be an improvement over the equilibrium adsorption model, Ref. 54, it was not evaluated with the single component data.

Initial attempts to evaluate the original mathematical model, Ref. 54, using the convolution procedure showed the calculations to be unstable for various values of the parameters Pe, N_{tOG}, and mR_0. Numerical calculations for this model were reprogrammed using different numerical techniques, Ref. 57, and previous computational problems were solved.

Representation of the twenty sets of single component data, Ref. 34, 57, by the nonequilibrium and equilibrium models are summarized in Table 14. The adequacy of the models is measured by the average squared deviation between the particular model's convolved response and

TABLE 13

NON-EQUILIBRIUM ADSORPTION MODEL

$$y(1,\theta) = c\cdot(y_1 + y_2)$$

where:

$$c = \frac{A}{2}\left(\frac{Pe}{\pi}\right)^{0.5}\cdot \exp\left\{\frac{Pe}{2}\right\}\cdot \exp\left\{-N_{tog}\cdot mR_o\cdot\theta\right\}$$

$$y_1 = \frac{1}{\theta^{1.5}}\ \exp\left\{-\frac{Pe}{4\cdot\theta} - \frac{Pe\cdot\theta}{4} - N_{tog}\cdot\theta + N_{tog}\cdot mR_o\cdot\theta\right\}$$

$$y_2 = 2\cdot N_{tog}^2\cdot mR_o\cdot\int_0^{\theta}\frac{I_1\left[2\cdot(N_{tog}^2\cdot mR_o\cdot(\theta-x)\cdot x)^{0.5}\right]}{2\cdot(N_{tog}^2\cdot mR_o\cdot(\theta-x)\cdot x)^{0.5}}\cdot\frac{1}{(x)^{0.5}}$$

$$\cdot\exp\left\{-\left(\frac{Pe}{4x} + \frac{Pe\cdot x}{4} + N_{tog}(1-mR_o)\cdot x\right)\right\}\cdot dx$$

TABLE 14

COMPARISON OF EQUILIBRIUM AND NON-EQUILIBRIUM ADSORPTION MODELS WITH CHROMATOGRAPHIC DATA

System	Column	Equilibrium Model Avg. Squared Dev.	Non-Equilibrium Model Avg. Squared Dev.
Nitrogen, 20°C	Molecular Sieve	0.00743	0.00741
Oxygen, 20°C	"	0.00486	0.00570
Pentane, 150°C	Chromosorb 102	0.000575	0.000580
Pentane, 200°C	"	0.000192	0.000195
Heptane, 150°C	"	0.000481	0.000464
Heptane, 200°C	"	0.000228	0.000202
Acetone, 125°C	"	0.000877	0.000863
Acetone, 100°C	"	0.0000386	0.0000387
Acetone, 125°C	"	0.0000266	0.0000270
Acetone, 150°C	"	0.0000104	0.0000108
Acetone, 175°C	"	0.0000051	0.0000046
Acetone, 200°C	"	0.0000457	0.0000406
Ethylene, 20°C	"	0.0130	0.0122
Ethylene, 28°C	"	0.0141	0.0132
Ethylene, 50°C	"	0.0296	0.0283
Ethylene, 75°C	"	0.0560	0.0539
Ethylene, 100°C	"	0.0747	0.0730
Ethylene, 125°C	"	0.0797	0.0781
Ethylene, 150°C	"	0.0867	0.0853
Ethylene, 175°C	"	0.0828	0.0769

the actual output data. This squared deviation is obtained over that portion of time where finite responses occur, not over the entire time domain. Table 14 may be summarized as follows:

1. Both models perform similarly with respect to the prediction of output chromatograms.

2. The predictions for the acetone system are superior to predictions for other systems.

3. Predictions for the ethylene system are the worst of all.

4. The improvement in prediction by including a finite value of N_{tOG} in the system model is at best minor, at least for the conditions studied. Equilibrium adsorption implies an infinite value for N_{tOG}, whereas in the experiments of Table 14, the value ranged from 62,000 to 148,000. It appears for these values of N_{tOG} that adsorption equilibrium is approached. Under other circumstances, e.g., with a much shorter column, the terms involving N_{tOG} will have more influence on the prediction.

5. Within each system group, especially acetone and ethylene, the quality of prediction depends strongly upon temperature. For acetone, heptane and pentane, the model representation improves as the temperature increases, whereas for ethylene, the trend is opposite. This implies different mechanisms controlling the adsorption-desorption-transport process are involved and that further model improvement is required.

In addition to comparing the models with data, it was shown that the moment analysis as outlined by Voytus, Ref. 55, and Taylor, Ref. 54, is valid. This suggests that the gross characteristics of the chromatogram -- the mean, the mode, and an estimate of the dispersion -- can be estimated directly from the Laplace transforms of the basic differential equations, without resorting to the final analytical solution.

The present models represent fairly well the chromatograms of acetone, pentane, and heptane on Chromosorb 102. In the light gas systems -- ethylene, nitrogen, and oxygen -- agreement between the theoretical prediction and experimental data are not as satisfactory, suggesting that other transport processes have not been included in the model. It is noted that the adsorbent used, Chromosorb 102 in most cases and Molecular Sieve 5A in two experiments, are porous. The lighter materials, such as ethylene, nitrogen, and oxygen, may adsorb internally within the adsorbent particles, whereas the larger acetone, pentane, and heptane may be confined to the external adsorbent surface. Thus the process of intraparticle diffusion, which was neglected in the model derivation, may be appreciable and hence responsible for the observed discrepancies. This additional mechanism is further suggested from an examination of the temperature behavior of the thermodynamic parameter mR_0. Over the temperature range considered, the activation energy for

mR_Q for the acetone system is of the order of 6 kcal/mole, an indication that the controlling mechanism is probably a physical adsorption process as proposed by the model. For the ethylene system, the corresponding activation energy varies from about 1.5 kcal/mole at 175°C to 4 kcal/mole at 28°C. Intraparticle diffusion (a low activation energy process) superimposed upon physical adsorption (a high activation energy process) would exhibit such temperature behavior, with the adsorption process controlling at the lower temperatures. The effect of temperature upon the quality of prediction for the ethylene data given in Table 14 further substantiates such a proposal.

Work in the immediate future will incorporate intraparticle diffusion into the mathematical models. Consideration of this diffusion further complicates the mathematical models, and a workable, analytical solution may not be obtained. If this is the case, direct numerical techniques will be employed. The resulting mathematical model will subsequently be evaluated with the experimental data to establish the importance of this mechanism.

D.4. Transport Parameter Estimation - P.K. Lashmet

Mathematical representation of the chromatograph requires a priori estimates of the transport parameters Pe and N_{tOG} as well as other properties which depend upon the complexity of the mathematical model. This task has as its objective the development of suitably accurate methods for estimating the above two parameters.

The Peclet number, which is a dimensionless measure of diffusion of the sample in the direction of carrier gas flow, is defined as

$$Pe = v\ L/D$$

where

v = mean velocity of the carrier gas

L = length of chromatographic column

D = effective diffusion or dispersion coefficient

This Peclet number is a function of the fluid mechanics of the system as well as the physical properties of the chemical sample and carrier gas. As a first approximation, the dimensionless Reynolds number Re and Schmidt number Sc represent these effects:

$$Re = d\ v\ \rho\ /\mu$$

$$Sc = \mu/\rho\ D_M$$

where

d = diameter of particle

ρ = carrier gas density

μ = carrier gas viscosity

D_M = molecular diffusivity of sample in carrier gas

Prior attempts to compute the Peclet number from theoretical considerations and other measured transport properties of the system were not completely successful, Ref. 59. In the meantime, numerous sets of experimental Peclet number data, both published and unpublished, have been obtained. Also a correlation based on two additional sets of data, Ref. 60, appears adequate for the present studies. Further work on this subject will include an evaluation of the correlation using other available data and an estimate of the uncertainty in predicting the Peclet number.

Prediction of the number of transfer units N_{tOG} was discussed earlier, Ref. 32. This correlation which applied to fluid flow around single particles, was extrapolated to the multiparticle column of the chromatograph. This was somewhat uncertain, and other correlations were investigated. A predictive method for liquids in packed beds, Ref. 61, was compared with available data for gaseous sytems and was found acceptable for this project.

These prediction techniques have been computerized to reduce the data reduction effort. Both prediction methods require values of the Schmidt number Sc, and a separate estimating procedure based on the theoretical work of Bird, Hirschfelder and Curtiss, Ref. 62 and others, which uses measured physical properties has been developed and is operational.

This task is essentially complete. The remaining effort involves estimating uncertainties for the predictions and completing a technical report on the subject.

REFERENCES

1. Burke, J.D. and Moore, J.W., "An Exploratory Investigation of a 1979 Roving Vehicle Mission," Dec. 1, 1970, 760-58, Jet Propulsion Laboratory, California Inst. of Technology, Pasadena, California.

2. Cobb, W.A., "Dynamic Evaluation of a Scaled Four Wheel Martian Roving Vehicle," Master of Engineering Project Report, Rensselaer Polytechnic Institute, Troy, N.Y., June 1972.

3. Steinbock, A.F., "Obstacle Negotiation of a Mars Roving Vehicle," Senior Project Report, Rensselaer Polytechnic Institute, Troy, N.Y., June 1972.

4. Janes, T.M., "Collapsibility and Deployment of a Four Wheeled Martian Roving Vehicle," Master of Engineering Project Report, Rensselaer Polytechnic Institute, Troy, N.Y., June 1972.

5. Klette, C., "Martian Roving Vehicle Wheel Test Apparatus," Master of Engineering Project Report, Rensselaer Polytechnic Institute, Troy, N.Y., June 1972.

6. Kobus, J.A., "Deflection Characteristics of an All Metal Toroidal Hoop Wheel," Senior Project Report, Rensselaer Polytechnic Institute, Troy, N.Y., May 1972.

7. Baker, J., Goldberg, A., and Pavarini, C., "An Optimal System Design Process for a Mars Roving Vehicle," RPI Technical Report MP-24, Rensselaer Polytechnic Institute, Troy, N.Y., November 1971.

8. Glasstone, Samuel, The Book of Mars, NASA SP-179, NASA 1968.

9. Pavarini, Baker and Goldberg, "An Optimal System Design Process for a Mars Roving Vehicle," RPI Technical Report MP-24, Rensselaer Polytechnic Institute, Troy, N.Y., November 1971.

10. Fiacco, Anthony V. and McCormick, Garth P., Nonlinear Programming: Sequential Unconstrained Minimization Techniques, New York, Wiley, 1968.

11. "An Exploratory Investigation of a 1979 Mars Roving Vehicle Mission," JPL Report 760-58.

12. Quelle, Fred W., Jr., "Alternatives to Q-Spoiled Ruby Rangefinders," Proceedings SPIE, Oct. 1967, pp. 7.

13. Torrance, K.E., Sparrow, E.M., "Theory for Off-Specular Reflection from Roughened Surfaces," Journal of the Optical Society of America, Vol. 57, No. 9, Sept. 1967, pp. 1105-1114.

14. Koechner, Walter, "Optical Ranging System Employing a High Power Injection Laser Diode," IEEE Transactions on Aerospace and Electronic Systems, Vol. AES-4, No. 1, Jan. 1968, pp. 81-91.

15. Stoller, Millan D., "Vulnerability of Lead Sulfide Detectors to Laser Radiation," Ballistic Research Labs, Aberdeen Proving Ground, Md., June 1971, AD 730 639.

16. Melchior, Hans, et al, "Photodetectors for Optical Communication Systems," Proceedings of the IEEE, Vol. 58, No. 10, Oct., 1970, pp. 1466-1483.

17. Geusic, et al, "Coherent Optical Sources," Proceedings of the IEEE, Vol. 58, No. 10, Oct., 1970, pp. 1429.

18. RCA Publication #OPT-100, "Gallium Arsenide Lasers and Emitters," 1970.

19. Ross, Monte, Laser Applications, Academic Press, 1971, pp. 282.

20. Advertisement by Coherent Optics Inc., Laser Focus, Feb. 1970, pp. 13.

21. Advertisement by Orlando Research Corp., Laser Focus, March 1970, pp. 53.

22. Pavarini, C. and Chrysler, J.H., "Terrain Modeling and Path Selection by an Autonomous Martian Exploratory Vehicle," RPI Technical Report MP-14, NASA Grant 33-018-091, June 1970.

23. Rautio, A., "Analysis of the Effect of Sensor Errors on a Long-Range Terrain Modeling System and a Study of Short-Range Terrain Modeling for an Autonomous Roving Vehicle," RPI Master of Engineering Project Report, Rensselaer Polytechnic Institute, Troy, N.Y., June 1971.

24. Moore, J. and Burke, J., "An Exploratory Investigation of a 1979 Mars Roving Vehicle Mission," JPL Document No. 760-58, Dec. 1, 1970.

25. Eleccion, M., "Technology; The Family of Lasers," IEEE SPECTRUM, March 1972.

26. Redeker, R.H., "Semiconductor Lasers: Still at the Temperature Barrier," LASER FOCUS, March 1969.

27. Smith, W.V. and Sorokin, P.P., The Laser, McGraw-Hill Book Co., 1966.

28. Zuraski, G., "Laser Range Measurement for a Satellite Navigation Scheme and Mid-Range Path Selection and Obstacle Avoidance," RPI Technical Report MP-26, Rensselaer Polytechnic Institute, Troy, N.Y., June 1972.

29. Bryson, A.E. and Ho, Y.C., "Applied Optimal Control," Ginn-Blaisdell Publishing Co., 1969, Chapter 12.

30. Close, C., Roy, R., and DeRusso, P., "State Variables for Engineers," Wiley & Sons.

31. Purdon, W., "Development of a Path Selection System Simulation for an Autonomous Mars Exploratory Vehicle," Master of Engineering Project Report, Rensselaer Polytechnic Institute, Troy, N.Y., June 1972.

32. Mounce, W., "Discrete Obstacle Detection," Master of Engineering Project Report, Rensselaer Polytechnic Institute, Troy, N.Y., June 1972.

33. Sliva, T.F., "Chromatographic Systems Analysis: First-Order Model Evaluation," RPI Technical Report MP-1, Rensselaer Polytechnic Institute, Troy, N.Y., September 1968.

34. Benoit, G.L., "Reduction of Chromatographic Data and Evaluation of a GC Model," RPI Technical Report MP-22, Rensselaer Polytechnic Institute, Troy, N.Y., June 1971.

35. Bentley, K.E., Giffen, C.E., Whitten, D.G., and Wilhite, W.F., "Detection of Life-Related Compounds on Planetary Surfaces by Gas Chromatography - Mass Spectrometry Techniques," Tech. Rept. 32-713, Jet Propulsion Lab., Pasadena, California, August 1965.

36. "Gas Chromatograph/Mass Spectrometer," JPL Space Programs Summary 37-61, v. I, pp. 22-28, Jet Propulsion Lab., Pasadena, California, January 31, 1970.

37. Viking Management, "1973 Viking Voyage to Mars," Astronaut. Aeronaut. 7, (11), 30-59, November 1969.

38. Engineering Model GC/MS Design Review: Mass Spectrometer Subsystem, pp. 12-65, Jet Propulsion Lab., Pasadena, California, January 27, 1971.

39. Hanson, W.B., "OGO-F-06 Ion Mass Spectrometer. Final Report, March 1966-June 1970," Report NASA-CR-111146, Natl. Aeronaut. Space Admin., Washington, D.C., August 1970.

40. Johnson, F.S., "High-Sensitivity Miniaturized Magnetic Sector Mass Spectrometer for the ALSEP Program. Final Report," Report NASA-CR-114774, Natl. Aeronaut. Space Admin., Washington, D.C., June 1970.

41. McMurray, W.J., Greene, B.N., and Lipsky, S.R., "Fast Scan High Resolution Mass Spectrometer. I. Operating Parameters and Its Tandem Use with Gas Chromatography," Anal. Chem., 38, 1194-1204, 1966.

42. McDowell, C.A., "Mass Spectrometry," McGraw-Hill, New York, 1963, pp. 201-271.

43. Morris, E.E., "Glass-Fiber-Reinforced Metallic Tanks for Cryogenic Service," "Advances in Structural Composites," Sci. Adv. Mater. Process Eng., 12, Paper No. AS-4, 1967.

44. Dushman, S., "Scientific Foundations of Vacuum Techniques," 2nd ed., (J.M.Lafferty, ed.), Wiley, New York, 1962.

45. Guthrie, A., and Wakerling, R.K., ed., "Vacuum Equipment and Techniques," McGraw-Hill, New York, 1949.

46. "Dynamic Response of a Gas Chromatograph-Mass Spectrometer Combination," JPL Space Programs Summary 37-62, v. I, pp. 28-33, Jet Propulsion Lab., Pasadena, California, March 31, 1970.

47. McFadden, W.H., "Introduction of Gas-Chromatographic Samples to a Mass Spectrometer," Separ. Sci., 1, 723-746 (1966).

48. Engineering Model GC/MS Design Review: Gas Chromatograph Subsystem, pp. 6-1 to 6-29, Jet Propulsion Lab., Pasadena, California, January 28, 1971.

49. Wise, E.M., "Palladium Recovery, Properties and Uses," Academic Press, New York, 1968, pp. 149-156.

50. Lovelock, J.E., Charlton, K.W., and Simmonds, P.G., "The Palladium Transmodulator: A New Component for the Gas Chromatograph," Anal. Chem., 41, 1048-1952 (1969).

51. Lucero, D.P., and Haley, F.C., "Sample Enrichment Techniques for a Gas Chromatograph/Mass Spectrometer Analysis System," J. Gas Chromatog., 6, 477-482 (1968).

52. Lovelock, J.E., Simmonds, P.G., and Shoemaker, G.R., "The Palladium Generator-Separator: A Combined Electrolytic Source and Sink for Hydrogen in Closed Circuit Gas Chromatography," Anal. Chem., 42, 969-973 (1970).

53. Lewis, F.A., "The Palladium Hydrogen System," Academic Press, New York, 1967, pp. 47-49.

54. Taylor, P.N., "Chromatographic Systems Analysis: Second-Order Model Development," M. Eng. Project Report, Rensselaer Polytechnic Institute, Troy, New York, June 1970.

55. Voytus, W.A., "Chromatographic Systems Analysis: Moment Analysis of the Equilibrium Adsorption Model," RPI Technical Report MP-9, Rensselaer Polytechnic Institute, Troy, N.Y., August 1969.

56. Baer, S.R., and Benoit, G.L., "Chromatographic Test Facility, RPI Technical Report MP-19, Rensselaer Polytechnic Institute, Troy, N.Y., March 1971.

57. Keba, P.S. and Woodrow, P.T., "A Comparison of Two Gas Chromatograph Models and Analysis of Binary Data," Master of Engineering Project Report, Rensselaer Polytechnic Institute, Troy, N.Y., June 1972.

58. Lapidus, L., and Amundson, N.R., "Mathematics of Adsorption in Beds, VI. The Effect of Longitudinal Diffusion in Ion Exchange and Chromatographic Columns," J. Phys. Chem., 56, 984-988, (1952).

59. Reichman, D.A., "Chromatographic Systems Analysis: Dispersion Parameter Evaluation," Master of Engineering Project Report, Rensselaer Polytechnic Institute, Troy, N.Y., September 1969.

60. Gunn, D.J., "Theory of Axial and Radial Dispersion in Packed Beds," Trans. Inst. Chem. Eng., 47, T351-T359 (1969).

61. Wakao, Noriski, Oshima, Takashi, and Yagi, Sakaer, "Mass Transfer from Packed Beds of Particles to a Fluid," Kagaku Kogaku, 22, 780-785 (1958).

62. Bird, R.B., Hirschfelder, J.O., and Curtiss, C.F., "Theoretical Calculations of the Equation of State and Transport Properties of Gases and Liquids," Trans. ASME, 76, 1011-1038 (1954).